Development and application of titanium dioxide coated magnetic particles for photocatalytic oxidation of aqueous phase organic pollutants

vorgelegt von

Diplom-Ingenieur

Marcelo José González Salazar

aus Santiago de Chile

von der Fakultät III - Prozesswissenschaften

der Technischen Universität Berlin

zur Erlangung des akademischen Grades

Doktor der Ingenieurwissenschaften

-Dr.-Ing.-

genehmigte Dissertation

Promotionsausschuss:

Vorsitzender: Prof. Dr.-Ing. Sven-Uwe Geißen

Gutachter: Prof. Dr.-Ing. M. Jekel

Gutachter: Prof. Dr.-Ing. M. Franzreb, Karlsruher Institut für Technologie

Tag der wissenschaftliche Aussprache: 25. Juni 2010

Berlin 2010

D 83

ACKNOWLEDGMENTS

ABSTRACT

Photocatalysts with magnetic characteristics were synthesized based on a sol-gel technique by coating magnetic particles with titanium dioxide. The magnetic photocatalyst is thought to be used in slurry systems to remove organic pollutants. After the photocatalytic degradation the catalyst can be easily recovered by the application of an external magnetic field.

Composition and size of the synthesized material was determined by X-Ray powder diffraction (XRD), particle size distribution and environmental scanning electron microscopy (ESEM). The specific surface area was estimated based on BET theory. Additionally, measurements to determine the magnetic saturation, zeta potential and solid/liquid magnetic separation of the synthesized photocatalyst were carried out.

Results showed that titanium dioxide was successfully coated onto the surface of magnetic particles, whereas TiO_2 is used for the photocatalytic oxidation of organic compounds and the magnetic core is used as a carrier for the solid/liquid separation by the application of a magnetic field. Two photocatalysts were synthesized, Fe_3O_4/TiO_2 and $Fe_3O_4/SiO_2/TiO_2$, exhibiting different physicochemical characteristics.

The photocatalysts were used in the degradation of the three model compounds benzoic acid (BA), methyl orange (MO) and sulforhodamine B (SRB). The degradation experiments were carried out in a batch photocatalytic system, which involved a slurry reactor with pH, temperature, stirring and air injection control; a UV-lamp directed through the bottom of the reactor was used as light source.

The influences of different parameters such as amount of catalyst, substrate concentration, pH and temperature were studied. In order to evaluate the efficiency of the photocatalytic degradation of the model compounds, the degradation rate was deduced. It was observed that a complete degradation of the model substances could be reached within a few hours of illumination.

The dependence of the degradation rate on the substrate concentration could be described according to the Langmuir-Hinshelwood relationship for the oxidation of benzoic acid, methyl orange and sulforhodamine with suspended Fe_3O_4/TiO_2 and $Fe_3O_4/SiO_2/TiO_2$. It was also possible to establish a relation between the adsorption and the photocatalytic reaction.

The influence of the amount of catalyst by means of the k_{app} values was studied. It was seen that an increase of the catalyst amount leads to an increase in the k_{app} values according to a

function $(C_{cat})^n$. The amount of catalyst selected for the degradation of the organic compounds was 0.5 g L^{-1} for both photocatalysts.

The photocatalytic process was found to depend strongly on the pH of the solution, showing considerable differences in the k_{app} value. Thus, the pH values found to promote maximum degradation for each model compound was used for further reactions. The effect of pH on the oxidation process can be explained by its effect on the adsorption.

Reusability studies of both photocatalysts were evaluated for the three model compounds at least for five cycles, separating the catalyst from the solution at the end of each cycle by using a magnet. The practical implementation of this process can only be successful presuming that the catalyst is effectively and economically recycled. It was shown that the solid/liquid separation of the catalysts by means of the application of a magnetic field was effective and that a repeated use of the recycled catalysts showed reproducible photocatalytic activity.

Finally, with the constants obtained from the photooxidation experiments with different amounts of catalyst and different initial organic concentrations a kinetic model was proposed. Thus, using this kinetic model the degradation rate of a particular compound can be estimated.

ZUSAMMENFASSUNG

Photokatalysatoren mit magnetischen Eigenschaften wurden im Sol-Gel-Verfahren aus mit Titandioxid beschichteten magnetischen Partikeln synthetisiert. Dieser magnetische Photokatalysator wurde in Suspensionsreaktoren angewandt, in denen er nach jedem photokatalytischen Abbauzyklus leicht durch die Anwendung eines äußeren Magnetfeldes zurückgewonnen und wieder verwendet werden konnte.

Die physikalisch-chemischen Eigenschaften des synthetisierten Photokatalysators wurden durch Röntgenbeugung (XRD) und atmosphärische Rasterelektronenmikroskopie (A-REM, Environmental Scanning Electron Microscopy (ESEM)) analysiert. Zudem wurden die spezifische BET-Oberfläche, die Magnetisierung der Partikeln als Funktion der angelegten Feldstärke mit einem Alternating-Gradient Magnetometer (AGM) und das Zeta-Potential bestimmt sowie Tests zur physikalischen Stabilität durchgeführt.

Die Ergebnisse zeigten, dass Titandioxid erfolgreich auf die Oberfläche der magnetischen Partikeln in Form einer TiO_2-Schicht fixiert wurde, wodurch eine photokatalytische Oxidation an der Oberfläche stattfinden konnte. Der magnetische Kern als Träger dieser Schicht ermöglichte die Abtrennung durch ein Magnetfeld. Insgesamt wurden zwei Photokatalysatoren synthetisiert, Fe_3O_4/TiO_2 und $Fe_3O_4/SiO_2/TiO_2$, welche jeweils verschiedene physikalisch-chemischen Eigenschaften aufwiesen.

Die Photokatalysatoren wurden bezüglich ihrer Kapazität, die Verbindungen Benzoesäure (BA), Methylorange (MO) und Sulforhodamin B (SRB) abzubauen, untersucht. Die Versuche wurden in einem photokatalytischen Batch-System durchgeführt. Dies beinhaltete einen gerührten und mit Lufteinblasung versehenen Suspensionsreaktor, wobei die Beleuchtung durch eine UV-Lampe durch den Boden des Reaktors erfolgte.

Bezüglich des Abbauverhaltens der drei Verbindungen wurden Einflüsse verschiedener Parameter wie Katalysatormenge, Substratkonzentration, pH-Wert und Temperatur. Um die Einflüsse auf die photokatalytische Oxidation auswerten zu können, wurde die Anfangsabbaugeschwindigkeit r_0 genutzt. Es wurde beobachtet, dass unter UV-Bestrahlung ein vollständiger Abbau des Modellstoffs innerhalb von wenigen Stunden erzielt werden konnte.

Der zeitliche Verlauf der Substratkonzentrationen während des Abbaus konnte für die Oxidation von Benzoesäure, Methylorange und Sulforhodamin mit beiden Katalysatoren

Fe_3O_4/TiO_2 und $Fe_3O_4/SiO_2/TiO_2$ durch das Langmuir-Hinshelwood-Modell beschrieben werden. Zudem war es möglich, einen Zusammenhang zwischen der Adsorption und der photokatalytischen Reaktion aufzuzeigen.

Der Einfluss der Katalysatormenge durch die K_{app}-Werte wurde untersucht. Die k_{app}-Werte erhöhen sich mit steigender Menge des Katalysators gemäß einer Funktion $(C_{cat})^n$. Für den Abbau der organischen Verbindungen wurde im Falle beider Photokatalysatoren eine Konzentration von 0,5 g L^{-1} gewählt.

Der photokatalytische Prozess erwies sich stark pH-abhängig, was sich in deutlichen Unterschieden in die k_{app}-Werte äußerte. Optimale pH-Werte mit entsprechend maximaler Abbaugeschwindigkeit wurden für alle Modellverbindungen bestimmt. Der Einfluss des pH-Wertes auf die Oxidation kann durch seine Auswirkungen auf die Adsorption erklärt werden.

Die Wiederverwendbarkeit der beiden Photokatalysatoren für die drei Modell-Verbindungen wurde in mindestens fünf Zyklen gezeigt, wobei die Abtrennung des Katalysators aus der Lösung am Ende eines jeden Zyklus mittels Magneten erfolgte. Die praktische Umsetzung dieses Prozesses kann nur erfolgreich sein, wenn der Katalysator effektiv und kostengünstig wieder verwendet werden kann. Es wurde gezeigt, dass der Katalysator durch Fest-Flüssig-Trennung effektiv recycelt werden konnte und dass das wieder gewonnene Material bezüglich seiner photokatalytischen Aktivität reproduzierbare Ergebnisse lieferte.

Abschließend wurde ein Kinetisches Modell mit den Konstanten, die aus der photokatalytischen Oxidation bei variierter Katalysatormenge und Substratkonzentration erhalten wurden, vorgeschlagen. Somit kann die Abbaugeschwindigkeit für die bestimmte organische Substanz theoretisch geschätzt werden.

TABLE OF CONTENTS

x

LIST OF TABLES

LIST OF FIGURES

1   INTRODUCTION

The aquatic environment and related issues have been a major concern of the public because most of our ecological water systems are being continuously contaminated. The presence of harmful organic compounds in water supplies as well as in discharged wastewater is mainly due to the contribution of chemical industries, power plants, landfills, and agricultural sources. Surface runoff may also contribute (Reemtsma and Jekel 2006). The existence of these chemicals in the environment constitutes a threat to humans because of their toxicity and the potential pollution to the food chain. As a result, increasingly stringent restrictions are being imposed on the release of these compounds by various regulatory bodies.

Conventional water treatment processes include filtration and flocculation, biological treatment, thermal and catalytic oxidation, and chemical treatment using chlorine, potassium permanganate, ozone and hydrogen peroxide (Ollis and Serpone 1989; Legrini, Oliveros et al. 1993; Mills, Davies et al. 1993; Baruth, American Society of Civil et al. 2005). Many of the previously mentioned technologies simply transfer the pollutant from the water into another phase, requiring additional treatment and/or disposal of the compound; are not suitable against non-biodegradable products or requires strong chemical oxidants of hazardous and therefore, undesirable nature (Ollis and Serpone 1989; Mills, Davies et al. 1993). Adsorption and air stripping are the most common treatment methods for waters contaminated with organic compounds. However, as non-destructive technologies, they merely transfer contaminants from the water to the adsorbents or to the air. Moreover, some toxic organic compounds are not removed by adsorption or air stripping because they are only poorly adsorbed or have low volatilities (Ollis 1987; Matthews 1993; Zhang, Crittenden et al. 1994; Crittenden, Liu et al. 1997).

In recent years, the research attention has been focused on processes that lead to an improved oxidative degradation of organic pollutants. Thus, one of the major advantages of these processes compared with the existing technologies is that there is no further requirement for secondary disposal methods. These processes include the so-called advanced oxidation processes (AOPs) which usually operate at or near room temperature and pressure (Glaze, Kang et al. 1987). AOPs include several methods such ozonation, Fenton oxidation, photo-Fenton and photocatalysis which differ in the way to generate the hydroxyl radicals. AOPs are processes with formation of the powerful hydroxyl radical $^\bullet OH$, which has a relatively high redox potential (2.8V) (among all known oxidants, only fluorine has a higher oxidation

potential). Hydroxyl radicals act as non-selective oxidation agents responsible for the degradation of organic pollutants.

AOPs are particularly useful for pre-treatment of water containing non-biodegradable contaminants prior to a biological treatment step (Scott and Ollis 1995).

The efficiency of these technologies is basically due to the reactions of hydroxyl radicals. The hydroxyl radicals are capable to attack almost all the organic compounds and their time of reaction is 10^6-10^{12} times faster than that of alternative oxidizing agents like ozone (Vidal, Sanchez et al. 1994).

Table 1.1 shows a comparison of the rate constants between hydroxyl radical and ozone with different organic compounds (Jornitz and Meltzer 2007).

Table 1.1: Rate constants (k in L mol^{-1} s^{-1}) of hydroxyl radical and ozone.

Compound	$^{\bullet}$OH	O_3
Phenols	10^9 - 10^{10}	10^3
Aromatics	10^8 - 10^{10}	1 - 10^2
Ketones	10^9 - 10^{10}	1
Alcohols	10^8 - 10^9	10^{-2} - 1
Alkanes	10^6 - 10^9	10^{-2}

Among the AOPs photocatalysis appear as a promising technology through which a wide spectrum of organic contaminants may be degraded or completely mineralized. An advantage of photocatalysis compared with other AOPs, especially those employing oxidants such as hydrogen peroxide and ozone, is the non-consumption of expensive oxidizing chemicals because the atmospheric oxygen is used as oxidant. Photocatalysts are also self regenerated and can be reused or recycled. It is a heterogeneous catalysis process. Photocatalysts used in UV or near-UV light-activated processes are typically semiconductor materials such as TiO_2, ZnO or CdS. Among them, titanium dioxide is the semiconductor which provides the best compromise between photocatalytic performance and stability in aqueous media; its low toxicity and its availability at low cost are further advantages. As a consequence, it is by far the most commonly used photocatalyst material (Hidaka, Zhao et al. 1992; Watson, Beydoun et al. 2002; Fabbri, Prevot et al. 2006).

The photocatalytic reaction may be carried out either in a slurry-type reactor (where the catalyst particles are suspended in the contaminated water to be treated), or in an immobilized-catalyst type reactor (where the catalyst particles are onto the surface of various inert substrates). The slurry system approach requires an additional separation step to remove the catalyst from the treated water. In this separation step, various techniques can be used like filtration, decantation and/or centrifugation but all these techniques involve additional expenses in a continuous treatment process. This presents the major drawback for the application of such a system. Immobilized catalysts provide a solution to the solid/liquid separation problem, but also presents a disadvantage as a restricted processing capacity due to possible mass transfer limitations (Matthews and McEvoy 1992).

TiO_2 particles in aqueous suspension, would offer significant advantages if an easy way could be found for the separation step after the photocatalytic treatment.

This research work is related to the separation and recycle of TiO_2 in a slurry photocatalytic system. The obstacles presented in the slurry system may be overcome by means of the preparation of magnetically separable photocatalyst.

A photocatalyst with magnetic properties allows the use of the technique of magnetic separation which is one of the most effective and simple methods for removing suspended solids from wastewater without the need for further separation processes. The magnetic photocatalyst allows its use as a suspended material, providing the advantage to have a high surface area for reaction.

The overall aim of this PhD thesis was to develop a photocatalyst that possesses two main characteristics, magnetic and photoactive for obtaining the organic pollutants degradation, and an easy removal and recovery from slurry systems.

In order to have a better understanding of the photocatalytic process, a photocatalytic reaction system was designed. Different organic compounds were used for testing the parameters involved in the photocatalytic process. The specific aims of the research work were summarized in the following points:

- Synthesis of photocatalyst particles with magnetic characteristics, photoactive and stable using a coating technique in which the photoactive titanium dioxide is deposited onto the surface of magnetic particles.
- Investigation of the structure and physico-chemical properties of the photocatalytic particles.

- Selection of organic compounds to be used as a model in the photocatalytic degradation as well as their respective methods of identification and quantification.

- Investigation of the equilibrium of adsorption.

- Investigation of the photooxidation of the model compounds using the magnetically separable photocatalyst and Degussa P25 TiO_2 (used as a reference material).

All the points previously listed were widely discussed in the subsequent chapters on this research work.

2   GENERAL ASPECTS

2.1   Photocatalysis

Heterogeneous photocatalysis has been found as an emerging treatment option for the removal of contaminants in water. In 1972 it was discovered that the photocatalytic splitting of water is induced on TiO_2, this means that water molecules can be decomposed, using UV irradiation, into oxygen and hydrogen, without the application of an external voltage (Fujishima and Honda 1972). Since then, many other principles, mechanisms and applications of photocatalysis have been studied and published by a large quantity of authors/publications, (Hoffmann, Martin et al. 1995; Linsebigler, Lu et al. 1995; Serpone 1995; Blake, Maness et al. 1999; Herrmann 1999). A variety of organic compounds can be photocatalytically oxidized and eventually mineralized to CO_2, H_2O and other non toxic products (e.g. residual ions such as Cl^-, if chlorinated compounds are involved).

2.2   Photocatalyst

2.2.1   Semiconductor

A semiconductor, by solid state definition, is a material whose valence band (VB) and conduction band (CB) are separated by an energy gap or band gap (E_{bg}). A conductor is distinguished by having a partially filled conduction band, the valence band overlaps the conduction band and there is no energy band gap. If the energy separation between the valence band and the conduction band is large (greater than 5 eV), the material is an electrical insulator.

Activation of a semiconductor photocatalyst is achieved by means of the adsorption of a photon energy (E_{ph}) which results in the promotion of an electron, e^-, from the valence band into the conduction band with the generation of a hole, h^+, in the valence band of the catalyst, according to Eq. 2.1 and the reaction illustrated in Figure 2.1 (Mills, Davies et al. 1993).

$$photocatalyst \xrightarrow{\ E_{ph} \geq E_{bg}\ } e^- + h^+ \qquad\qquad \text{Eq. 2.1}$$

In metals, where there is a continuum of energy states, the light-generated electrons deactivate easily and the lifetime of the electron-hole pair is so short that they cannot be harvested. The existence of a band gap in semiconductors prevents rapid deactivation of the excited electron-

hole pairs, which can be deactivated only by recombination. This assures that an electron-hole pair lifetime is sufficiently long to participate in interfacial electron transfer (Ollis and Serpone 1989). In an oxygenated aqueous suspension, redox reactions are produced which can oxidize organic compounds (Crittenden, Liu et al. 1997).
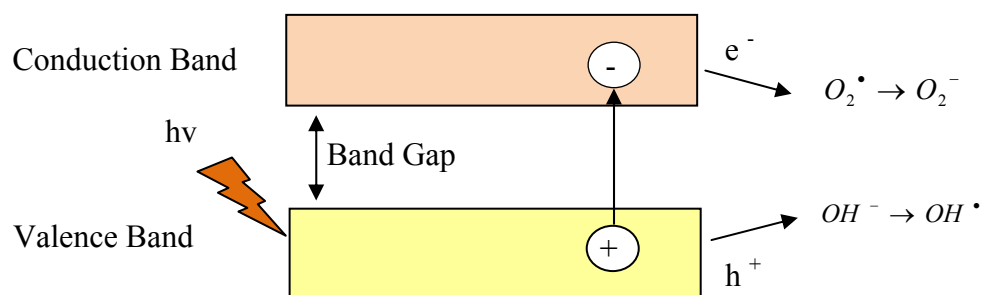
Figure 2.1: Conduction and valence bands and electron-hole pair generation in semiconductor (Agustina, Ang et al. 2005).

Various chemical steps occur in the photocatalytic reactions, following the initiation step of pair electron-hole formation. This lead to the utilization of both the electron hole h^+ for the oxidation processes and eventually to the capture of the e^- electron for the reduction processes, as well the potential formation of super oxide anions and hydrogen peroxide from oxygen (de Lasa, Serrano et al. 2005).

A criterion for the organic compound degradation is that the redox potential of the pair $H_2O/^\bullet OH$ ($OH^- \rightarrow {}^\bullet OH + e^-$; $E° = -2.8V$) couple lies within the band gap of the semiconductor (Hoffmann, Martin et al. 1995). Various semiconductor particles have band gap energies that are high enough to be used in photocatalytic studies. In <u>Table 2.1</u> (Rajeshwar and Ibanez 1997) the band gap energies of common semiconductors used in photocatalysis are listed.

Cadmium sulfide (CdS) and cadmium selenide (CdSe) act as photocatalysts; unfortunately these materials exhibit photoanodic corrosion in aqueous media and they are also toxic (Hoffmann, Martin et al. 1995; Warad, Ghosh et al. 2005).

Iron oxides are no suitable semiconductors, even though they are inexpensive and have high band gap energies, because they readily undergo photocathodic corrosion (Hoffmann, Martin et al. 1995). ZnO appears suitable for photocatalysis due to its band gap energy is (3.2 eV), however, ZnO is generally unstable in solution even without irradiation, especially at low pH (Angelidis, Koutlemani et al. 1998). Utilization of WO_3 as a photocatalyst has also been

6

investigated; nevertheless it shows a lower photocatalytic activity than TiO_2 (Angelidis, Koutlemani et al. 1998; Fujishima and Zhang 2006).

Table 2.1: Band Gap Energies of Various Semiconductors.

Semiconductor	Band gap energy (eV)
TiO_2 (rutile)	3.0
TiO_2 (anatase)	3.2
ZnO	3.2
ZnS	3.6
CdS	2.4
Fe_2O_3	2.3
WO_3	2.8

Among the semiconductors of Table 2.1 TiO_2 is the most commonly applied catalyst due to several favorable factors: it is highly photoactive, very photostable, biologically and chemically inert, non-toxic and also inexpensive (Mills, Davies et al. 1993; Hoffmann, Martin et al. 1995; Crittenden, Liu et al. 1997; Fabbri, Prevot et al. 2006).

2.2.2 TiO_2

Titanium dioxide (TiO_2) is used as a white pigment in paints, paper, rubber, plastic and cosmetics. Irradiated TiO_2 shows a strong photocatalytic power for the destruction of pollutants (Hidaka, Zhao et al. 1992; Hoffmann, Martin et al. 1995; Zhao, Wu et al. 1998), for production of hydrogen (Duonghong, Borgarello et al. 1981; Liu, Wu et al. 1999) and for removal of metal ions (Ollis, Pelizzetti et al. 1991; Karakitsou and Verykios 1993). Titanium dioxide or titania has been widely studied for widespread environmental treatment and other applications. Furthermore, a TiO_2 photocatalyst presents high activity for the oxidation of volatile organic compounds under UV irradiation and offers an economically and technically practical means to clean air and water (Kwon, Fan et al. 2008).

Titanium dioxide has three main crystal structures: anatase, which tends to be more stable at low temperature; brookite, which is usually found in minerals and has an orthorhombic crystal structure, and rutile, which is the stable form at higher temperature (Rao, Yoganarasimhan et

al. 1961). Both rutile and anatase TiO_2 are tetragonal structures (Figure 2.2) with unit cells consisting of 6 and 12 atoms, respectively (Stashans, Lunell et al. 1996; Diebold 2003). Generally, anatase TiO_2 shows higher photocatalytic activity than other types of titanium dioxide due to its band gap, number of hydroxyl groups, surface area and porosity (Tayade, Surolia et al. 2007).
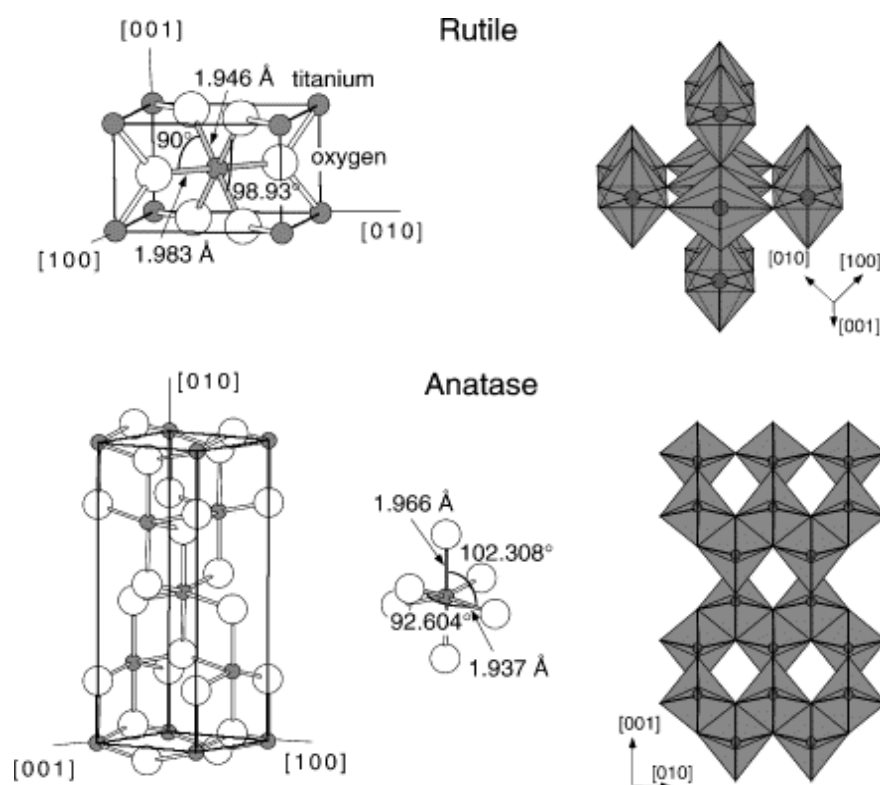
Figure 2.2: Crystal structures of titanium oxide: rutile and anatase (Diebold 2003).

Among the different commercially available titanium dioxides, the commercial Degussa product P25 is one of the most frequently applied ones in photocatalysis because it shows high activity for many kinds of photocatalytic reactions, probably due to its exceptional structure. It has often been proposed for the degradation of pollutants in water or air. The product is manufactured by flame hydrolysis (Aerosil process). The specifications of the product P25 TiO_2 are listed in Table 2.2 (Zhang, Yang et al. 2007; Ciston, Lueptow et al. 2008).

8

Table 2.2: Technical data of the commercial Degussa P25 TiO$_2$.

Specification	
Crystalline type	Anatase (80%) + Rutile (20%)
Crystallite size	25 nm
BET specific surface area	50 m^2 g^{-1}

In the frame of this investigation Degussa P25 TiO$_2$ was used as a reference material.

2.2.3 Methods for the preparation of TiO$_2$

Titanium dioxide is obtained either from minerals or from a solution of titanium salts or alkoxides. There are many synthetic methods for the preparation of TiO$_2$, a wide variety of approaches including flame synthesis, ultrasonic irradiation, chemical vapor deposition, as well as sol–gel reactions have been reported (Morrison, Raghavan et al. 1997; Murakami, Matsumoto et al. 1999; Zaban, Aruna et al. 2000; Zhu, Yang et al. 2007). The application of sol-gel technique is gaining interest basically due to several advantages including; good homogeneity, ease of chemical composition control, low processing temperature, large area coatings, low equipment cost, and good photocatalytic properties (Kajitvichyanukul, Ananpattarachai et al. 2005). Sol-gel processing is a wet chemical synthesis approach that generates inorganic oxides via gelation, precipitation or hydrothermal treatment (Ying and Sun 1997). It involves the use of a molecular precursor, either an inorganic salt or a metal alkoxide, as a starting material (Castillo, Morán-Pineda et al. 1998).

2.2.4 Sol-gel technique using TiCl$_4$

The preparation of nanocrystalline TiO$_2$, anatase or mixed phase, is obtained using titanium tetrachloride (TiCl$_4$) and water (H$_2$O) as starting materials in a hydrolysis process (Zhang, Gao et al. 1999). Hydrolysis occurs by contacting TiCl$_4$ with H$_2$O. As a result, titania precipitates after hydrolysis and condensation reactions of TiCl$_4$. Heating TiCl$_4$ aqueous solution that contains TiCl$_4$ and water would accelerate the reaction (Hong Kyu Park 1997).

2.2.5   Particle coating using sol-gel technique

Modifying the properties of one material by coating it with another type of material has been a popular approach widely documented in the literature (Ocaña, Matijevic et al. 1991; Inel and Ertek 1993; Beydoun, Amal et al. 2000; Watson, Beydoun et al. 2002). The concept of coating one material with another is used to develop a magnetic photocatalyst. Some researchers reported a kind of magnetically separable photocatalyst which could be separated easily from the solution by a magnetic field and had a photocatalytic activity (Chen and Zhao 1999; Beydoun, Amal et al. 2000; Watson, Beydoun et al. 2002; Gao, Chen et al. 2003). The magnetic cores are ideal as support of TiO_2 because they allow an easy particle separation in the range of micrometer and submicrometer by an applied magnetic field (Beydoun, Amal et al. 2000). Smaller particles sizes offer larger surface area for a better mass transfer.

Sol-gel process allows the production of nanocrystalline materials with a low capital cost of equipment compared to gas phase synthesis (Ying and Sun 1997). The reaction between the starting material and water is a two step process and involves both hydrolysis and condensation (polymerization) reactions. The addition of water generates the hydrolysis process where the M-OH bond is produced, then the condensation reaction occurs once the OH^- groups are created (Gopal, Moberly Chan et al. 1997). Thermal treatment is generally used to obtain crystal structures from amorphous structures.

The presence of seed particles in a dispersion solution when other particles begin to precipitate affects the system and, the precipitation and formation of the particles is given in a new phase. Some possible processes may be suggested in this new phase.

The first one is the heterogeneous nucleation; this is the mechanism by which the formation of a new phase is catalyzed by the presence of seed particles (solid phase). Here, the reactants are adsorbed on the surface of the seed particles, and the new phase can precipitate directly onto them. The adsorption of the metal ions onto the surface of the seed particles provides sites for the surface nucleation, which act as precursors to nucleation (Gherardi and Matijevic 1986).

In the second possibility, the particles precipitate separately in solutions (homogeneous nucleation), which interact with and adhere to the surface of the seed particles, this process is known as a heterocoagulation mechanism (Garg and de Jonghe 1990).

Finally, another possibility is given when the interaction between the reactants and the seed particles does not exist or is too weak. In this case, the result is a mixed system in which the

seed particles and the new particles can coexist as a separate phases (Gherardi and Matijevic 1986).

2.3 Oxidation of Organic Pollutants

Photocatalytic oxidation has been studied for a wide range of organic compounds. The general classes of these compounds are summarized in Table 2.3. Many of these compounds are not completely mineralized (Hoffmann, Martin et al. 1995).

Table 2.3: Classes of organics able to be photomineralized.

Substrates		
Alkanes	Aromatics	Polymers
Haloalkanes	Haloaromatics	Surfactants
Aliphatic alcohols	Nitrohaloaromatics	Herbicides
Aliphatic carboxylic acids	Phenols	Pesticides
Alkenes	Halophenols	Dyes
Haloalkenes	Aromatic carboxylic acids	Hormones

2.3.1 Aromatic compounds

Aromatic compounds are common pollutants in the waste effluent from many industrial sectors, such as petroleum refineries, synthetic chemical plants, pulp and paper, textiles, detergent, pesticide and herbicide, and pharmaceutical factories. Among them phenol, benzoic acid and their derivates has been widely studied in photocatalytic processes (Chen and Ray 1999; Assabane, Ait Ichou et al. 2000).

The photocatalytic degradation of phenol using TiO_2 has achieved fairly good results, but the process shows a different behaviour depending on the initial phenol concentration. Two different degradation mechanisms have been mentioned related to the existence of a different surface activation.

At small concentrations of phenol (0.1 g L^{-1}), the insertion of $^{\bullet}OH$ in the phenol molecule is favored (Araña, Tello Rendón et al. 2001). The presence of small adsorbate concentrations does not affect the yield of this radical. Phenol degradation at large concentrations (1.0 g L^{-1})

seems to occur onto the surface of the catalyst by means of peroxo-compounds generation (Araña, Tello Rendón et al. 2001), which is not affected by the $^{\bullet}$OH insertion process. The formation of these compounds on the catalyst is favored by the large amount of chemisorbed phenol molecules, hence a smaller number of photons that reach the surface and a smaller amount of $^{\bullet}$OH are formed.

It may be concluded that in solutions of large concentrations of phenol, the chemisorption on the catalyst can cause the breakdown of the molecule, in contrast at small concentrations of phenol the mechanism suggested to the ring break is through successive $^{\bullet}$OH insertion. From these results it is possible to conclude that the photocatalytic process may be also applicable to concentrated pollutants, in combination with a catalyst reactivation method if necessary.

The photodegradation rate of the polycarboxylic (hemimellitic (Hem), trimellitic (Tri) and pyromellitic (Pyro)) benzoic acids follows the order Pyro > Hem > Tri, a complete mineralization is reached with different reaction times depending on their nature (Assabane, Ait Ichou et al. 2000).

2.3.2 Dyes

Dyeing and finishing of textile industries are extremely important processes in which large amounts of water and energy are required, along with various chemicals as dyes, detergents, chelating agents and formic acid. This all becomes an environmental concern, because of high energy consumption and wastewater containing hazardous chemicals. The removal of textile dyes and other commercial dyestuffs is of great concern, and have become a focus of attention in the last few years (Ganesh, Boardman et al. 1994). Annually worldwide produced 700.000 tons of dyes and about 50% of them are azo dyes. It is estimated that approximately 15% of the world production of dyes are released into the textile effluents during the dyeing process (Bauer, Jacques et al. 2001). Traditional physical methods, such as coagulation and adsorption, for the treatment of dyes pollutants can be used efficiently. Nevertheless, they are non-destructive, since they just transfer organic compounds from water to another phase (Tang and Huren 1995; Kuo and Ho 2001). Due to the large number of aromatic rings present in the dye molecules and the stability of modern dyes, conventional biological treatment methods are ineffective for decolorization and degradation (Patil and Shinde 1988; Arslan and Balcioglu 1999). Furthermore, the majority of dyes is only adsorbed on the sludge and is not degraded (Pagga and Taeger 1994).

One of the most recent methods of wastewater treatment containing dyes is their photocatalytic degradation in solutions illuminated with UV-irradiation, which contain a suitable photocatalyst, mainly TiO_2.

In the photocatalytic degradation of azo dyes, the first step consists in the cleavage of azo double bond, inducing in the visible region (Vinodgopal, Wynkoop et al. 1996). Triphenylmethane dyes are found to be bleached easier than anthraquinone dyes (Epling and Lin 2002). It is also observed that food dyes are in general easier to be bleached than other dyes (Epling and Lin 2002). The rates of photobleaching differ significantly depending on the different functional groups of various dyes.

Additional factors such adsorption characteristics on the TiO_2 surface (Hu, Tang et al. 2003), aqueous solubility of the dyes, light source (Epling and Lin 2002), and presence of inorganic salts (Sökmen and Özkan 2002) may play an important role in the control of photobleaching and mineralization rates (Epling and Lin 2002).

2.4 Photocatalytic Reactor Design

The development of a viable and practical reactor system for water treatment with heterogeneous photocatalysis on industrial scales has not yet been successfully achieved. The photocatalytic reactor design is much more complicated than that of a conventional catalytic reactor because it involves additional engineering factors, thus, the light illumination of catalyst becomes relevant, besides mixing, mass transfer, reaction kinetics, amount of catalyst, etc. The high degree of interactions among the transport processes, reaction kinetics, and light absorption leads to a strong coupling of physicochemical phenomena and a major obstacle in the development of photocatalytic reactors (Ray 1999).

Several problems have to be solved for the effective design of photocatalytic reactor (Ray and Beenackers 1996). (i) the efficient exposure of the catalyst to light irradiation must be achieved since the catalyst shows no activity without photons of appropriate energy; (ii) the photocatalytic reaction rate is usually slow compared to conventional chemical reaction rates, due to small concentration levels of the pollutants; (iii) large amounts of active and stable catalyst must be provided inside the reactor to provide large processing capacity (Preety S. Mukherjee 1999). Among these restrictions, the most important factor is the illumination since the amount of catalyst that can be activated determines the water treatment capacity of the reactor. Efficient reactor design must expose the highest amount of the activated stable

catalyst to the illuminated surface and must have a high density of active catalyst in contact with the liquid to be treated inside the reactor.

2.4.1 Reactors for water treatment

There are several methods to classify the photocatalytic reactors between them the reactors for water treatment can be classified according to their design characteristics.

Based on the light type, reactors can be divided into two categories: reactors using solar irradiation, and those using artificial UV lamps. The design of TiO_2-based photocatalytic reactors has mainly focused on using either slurry or immobilized configurations. In slurry reactors, the catalyst particles are freely dispersed in the fluid phase (water) and consequently, the photocatalyst is fully integrated in the liquid mobile phase. The immobilized catalyst reactor design features a catalyst anchored to a fixed support, dispersed on the stationary phase. Based on the position of the irradiation source, basically photocatalytic reactor systems can be categorized as: (a) immersion type with lamps placed within the reactor, (b) external type with lamps outside the reactor or (c) distributive type where the irradiation is transported from the source to the reactor by optical means as reflectors or optical fibers.

2.4.2 TiO₂ slurry reactors

The majority of the photocatalytic reactors are of well-mixed slurry variety (Augugliaro, Davì et al. 1990). Slurry systems have shown the largest photocatalytic activity when compared to photocatalytic reactors with immobilized photocatalyst (Matthews and McEvoy 1992; Parent, Blake et al. 1996; Pozzo, Baltanás et al. 1999). Slurry reactor configuration has two main advantages which are: (a) a large illuminated surface area per unit volume of catalyst is available and (b) minimum mass transfer limitations.

In addition, slurry systems require separation of the fine catalyst particles from the water suspension. Separation steps complicate the treatment process and decrease the economical viability of the slurry reactor approach. Several techniques have been proposed including centrifugation, high-cost ultra-centrifugation, inexpensive overnight particle settling, and flocculation.

2.4.3 Immobilized system

The photocatalyst are immobilized onto a fixed support such as the fiber mesh, reactor wall, ceramic or glass bead. Therefore, the problem of separation process presented with slurry systems can be avoided by using the immobilized system. Unfortunately, the photocatalytic efficiency of immobilized systems is often lower than those of slurry systems because supported catalysts have a low surface area per reactant volume and may suffer transfer mass limitations.

The advantages and disadvantages of slurry and immobilized photocatalytic reactors are summarized in the Table 2.4 (Ollis, Pelizzetti et al. 1991; Parent, Blake et al. 1996; Alfano, Bahnemann et al. 2000).

Table 2.4: Suspended versus immobilized photocatalytic systems.

Slurry reactors	Immobilized reactors
Advantages	
- Fairly uniform catalyst distribution	- Continuous operation
- Large illuminated surface area per unit volume of catalyst	- Improved removal of organic material from water phase while using support with adsorption properties
- Minimum mass transfer limitations	
- Minimum catalyst fouling effects due to the possible continuous removal and catalyst replacement	- No need for an additional catalyst separation operation
- Well mixed particle suspension	
- Low pressure drop across the reactor	
Disadvantages	
- Requires-post process separation	- Poor light utilization efficiencies due to light scattering by immobilized photocatalyst
- Absorption and scattering of light by the suspended particles	
	- Restricted processing capacities due to possible mass transfer limitations
	- Possible catalyst deactivation

3 THEORETICAL BACKGROUND

3.1 General Mechanisms of Photocatalysis

The general mechanism for heterogeneous photocatalysis on TiO_2 is complicated and still under discussion. The most widely accepted mechanism can be represented with the steps shown by Eq. 3.1 to Eq. 3.9 (Hoffmann, Martin et al. 1995).

$$TiO_2 + h\nu \rightarrow h_{vb}^+ + e_{cb}^- \qquad \text{Eq. 3.1}$$

$$h_{vb}^+ + > Ti^{IV}OH \rightarrow \{> Ti^{IV}OH^\bullet\}^+ \qquad \text{Eq. 3.2}$$

$$h_{vb}^+ + H_2O_{(ads)} \rightarrow OH^\bullet_{(ads)} + H^+ \qquad \text{Eq. 3.3}$$

$$e_{cb}^- + > Ti^{IV}OH \leftrightarrow \{> Ti^{III}OH\} \qquad \text{Eq. 3.4}$$

$$e_{cb}^- + O_{2(ads)} \rightarrow O_2^{\bullet-}{}_{(ads)} \qquad \text{Eq. 3.5}$$

$$e_{cb}^- + \{> Ti^{IV}OH^\bullet\}^+ \rightarrow > Ti^{IV}OH \qquad \text{Eq. 3.6}$$

$$h_{vb}^+ + \{> Ti^{III}OH\} \rightarrow > Ti^{IV}OH \qquad \text{Eq. 3.7}$$

$$e_{cb}^- + A \rightarrow A^{\bullet-} \qquad \text{Eq. 3.8}$$

$$h_{vb}^+ + D \rightarrow D^{\bullet+} \qquad \text{Eq. 3.9}$$
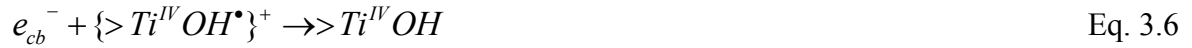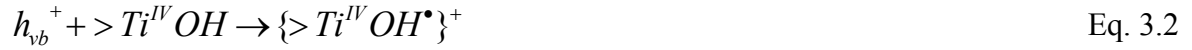
where >TIOH represent the primary hydrated surface functionality of TiO_2, $\{> Ti^{IV}OH^\bullet\}^+$ represent the surface-trapped valence band hole (surface-bond hydroxyl radical), e_{cb}^- is a conduction band electron, h_{vb}^+ is a valence band hole, A represents electron acceptors, D electron donors, and $\{> Ti^{III}OH\}$ is the surface-trapped conduction band electron.

Since the surface of TiO_2 is mainly hydrated, these holes can oxidize surface-bound OH^- ($Ti^{IV}OH$) or water to generate hydroxyl radicals, $^\bullet OH$, in particles (Eq. 3.2 and Eq. 3.3 respectively). The process is thought to occur by initial dynamic trapping of the conduction band electron (e_{cb}^-) in shallow traps at surface $>Ti^{IV}OH$ groups to form $>Ti^{III}OH$ groups (Eq. 3.4) and react with a surface adsorbed oxygen to form an effective oxygenation agent, superoxide species (O_2^-) (Eq. 3.5). These trapped charge carriers may then recombine at the

surface (Eq. 3.6 - Eq. 3.7), or may participate in reduction or oxidation of adsorbed organic molecules (Eq. 3.8 - Eq. 3.9), and/or may diffuse from the TiO_2 surface and contribute to the degradation in the bulk solution. The overall quantum efficiency for interfacial charge transfer is determined by two critical processes (Hoffmann, Martin et al. 1995). One is the competition between charge carrier recombination (the reverse of Eq. 3.1) and trapping of charge carriers (Eq. 3.2 - Eq. 3.5, and perhaps Eq. 3.8 - Eq. 3.9) and the other one is the competition between trapped carrier recombination (Eq. 3.6 - Eq. 3.7) and interfacial charge transfer with organic substrate. Any action that can either increase the lifetime of the charge carriers or interfacial charge transfer would be beneficial to the overall photocatalytic process (Katoh, Furube et al. 2004). The mechanism emphasizes the importance of the site defects in the TiO_2 particles and the importance of the adsorption of organic substrates on the surface.

Two principal pathways have been proposed for photocatalytic reactions. One pathway proceeds through an indirect oxidation via a surface-bound hydroxyl radical (Turchi and Ollis 1990; Mills and Hoffmann 1993). The second pathway involves direct hole oxidation of the organic substrate via the valence band hole (Draper and Fox 1990). Values of oxidation potential of hydroxyl radicals and other species are shown in Table 3.1.

Table 3.1: Oxidation potential and relative oxidation power of some species (Munter 2001).

Oxidizing Species	Oxidation Potential (Volts)	Relative Oxidation Power (Chlorine as reference)
Chlorine	1.38	1.00
Hypochlorous acid	1.5	1.10
Permanganate	1.69	1.24
Hydrogen peroxide	1.77	1.31
Ozone	2.07	1.52
Atomic oxygen	2.4	1.78
Hydroxyl radical	2.8	2.05
Positively charged hole on titanium dioxide, TiO_2^+	3.2	2.35

Supporting the proposed reaction pathway for the surface-bound hydroxyl radical, there is the observation of hydroxylated structures detected as intermediates in the course of the photocatalytic degradation of halogenated aromatics. These hydroxylated intermediates are also found when similar aromatics are reacted with a known source of hydroxyl radicals. Generally, molecular oxygen enhances the rates and efficiencies of photocatalytic oxidation, which act as an acceptor species in the electron-transfer reaction (Eq. 3.5), suppressing electron-hole recombination. Super-oxide anions, (Eq. 3.5), can subsequently be involved in the following reactions (Eq. 3.10 - Eq. 3.11), where hydrogen peroxides arises from direct dioxygen reduction by conduction band electrons (e^-_{cb}) (Hoffmann, Martin et al. 1995). It is interesting to mention the role of O_2 in the photoactivity of polymorphous TiO_2. It has been commented earlier that the structure of rutile has been found to be less photoactive than anatase (although both forms of TiO_2 are thermodynamically able to reduce O_2), due to its low capacity to adsorb O_2, which leads to a faster electron-hole recombination (Fox and Dulay 1993). H_2O_2 may also contribute to the degradation of organic and inorganic electron acceptors or as a direct source of $^{\bullet}OH$ radicals (Eq. 3.12 - Eq. 3.13). Finally, hydroxyl radicals ($^{\bullet}OH$), as described by Eq. 3.14, oxidize organic adsorbed pollutants (RX_{ad}) on the surface of titanium dioxide particles.

$$O_2^{\bullet-}{}_{(ads)} + H+ \rightarrow HO_2^{\bullet} \qquad \text{Eq. 3.10}$$

$$H^+ + O_2^{\bullet-} + HO_2^{\bullet} \rightarrow H_2O_2 + O_2 \qquad \text{Eq. 3.11}$$

$$H_2O_2 + e_{cb}^- \rightarrow OH^{\bullet} + OH^- \qquad \text{Eq. 3.12}$$

$$H_2O_2 + O_2^{\bullet-} \rightarrow OH^{\bullet} + OH^- + O_2 \qquad \text{Eq. 3.13}$$

$$OH^{\bullet}{}_{(ads)} + RX_{(ads)} \rightarrow Intermediate \qquad \text{Eq. 3.14}$$
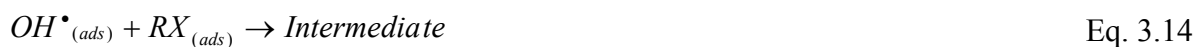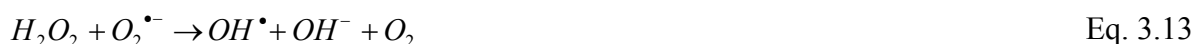
3.2 Adsorption of Aqueous Organic Substrates on TiO_2

In order to successfully represent the dynamic adsorptive behaviour of any substance from the fluid to the solid phase, it is important to have a satisfactory description of the equilibrium state between the two phases of the adsorption system.

3.2.1 Sorption Equilibrium

Adsorption of molecules can be represented as a chemical reaction (Eq. 3.15):

$$A + B \Leftrightarrow A \cdot B \qquad\qquad\qquad \text{Eq. 3.15}$$

where *A* is the adsorbate, *B* is the adsorbent, and *A·B* is the adsorbed compound. Sorbates are held on the surface by various types of chemical forces such as hydrogen bonds, dipole-dipole interactions, and van der Waals forces. If the reaction is reversible, molecules continue to accumulate on the surface until the rate of the forward reaction (adsorption) equals the rate of the reverse reaction (desorption). If this condition exists, equilibrium has been reached and no further accumulation will occur.

One of the most important characteristics of an adsorbent is the quantity of adsorbate that it can accumulate. The state of equilibrium is described by means of adsorption isotherms. The relationship can be based on two general approaches, theoretical and empirical models. Theoretical models seek to describe a system based on the thermodynamic principles. Empirical models provide a mathematical description of observed experimental data by measuring the concentrations and loadings.

3.2.2 Experimental determination of sorption isotherms

The state of equilibrium of the sorption of a single component can be derived from experimental data by means of mass balances. In batch methods the equilibrium is determined by contacting a solution of a given composition with a sorbent material of known solid-phase composition.

In the case of a binary system the mass balance of the system is described by Eq. 3.16, where V_L is a volume of liquid phase with an initial concentration of sorptive C_0 and with a sorbent mass m is placed in contact.

$$m \cdot q_0 + V_L \cdot C_0 = m \cdot q + V_L \cdot C \qquad\qquad \text{Eq. 3.16}$$

If the initial loading is zero (q_0=0), one obtains from Eq. 3.16

$$q = \frac{V_L}{m} \left(C_0 - C \right) \qquad\qquad\qquad \text{Eq. 3.17}$$

This equation describes the so-called operation line from the initial state of the system (c_0, q_o=0) to the state of equilibrium.

By varying either the initial concentration or the mass of sorbent added to the constant volume of solution, several points of the isotherm may be obtained.

Numerous studies have shown that the adsorption of organic compounds on the surface of semiconductors can be described by means of a Langmuir relationship (Fox and Dulay 1993; Hoffmann, Martin et al. 1995; Mills and Le Hunte 1997).

3.2.3 Langmuir isotherm

Langmuir developed the adsorption theory to describe adsorption of gases on solid surfaces (Langmuir 1918). The derivation of the Langmuir adsorption isotherm involves some implicit assumptions: a) the adsorption is at a fixed number of localized sites; b) there is only a monolayer of adsorbed molecules; c) the surface is homogeneous, that mean, all the adsorption sites are equivalent; d) there is no lateral interaction between adsorbate molecules; e) the equilibrium is characterized by the fact that the rates of adsorption and desorption are equal. The Langmuir isotherm describes the relationship between the amount adsorbed at equilibrium (q_e) and its equilibrium concentration (C_e) by the equation Eq. 3.18

$$q_e = q_{max} \frac{K_L C_e}{1 + K_L C_e} \qquad \text{Eq. 3.18}$$

where q_{max} and K_L are the Langmuir constants which are related to the adsorption capacity and adsorption energy, respectively. There are two limiting cases for the Langmuir relationship:

At small sorbate concentrations, the denominator of Eq. 3.18 tends to 1 and the equation simplifies to:

$$q_e = q_{max} K_L C_e \qquad \text{Eq. 3.19}$$

This relationship corresponds to the Henry´s law, which gives a linear adsorption isotherm expressed by the product of K_L and q_{max}.

At large concentrations, the equation simplifies to:

$$q_e = q_{max} \qquad \text{Eq. 3.20}$$

This means that the adsorbent loading is independent of the concentration. This is partly due to the filling up of a significant number of the total possible adsorption sites. This results in a smaller chance of an ion from the solution to find a vacant site, and therefore being adsorbed.

The Langmuir adsorption isotherm has the simplest form, an equally simple physical picture, and shows reasonable agreement with a large number of experimental isotherms. Therefore,

the Langmuir adsorption model is probably the most useful one among all isotherms describing adsorption, and often serves as a basis for more detailed developments (Snoeyink and Summers 1999).

The Langmuir constants (q_{max} and K_L) can be deduced from experimental values by means of linearization methods. There are three different possibilities to linearize the Langmuir relationship, Eq. 3.18 and to deduce the numerical values of the parameters. These are shown in Table 3.2.

3.2.4 Freundlich isotherm

The Freundlich isotherm is one of the earliest empirical equations used to describe equilibria data (Freundlich 1906). The Freundlich adsorption isotherm has often been found to fit liquid-phase adsorption data quite well, provided that the adsorption sites are not identical, and the total adsorbed amount is the same over all types of sites. The Freundlich isotherm is expressed as:

$$q_e = K_F \left(C_e \right)^{\frac{1}{n_F}}$$
Eq. 3.21

where K_F and n_F are the Freundlich constants related to the capacity and intensity of adsorption, respectively (Snoeyink and Summers 1999).

The Freundlich equation gives an expression encompassing the surface heterogeneity and the exponential distribution of active sites and their energies. According to the Freundlich equation, the amount adsorbed increases infinitely with increasing concentration or pressure. This equation does not change to a linear isotherm in the small residual concentration range and no maximum loading at high concentrations exists. The linear form of Freundlich isotherm is also shown in Table 3.2.

Table 3.2: Isotherm models and their linear forms.

Isotherm		Linear form	Plot
Langmuir-1	$q_e = q_{max} \dfrac{K_L C_e}{1 + K_L C_e}$	$\dfrac{1}{q_e} = \dfrac{1}{K_L q_{max}} \dfrac{1}{C_e} + \dfrac{1}{q_{max}}$	$\dfrac{1}{q_e} vs. \dfrac{1}{C_e}$
Langmuir-2		$\dfrac{C_e}{q_e} = \dfrac{1}{q_{max}} C_e + \dfrac{1}{q_{max} K_L}$	$\dfrac{C_e}{q_e} vs. C_e$
Langmuir-3		$\dfrac{q_e}{C_e} = -K_L q_e + K_L q_{max}$	$\dfrac{q_e}{C_e} vs. q_e$
Freundlich	$q_e = K_F (C_e)^{\frac{1}{n_F}}$	$\ln q_e = \ln K_F + \dfrac{1}{n_F} \ln C_e$	$\ln q_e vs. \ln C_e$

3.3 Reaction Kinetics

A variety of models have been derived to describe the rates of photodegradation of chemical compounds on semiconductor surfaces. The most commonly used is the Langmuir-Hinshelwood (L-H) kinetic expression (Ollis and Serpone 1989; Fox and Dulay 1993; Hoffmann, Martin et al. 1995; Mills and Le Hunte 1997).

According to the L-H model for heterogeneous catalytic reaction, the rate of a unimolecular surface reaction is proportional to the surface coverage, which may be related to the equilibrium concentration of the reagent in a homogeneous phase by the Langmuir adsorption isotherm. Thus, the kinetic model of L-H assumes that the Langmuir adsorption isotherm adequately describes the relationship between the surface coverage of the species A on the surface of the catalyst, and activity (or concentration) of the same species present in the fluid phase. This fact indicates that the species A are in equilibrium between the surface of the catalyst and the fluid phase (Cunningham and Al-Sayyed 1990). The mathematical relationship is shown in Eq. 3.22:

$$\theta = \frac{K''_{ads} a}{1 + K''_{ads} a} = \frac{K'_{ads} C\gamma}{1 + K'_{ads} C\gamma} = \frac{K_{ads} C}{1 + K_{ads} C} \qquad \text{Eq. 3.22}$$

where θ is the surface coverage, a is the equilibrium activity of the substrate in aqueous solution, C is the concentration of the substrate in solution , γ is the activity coefficient of the substrate and K_{ads} is the apparent adsorption equilibrium constant.

In accordance with the above considerations, the reaction rate can be expressed as:

$$r = -\frac{dC}{dt} = k_{eff}\theta = \frac{k_{eff}K_{ads}C}{1+K_{ads}C}$$ Eq. 3.23

where k_{eff} is the apparent effective reaction rate constant occurring at the active site on the photocatalyst surface.

Another implicit assumption of the L-H model is that the rate of surface adsorption of the substrate is greater than any subsequent chemical reaction and, therefore, the rate-limiting step is the reaction of adsorbed species on the surface of the semiconductor. Finally, it is also assumed that the reaction product does not block the photocatalytic site (Fox and Dulay 1993).

The formal interpretation of K_{ads} is different for each reaction scheme. Turchi and Ollis (Turchi and Ollis 1990) proposed four possible mechanisms, all based on $^\bullet$OH attack of the organic reactant in photocatalytic reactions on TiO_2. For all these mechanisms, the reaction rate equation has the same form as the equation proposed in Eq. 3.23. However, the interpretation of the constant K_{ads} is different in each case, and none is completely equivalent to the adsorption isotherm in the dark. It is worth mentioning that the values of K_L measured from dark adsorption isotherms tend to be lower than those obtained from kinetic studies of photocatalytic degradation (Mills and Morris 1993).

The apparent effective reaction rate constant (k_{eff}) is a proportionality constant that gives a measure of the intrinsic reactivity of the photoactivated surface with the substrate (Mills and Morris 1993). k_{eff} is proportional to I_a^p, where I_a is the rate of light adsorption, and p is an exponent equal to 0.5 or 1, at strong or weak light intensities respectively (Turchi and Ollis 1990; Mills and Morris 1993). In this way, it is only possible to compare the rate constants of different compounds when the catalyst and the light sources used are the same (Ollis and Serpone 1989).

Although k_{eff} and K_{ads} are assumed to be two independent parameters, they seem to be dependent on each other (Hoffmann, Martin et al. 1995). This behaviour is a result of the change by the adsorption equilibrium constant under the irradiation. In fact, irradiation can

induce the photoadsorption or photodesorption of substrates on the surface of a catalyst. In these cases, K_{ads} appears to be a function of the light intensity in the same way as k_{eff}.

The reaction rate equation Eq. 3.23 can then be rewritten as follows:

$$\frac{1}{r} = \frac{1}{k_{eff}} + \frac{1}{k_{eff}K_{ads}}\frac{1}{C} \qquad \text{Eq. 3.24}$$

Thus, the linearity of a plot of 1/r versus 1/C tests the validity of the L-H model, where $1/k_{eff}$ is the intercept and $1/k_{eff}K_{ads}$ is the slope. Many photocatalytic reactions show a good linearity in such graphs. Unfortunately, this setting cannot be taken as solid evidence of the substrate preadsorption because the same rate law can also describe the kinetic reactions that occur in homogeneous phases (Turchi and Ollis 1990).

In order to treat reactions involving the competition between two or more species for a single adsorption site, the following expression is suggested:

$$r = -\frac{dC}{dt} = k_{eff}\theta = \frac{k_{eff}K_{ads}C}{1 + K_{ads}C + \sum_i K_{ads,i}C_i} \qquad \text{Eq. 3.25}$$

where i is a competitively adsorbed species, that can be, e.g., a solvent molecule, an intermediate product of the reaction, some non-reactive component present in the dissolution or another reagent (Ollis and Serpone 1989; Fox and Dulay 1993). In the same way as in other areas of heterogeneous catalysis, the simultaneous adsorption has an influence on the kinetics of the reaction.

The L-H approach has some limitations (Fox and Dulay 1993). As has been seen previously, a basic assumption of the L-H kinetic model is the requirement of surface preadsorption. As a consequence, a wide range of photocatalytic reaction rates caused for the differences in adsorptive affinity of different substrates on a given semiconductor surface. However, the rate of reaction observed k_{eff} are quite similar in the different reactions that have been studied (Turchi and Ollis 1990).

3.4   Important Parameters Influencing the Photocatalytic Process

The photocatalytic process is a very complex process due to the several factors that affect the photocatalytic reaction rates. These factors can be classifying in two groups, extrinsic parameters and intrinsic parameters. Extrinsic parameters are external factors such as operating conditions. They include the light intensity, the pH of the solution, the initial

concentration of the organic compound, the amount of catalyst, the temperature, and the presence of ions in solution (Litter 1999; Xu, Shi et al. 1999).

Intrinsic parameters are those that only depend on the photocatalyst. Many studies have been developed in order to establish a relationship between the photocatalytic activity and the physicochemical properties of the catalyst. Usually, the photocatalytic activity of titania depends on its crystal phase, surface properties including the number of active sites (surface area), particle size, and porosity as well as the presence of surface acid or basic groups (Bacsa and Kiwi 1998; Xu, Shi et al. 1999). E.g., many studies have confirmed that the anatase phase of titania is a good photocatalytic material due to its low recombination rate of photogenerated electrons and holes (Hoffmann, Martin et al. 1995).

3.4.1   Extrinsic parameters

3.4.1.1   Effect of pH

Dependence of the photocatalytic reaction rate on the solution pH is often observed. The effect of pH on the reaction rate can be interpreted in terms of electrostatic interactions between charged TiO_2 particles and pollutants. This in turn is important because it affects the adsorption processes, and it is believed that the photocatalytic reactions are surface reactions. If TiO_2 is contacted with an aqueous media, it exhibits an amphoteric behaviour. The principal amphoteric surface functionality is the titanol fraction (>TIOH), therefore, a variation in pH also affects the surface speciation due to the amphoteric nature of the titanium dioxide particles (Jackson and Ahmed 2007); consequently affecting the adsorption and photocatalytic reactions of pollutants. The point of zero charge ($pH_{(PZC)}$) of metal oxide is defined as the pH at which the concentrations of protonated and deprotonated groups are equal, see Eq. 3.26.

$$pH_{PZC} = \frac{1}{2}\left(pk_1 + pk_2\right)$$
Eq. 3.26

The $pH_{(PZC)}$ of TiO_2 is 3.5-6.7, depending on the origin of sample. As a consequence of this amphoteric behaviour, the TiO_2 surface is predominantly negatively charged at pH > $pH_{(PZC)}$, and positively charged at pH < $pH_{(PZC)}$. E.g., methylene blue preferred to be absorbed on TiO_2 and readily degraded photocatalytically in alkaline solutions because its molecule and the surface of TiO_2 possess opposite charges; however, only little degradations were obtained in the acidic solutions (Hasnat, Siddiquey et al. 2005).

Moreover, the pH of the solution has an influence on the dispersion stability and also on the photodegradation rates (van Dyk and Heyns 1998).

3.4.1.2 Light intensity

The intensity of the light incident determines the rate of photoelectron and photohole generation and consequently the electron-hole concentrations in an illuminated semiconductor. It influences not only the photocatalytic degradation rate of organic matter but also the rate of photoelectron and photohole recombination (Mills and Hoffmann 1993; Hoffmann, Martin et al. 1995). Considering this, the light intensity affects the overall quantum efficiency of photocatalytic degradation. In a slurry system, at weak light intensity conditions, the photocatalytic degradation rates usually increase linearly with the light intensity (Hoffmann, Martin et al. 1995). Nevertheless, at strong light intensity conditions, the photocatalytic degradation rates varied with the square root of the light intensity (Ollis, Pelizzetti et al. 1991; Mills, Davies et al. 1993). The square root dependence of the reaction rate on the light intensity is often attributed to the enhanced recombination of photoelectrons and photoholes at strong light intensities (Mills and Hoffmann 1993).

3.4.1.3 Effect of initial concentration of pollutant

The pollutant concentration is always an important parameter to be considered in any water treatment process and, therefore, it is important to examine the effect of its initial concentration. The kinetics of photocatalytic degradation of many organic compounds in TiO_2 suspensions under UV irradiation follows a Langmuir-Hinshelwood reaction model described by Eq. 3.23. As becomes obvious, the kinetics of photocatalytic degradation depend of both the easiness with which it can be oxidized by the photogenerated hole and also how well it adsorbs on the surface of TiO_2.

It is also important to note that the absorption spectrum of the pollutant can significantly affect the kinetics of photocatalysis. In particular, if the pollutant is a strong UV absorber and its concentration is increased, then, it possibly begin to screen the TiO_2 from the photon absorption and the kinetics of photocatalytic degradation begin to deviate from Eq. 3.23, with the rate decreasing with increasing pollutant. This problem can be solved by choosing model pollutants that do not absorb significantly in the 300-400 nm wavelength region. Nevertheless, the effect of screening on the photocatalysis can be readily observed using

dyestuffs, by highly colored pollutants, or deposits of particulate matter on the surface of TiO_2 (Mills, Davies et al. 1993).

3.4.1.4 Effect of the amount of catalyst

The initial photodegradation rates increases proportionally with the amount of catalyst. This indicates a true heterogeneous photocatalytic regime. However, above a certain amount of catalyst the reaction rate reaches a limiting value. This plateau mainly results from the following two factors: a) aggregation of photocatalyst particles at high concentrations, causing a decrease in the number of photocatalytic sites, and b) increase in turbidity and light scattering at high concentrations, which masks part of the photosensitive surface, leading to a decrease in the penetration depth of the UV radiation.

The amount of catalyst is an important design parameter that has been extensively studied (Mengyne, Shifn et al. 1995; Mohammad Hossein Habibi 2004), e.g., in reactor systems as slurry types, for the effective use of the reactor space and photocatalyst (Chen and Ray 1999).

3.4.1.5 Effect of temperature

Experimental studies on the temperature dependence of the reaction rate for the degradation of organic compounds have been carried out since the 1970s (Gaya and Abdullah 2008). The variations of the initial rate of reaction observed over the range between 278-333 K for 4-Chlorophenol (Al-Sayyed, D'Oliveira et al. 1991) and 2-Chlorophenol (Rideh, Wehrer et al. 1997) have shown to be in accordance with Arrhenius law (see Eq. 3.27). However, the apparent activation energy is very small (5.5 kJ/mole and 6.23 kJ/mole respectively), which indicates that the thermally activated steps are negligible.

$$k = Ae^{-\frac{E_a}{RT}} \qquad\qquad \text{Eq. 3.27}$$

In the Arrhenius equation, k is the rate constant and T is the temperature (expressed in Kelvin K), where A is the frequency factor, R is the gas constant (8.314 J mol^{-1} K^{-1}) and E_a is the activation energy. Taking the natural logarithm of the Arrhenius equation yields:

$$\ln(k_{T_1}/k_{T_0}) = \frac{E_a}{R}(1/T_0 - 1/T_1) \qquad\qquad \text{Eq. 3.28}$$

If the chemical reaction obeys the Arrhenius equation, a plot of $\ln(k)$ versus T^{-1} gives a straight line whose slope and intercept can be used to determine E_a and A.

Generally, for TiO_2 photocatalyst, UV-light irradiation is the primary source of energy for electron-hole pair generation at room temperature as the band gap energy is too high to be overcome by thermal activation. Therefore, the slight increase in the rate constant can be attributed to the increasing collision frequency of molecules in solution that increases with increasing temperature (Chen and Ray 1998). An expected increase of the reaction rate constant with increasing temperature is possibly compensated by a decrease of the adsorption equilibrium constant. This feature is an advantage for practical application of photocatalytic process due to it can operate at or near room temperature.

3.4.2 Intrinsic parameters

There is a direct correlation between the degradation rate of organic pollutants and the surface coverage of TiO_2 (Guillard, Lachheb et al. 2003). It has also been demonstrated that the photocatalytic activity of TiO_2 strongly depends on its physical properties; a certain TiO_2 powder showed no appreciable activity but another powder was quite active. The physical properties such as crystal structure, surface area, and particle size are important parameters that influence the performance of photocatalysts in the photocatalytic oxidation. (Ding, Sun et al. 2005).

3.4.2.1 Crystal phase

The different behaviour in the photoactivity between anatase and rutile can be attributed to the different position of the conduction band (more positive for rutile) and the higher recombination rate of electron-hole pairs photoproduced in rutile (Okamoto, Yamamoto et al. 1985). Another explanation can be given with O_2 present in the medium, taking into account that O_2 has to be adsorbed on TiO_2 surface before reduction and the amount of O_2 that can be adsorbed depends on the hydroxylation degree of the adsorbing surface, and therefore on the acid-base superficial properties. These properties are different depending on the preparation method as well as on the thermal treatment (Sclafani, Palmisano et al. 1990).

In general the surface of anatase is highly hydroxylated and can lose water at the expense of superficial hydroxyl groups under thermal treatment. The decrease of superficial hydroxyl groups has been related with the decrease of the photocatalytic activity of TiO_2 (Campostrini, Carturan et al. 1994).

Rutile has a very low density of superficial hydroxyl groups, and its rehydroxylation even in contact with water is negligible (Primet, Pichat et al. 1971). From the previous considerations,

it seems to be that one of the fundamental reasons of the low photocatalytic activity of rutile is due to its poor adsorption capacity towards O_2 (Boonstra and Mutsaers 1975).

3.4.2.2 Particle size

The influence of particle size on the photocatalytic activity can be interpreted in terms of its effect on the surface area. The density of surface defects (or electron capture centers) increases as the particle size decreases. Reduction of the particle size might result in some electronic modification of TiO_2 and produce an enhancement of the activities of electrons and holes, and/or a suppression of the radiationless transfer of absorbed photon energies (Xu, Shi et al. 1999). Therefore, in nanocrystalline semiconductor particles, when particle size becomes extremely small (i.e. several nm in diameter), surface recombination becomes an important process (Serpone, Lawless et al. 1995).

3.4.2.3 Surface area

The photocatalytic reaction take place at the surface of a semiconductor, the increase of the surface area as a result of the decrease in the particle size is expected to cause increase in the activity. Often this may be true, but in contrast to conventional catalyses there are many factors that influence the photocatalytic activity. If the photocatalytic activity is affected by the amount of reactant at the surface, the surface area must be a factor of the activity. However, since the photocatalytic reactions occur in the vicinity of light absorption, the surface that is not reached by light does not contribute to the activity (Kaneko and Okura 2002).

On the other hand, powders with a large surface area are usually associated with large amounts of crystalline defects, which favours the recombination of electrons and holes leading to a poor photoactivity (Saadoun, Ayllón et al. 1999).

4   MATERIALS AND METHODS

4.1   Synthesis of Magnetic Photocatalysts

In this research, two types of magnetic photocatalysts (Fe_3O_4/TiO_2 and Fe_3O_4/SiO_2/TiO_2) have been synthesized. This synthesis involves the formation of titania powders as well as a coating technique. The synthesis route used to produce titania powders was the sol-gel technique by hydrolysis of titanium tetrachloride and a coating method was used to produce magnetic photocatalysts, this coating method involves the precipitation of titania onto the surface of seed magnetic particles (Fe_3O_4 and SiO_2/Fe_3O_4).

4.1.1   Preparation of TiO$_2$ powders

TiO_2 has been synthesized from $TiCl_4$ in aqueous solution by a modification of the procedure presented by Zhang *et al.* (Zhang, Gao et al. 1999). Titanium tetrachloride ($TiCl_4$, molecular mass=189.71, purity ≥99%) was purchased from Merck, and it is used as main starting material without further purification. The concentrated $TiCl_4$ solution was added dropwise into deionized water at 5°C. The concentration of titanium was adjusted to 3 mol L^{-1}. In order to promote crystallization of titania, a small amount of Degussa P25 TiO_2 (70 mg) was added into a $(NH4)_2SO_4$ solution. The 3 mol L^{-1} $TiCl_4$ solution was then added dropwise to a $(NH4)_2SO_4$ solution at a ratio [(Ti):(SO_4^{2-}) = 20:1] under stirring in a temperature-controlled bath (70°C) until the desired concentration of titanium (0.28 mol L^{-1}) was reached. Then the mixed solution was adjusted with 2.6 mol L^{-1} NH_4OH solution to pH 7. After 1 h, the precipitate formed in the solution was separated by filtration and washed thoroughly with deionized water to remove free chloride ions. Then, the precipitate was dispersed in anhydrous ethanol to remove any adsorbed water and to diminish the agglomeration during its drying process. The resulting sample was finally dried in a convection oven at 60°C for 48 h.

4.1.2   Preparation of silica coated magnetite (SiO$_2$/Fe$_3$O$_4$)

The method used to prepare silica coated magnetite had been reported previously by Chang *et al.* (Chang, Lin et al. 2006; Chang, Chang et al. 2008). Single-domain magnetite particles were prepared from ferric and ferrous chloride salts ($FeCl_3$ and $FeCl_2$) in an inert atmosphere and under stirring. The stoichiometric molar ratio of (Fe^{2+}/Fe^{3+}) was 0.5 to achieve

quantitative conversion via the addition of ammonia as precipitator. The temperature was kept at 80°C. After mixing for 3 min, magnetite formed was separated from the solution by means of a magnet and washed several times with deionized water. Subsequently, the obtained magnetite was contacted with an admixture, which was composed of ammonium hydroxide (25 vol. %), isopropanol, deionized water and tetraethylorthosilicates ($Si(OC_2H_5)_4$, TEOS). The total volume of the admixture was 2 L and the molar ratios were [(isopropanol):(water):(NH_4OH):(TEOS) = (30:2:7.8:1)]. After mixing for 5 h at a temperature of 40°C, the magnetic silica-coated particles were dried under an infrared-ray lamp overnight. The powder was then calcined at 400°C under a nitrogen atmosphere for 8 h to obtain magnetic silica-coated (SiO_2/Fe_3O_4). After washing several times the particles were dried at 100°C over night.

4.1.3   Preparation of Fe_3O_4/TiO_2 and $Fe_3O_4/SiO_2/TiO_2$

For the preparation of Fe_3O_4/TiO_2 and $Fe_3O_4/SiO_2/TiO_2$ particles, two starting materials were used. The commercial magnetite Bayoxide[®] E 8710 supplied by Lanxess was used for the synthesis of Fe_3O_4/TiO_2. This synthetic iron oxide Fe_3O_4 exhibits a surface area between 3-6 m^2 g^{-1}, a saturation magnetization between 84.8-91.7 emu g^{-1} and a predominant particle size of 0.5 μm. Silica coated magnetite, previously mentioned in section 4.1.2 was used for the synthesis of $Fe_3O_4/SiO_2/TiO_2$.

The synthesis was carried out based on the method of preparation of TiO_2 powders previously described in section 4.1.1. Magnetic particles were placed in an ultrasonic bath (Bransonic 2200, Danbury, USA) for 10 min, and then they were added to the reaction mix just before the addition of a 2.6 mol L^{-1} NH_4OH solution. Subsequently, the same procedure used to prepare TiO_2 powders followed. After 1 h of reaction the reactor was placed in an ice bath for 10 min to stop the reaction. The precipitate was separated by means of a magnet and washed thoroughly with deionized water and ethanol. The resulting sample was finally dried at 60°C for 48 h. In some cases, the samples were calcined at 400°C for 1 h. A flow chart of the method is shown in the Figure 4.1.
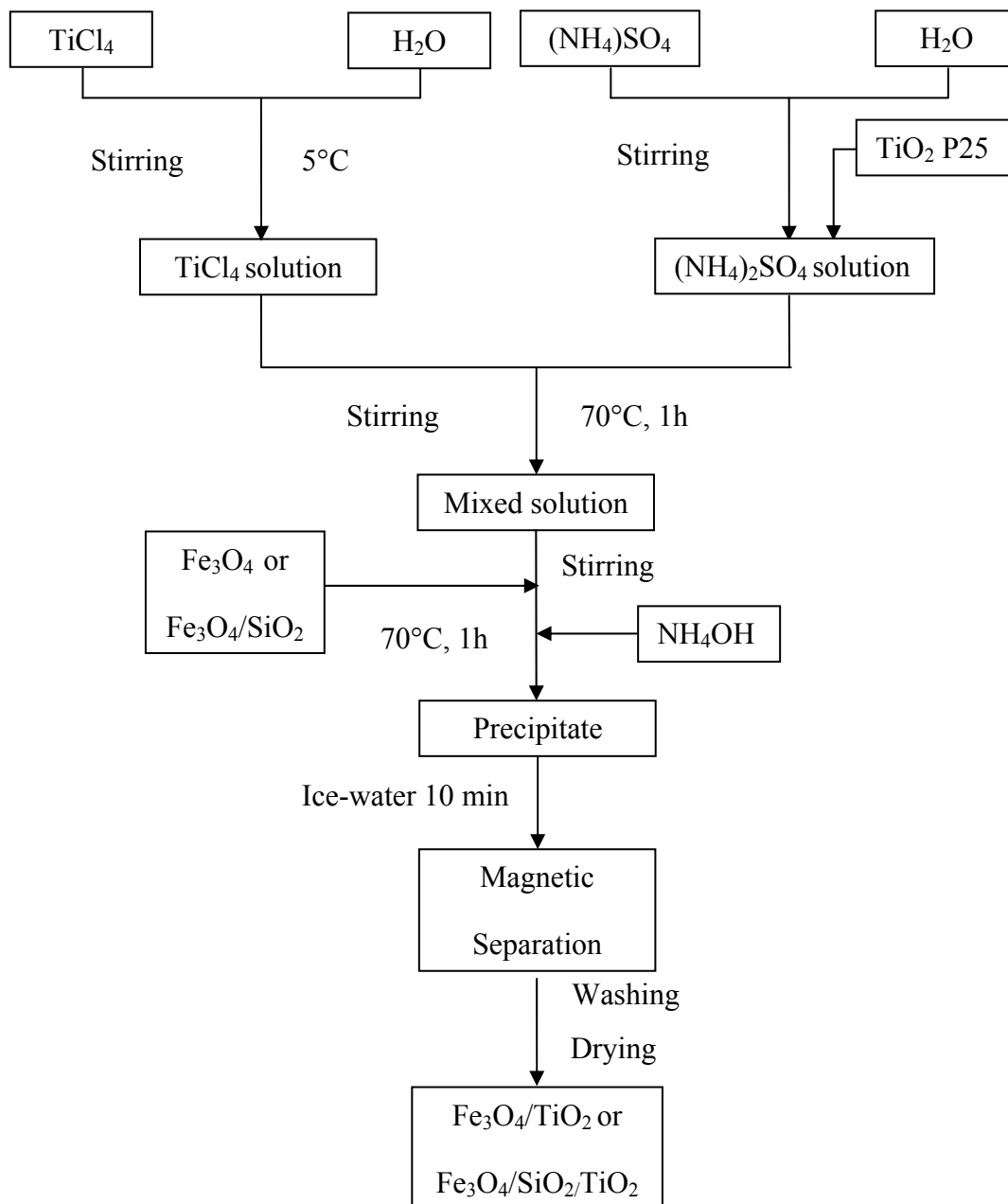
Figure 4.1: Flow chart of the steps involved in the preparation of Fe_3O_4/TiO_2 or $Fe_3O_4/SiO_2/TiO_2$.

4.1.4 Particle characterization

To obtain the physical characteristics of Fe_3O_4/TiO_2 and $Fe_3O_4/SiO_2/TiO_2$ particles, crystal structure, particle size distribution, morphology and surface area measurements were carried out. The magnetic properties, zeta potential and solid/liquid magnetic separation of the particles were also measured.

4.1.4.1   X-ray diffraction (XRD)

X-ray diffraction (XRD) analysis was performed for crystal phase identification and estimation of anatase, rutile, brookite and magnetite using CuK$_\alpha$ radiation in a Siemens D5000 automatic powder diffractometer system. Sample preparation for XRD analysis involved placing the finely ground catalyst in a sample holder.

4.1.4.2   ESEM

Environmental Scanning Electron Microscopy (ESEM) was used to determine the morphology of the particles. The equipment ESEM, XL30 ESEM-FEG (Philips, Netherlands) was used for this purpose. Using EDAX (energy dispersive X-ray microanalysis) the elemental composition of different particle surfaces was determined. Atoms in the sample are excited by an electron beam, where the sample emits X-rays with a specific energy of the elements. Thus, a qualitative or semi-quantitative determination of the chemical composition of the sample surface can be made. The samples used for ESEM analysis were subsequently used for EDAX analysis. Therefore, no further sample preparation was necessary.

4.1.4.3   Particle size distribution

The size distribution of the magnetic particles was determined in the range of 0.1-3600 μm by means of the particle size analysis system Eyetech (Ankersmid Ltd applied, Netherlands). Diluted suspensions of particles are introduced into a cuvette with mechanical stirrer.

4.1.4.4   Zeta potential

The zeta potential measurements were obtained using a Zetasizer 5000 (Malvern Instruments, Herrenberg, Germany). The particles were suspended in deionized water and the measurements of the zeta potential were obtained from electrophoretic mobility as a function of the pH. The pH was controlled using an automatic titrator (Mettler Toledo DL 25 titrator) and adjusted by adding 0.01mol L^{-1} NaOH solution or 0.01 mol L^{-1} HCl solution.

4.1.4.5   Specific surface area

The surface area of the particles was determined by the BET method with the device AUTOSORB1 (Quantachrome, Greenvale, USA) using a nitrogen atmosphere. Prior to the analysis, about 0.150 g particles were degased at 95°C for 12 h.

4.1.4.6 Magnetic characterization

Magnetic characterization of the particles was performed by means of an alternating gradient magnetometer (AGM) (Micromag 2900, Measurements, Princeton USA). The magnetization of the particles as a function of the applied field strength was measured.

4.1.4.7 Magnetic solid/liquid separation

To measure the solid/liquid magnetic separation a turbidity test was carried out. The catalyst loading for every test was 50 mg L^{-1}. Solutions of deionized water were used. The turbidity was determined using a turbidimeter (HACH model 2100 AN, Colorado, USA). The suspension was left to settle down in presence and absence of a hand magnet with dimension of 1.5 x 2 x 0.5 cm (NdFeB permanent magnet). The turbidity was measured at determined time intervals for 1 h.

4.2 Model Compounds

In this research three different organic compounds benzoic acid, methyl orange and Sulforhodamine B were chosen as model compounds. They were used for both adsorption and photocatalytic oxidation experiments.

All the solutions and suspensions were prepared with deionized water. The photocatalysts used were Fe_3O_4/TiO_2, $Fe_3O_4/SiO_2/TiO_2$ and P25 TiO_2.

4.2.1 Benzoic acid

Its molecular formula is $C_7H_6O_2$ (orC_6H_5COOH), its structure is shown in Figure 4.2 and its molecular mass is 122.12 (g mol^{-1}). In this research benzoic acid from Merck (for analysis) was used.
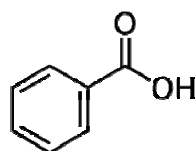
Figure 4.2: Structure of benzoic acid.

Benzoic acid can be found in nature in free and combined forms and is one of the most important aromatic carboxylic acids (Maki and Susuki 1985). The catalytic oxidation of toluene with air, it is the most common way to produce benzoic acid at industrial scale. Benzoic acid is used to produce a wide variety of organic chemicals. Its applications include intermediates for dyes, herbicides, pharmaceuticals, food, additives and perfumes. Benzoic acid is included in the US Environmental Protection Agency (EPA) list of priority pollutants, air toxics, or toxic release inventory (Blake 1995).

Benzoic acid is stable towards the usual oxidants as air, permanganate, chromic acid, hypochlorite and dilute nitric acid. In addition to its simple chemical structure with only one aromatic ring, it is an ideal substance as a model compound for photocatalytic oxidation of more complex phenolic compounds with less chemical stability. The UV absorption spectrum of benzoic acid exhibits a maximum at about 225 nm shown in Figure 8.1; benzoic acid does not absorb ultraviolet light between 320 and 400 nm.

4.2.2 Methyl orange

Methyl orange (sodium-4-dimethylamino-azobenzene 4´-sulfonate) is industrially synthesized by coupling diazotized sulphanilic acid with dimethlaniline. The acid dye is used for wool and silk colouring. Its molecular formula is $C_{14}H_{14}N_3NaO_3S$, the chemical structure is shown in Figure 4.3 and its molecular mass is 327.34 (g mol^{-1}). Methyl orange was obtained from Merck (Art. 1322).
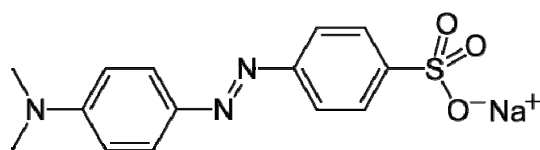
Figure 4.3: Structure of methyl orange.

Methyl orange is one of the most frequently employed acid-base indicators. The indicator changes its colour from red to yellow in the pH range 3.1 - 4.4.

4.2.3 Sulforhodamine B

Sulforhodamine B or Kiton Red is widely used in medical science as a fluorescent label. It has a high solubility in water. The acid form of sulforhodamine B (SRB) was purchased from Sigma-Aldrich (USA). Its molecular formula is $C_{27}H_{30}N_2O_7S_2$, the structural formula is

shown in Figure 4.4 and its molecular mass is 558.68 (g mol^{-1}). The colour of this dye turns into a bright orange under UV light.
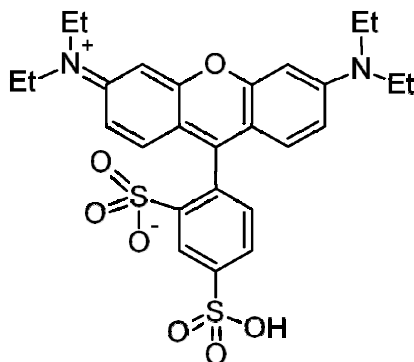
Figure 4.4: Structure of sulforhodamine B.

4.3 Analytical Methods

4.3.1 Determination of benzoic acid

The concentration of benzoic acid was determined by means of High Pressure (or Performance) Liquid Chromatography (HPLC) using a Dionex system (Dionex, Sunnyvale, CA,USA) containing a pump, an automated sample injector and an UV detector. Separation was performed on a Lichrosorb RP18-5μ column 250x4 mm (Merck, Darmstadt, Germany). A sample injection volume of 20μL was used. For data analysis Chromeleon software (Dionex, Sunnyvale, CA, USA) was used. The analysis was carried out at a wavelength of 225 nm and the eluent contained 80% 10 mmol L^{-1} ammonium acetate (NH$_4$OAc) and 20% methanol and was pumped through the system at a flow rate of 0.5 mL min^{-1}.

4.3.2 Determination of methyl orange and sulforhodamine B

The concentrations of methyl orange and sulforhodamine B were determined by UV-Vis spectroscopy using a spectrophotometer UV mini-1240 (Shimadzu, Kioto, Japan). Disposable cuvettes (Plastibrand, Germany) of 2.5 mL were used for sample preparation.

4.3.3 Determination of dissolved organic carbon (DOC)

The concentration of dissolved organic carbon was determined by using a TOC-Analyzer multi N/C 2000 (Analytik Jena, Gernany). The sample was acidified to pH 2 using HCl and

purged using oxygen. Then the sample was heated to 800°C in presence of a catalyst. At this temperature organic compounds are completely oxidized. The concentration of the resulting CO_2 was determined by IR absorption.

4.4   Adsorption of the Model Compounds

The batch adsorption tests were performed in absence of light (dark reaction). The concentration of photocatalyst was always the same 4 g L^{-1} for all the experiments. The benzoic acid concentration used was in the range of 0.003-0.065 mmol L^{-1}, the concentration of methyl orange between 0.0017-0.04 mmol L^{-1}, and the concentration of SRB between 0.003-0.047 mmol L^{-1}. The pH value was adjusted by adding 0.05 mmol L^{-1} NaOH or 0.05 mmol L^{-1} HCl. The reaction was performed in flasks with fixed volumes of 25 ml. The flask were sealed and agitated at room temperature on a shaker for 24 h. The photocatalyst was separated with a syringe filter (0.45 μm) before the concentration of a model substance was determined.

4.5   Photocatalytic Reactor Configuration

The degradation experiments were carried out in a photocatalytic system. This facility consists of a light source and a reactor as is shown in Figure 4.5.

4.5.1   Light Source

The irradiation source used was a UVASPOT 400/T lamp (Dr. Hönle, Germany) which is equipped with a 450 W metal halide high pressure bulb. A filter permitting the transmission of wave lengths between 315 and 400 nm was used.

The light intensity was measured with a UVA radiometer (Dr. Hönle, Germany), which has a spectral sensitivity in the range of 315-400 nm and a measuring range between 0-199.9 mW cm^{-2}. The intensity measured at the bottom of the reactor was 20 mW cm^{-2}; the intensity at 10 cm from the lamp without the reactor was 21.5 mW cm^{-2}.
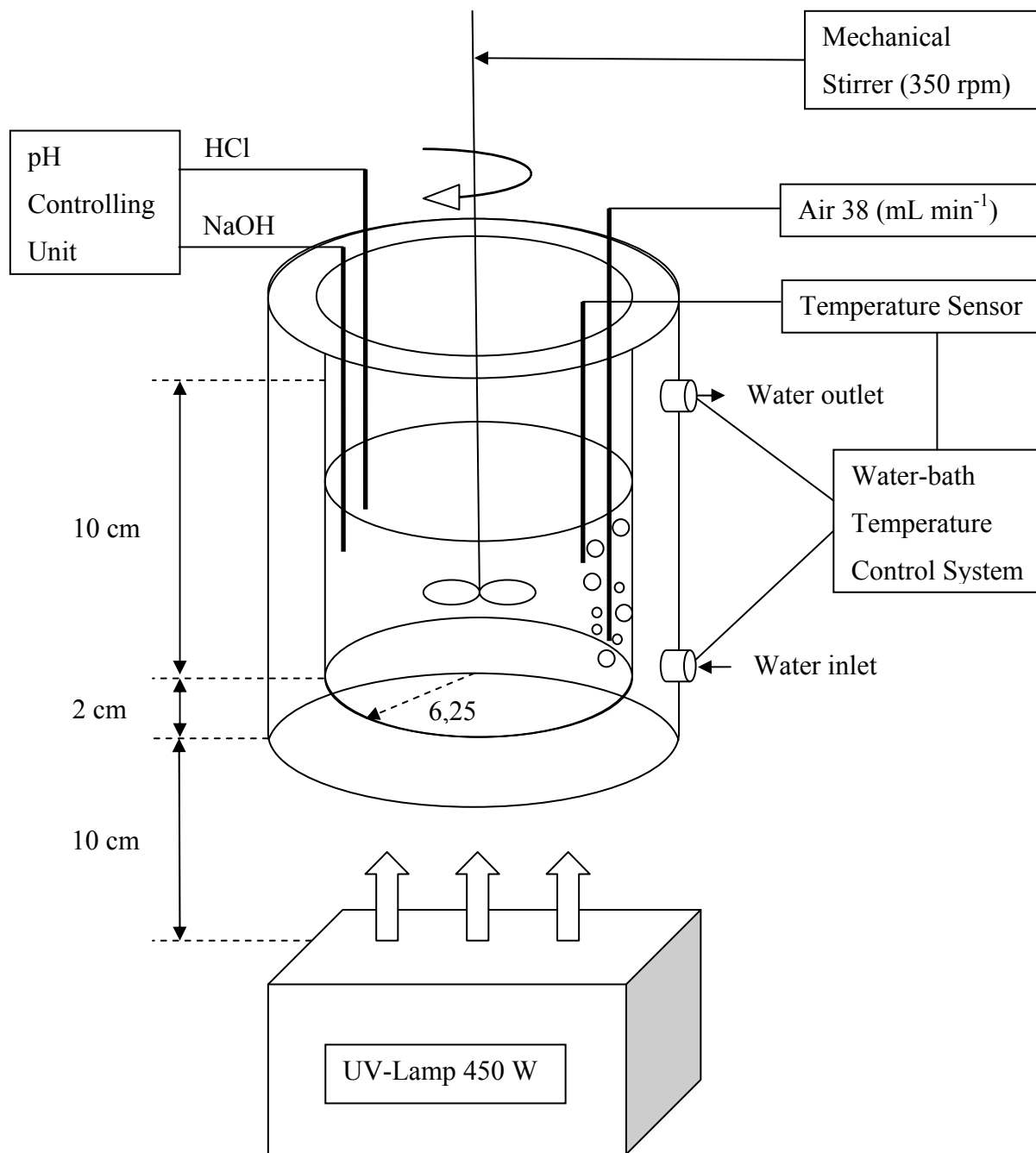
Figure 4.5: Photocatalytic sytem.

4.5.2   Reactor

A jacketed cylindrical borosilicate glass reactor (Duran®) was used as a batch reactor with the following dimensions: Internal diameter 6.25 cm and a height 10 cm. The reactor wall was covered with aluminum foil. The temperature of the water in the jacket was controlled by a thermostatic water bath RC6 (Lauda, Germany). The reaction was stirred at 350 rpm using a mechanical stirrer RZR 2051 control (Heidolph, Germany). The pH was controlled

automatically and kept constant during the entire reaction by using a pH control unit Dulcometer D1C (Prominent, Germany), a pH electrode H 6180 (Schott, Germany) and two dosage pumps Gamma/L (Prominent, Germany) for the addition of 0.05 mmol L^{-1} HCl or 0.05 mmol L^{-1} NaOH to the reaction mixture. Air was introduced into the reactor by using a peristaltic pump (Behr, Germany) at 38 mL min^{-1}.

4.6 Procedure of the Photocatalytic Oxidation

The experiments were carried out using different concentrations of photocatalyst as well as model compounds. The amounts of photocatalyst were in the range between 0.03 and 1 g L^{-1}. The initial concentrations of the model substances were between 0.08 and 0.98 mmol L^{-1} using benzoic acid, 0.03 and 0.3 mmol L^{-1} using methyl orange and 0.003 and 0.017 mmol L^{-1} using sulforhodamine. Before starting irradiation, both pH and temperature were adjusted and kept constant. Air was continuously introduced into the reactor; the reaction volume was 400 mL, containing both the photocatalyst and the organic compound. The suspensions were stirred in the dark for 30 min to assure adsorption/desorption equilibrium of the model substances.

In order to take samples 5 mL of the suspension were filtered through a syringe filter (0.45 μm) to separate the photocatalyst and to stop the photocatalytic reaction. Samples were taken at regular time intervals and stored in glass bottles for subsequent analysis of the concentration of the models compounds.

5   RESULTS AND DISCUSSION

5.1   Preparation of the Magnetic Photocatalyst

The preparation of the magnetic photocatalyst was carried out according to the coating concept where one material is deposited on another. In this case magnetic particles were used as a seed material and TiO_2 was the compound to be precipitated.

5.1.1   Synthesis conditions

For the synthesis of TiO_2 a modification of the Zhang procedure (Zhang, Gao et al. 1999) was carried out. A $Ti:SO_4^{2-}$ ratio of 20:1 was used because under these conditions the formation of anatase phase is favoured as investigated by Zhang. The addition of a small amount of SO_4^{2-} ions induces the growth of TiO_2 clusters to anatase phase. The parameters applied for the synthesis of the magnetic photocatalysts mentioned above are summarized in Table 5.1.

Table 5.1: Hydrolysis conditions applied for the synthesis of magnetic photocatalysts.

Particle	$TiCl_4$ (mmol/L)	$Ti:SO_4^{2-}$	Seed particle	Hydrolysis time (min)	Hydrolysis T (°C)	Dried (°C)
TiO_2 (T-60)	0.28	20:1	-	60	70	60
TiO_2 (T-400)	0.28	20:1	-	60	70	400
Fe_3O_4/TiO_2 (F/T)	0.28	20:1	Fe_3O_4	60	70	60
$Fe_3O_4/SiO_2/TiO_2$ (F/S/T)	0.28	20:1	Fe_3O_4/SiO_2	60	70	400

Various magnetic photocatalysts were prepared by precipitation of TiO_2 onto two different magnetic materials, Fe_3O_4 and Fe_3O_4/SiO_2. Among them, two photocatalysts have been selected to continue with the investigation of adsorption and photooxidation.

5.1.2 X-ray powder diffraction (XRD) analyses

Figure 5.1 shows the XRD patterns for samples T-60 and T-400 at temperatures of 60°C and 400°C respectively, along with the reference patterns for anatase and rutile. The X-ray peaks at 2θ equal to 25.3, 37.8 and 48 are generally attributed to an anatase phase (00-021-1272 JCPDS card number) and the peaks at 2θ equal to 54.4 are attributed to a rutile phase (00-21-1276 JCPDS card number), thus, the presence of both anatase and rutile phases are confirmed in both materials, T-60 and T-400. The analysis of XRD data suggests that T-60 consists of both crystalline and amorphous components where the amorphous part prevails. An effect of the temperature is also shown; when the sample is calcined at 400°C (T-400) the peak corresponding to the anatase phase becomes more intense indicating an increase in the crystallization of the amorphous trace. Changes in the crystal structure were not detected.

Encouraged by the fact that the thermal treatment was beneficial for the conversion of titanium dioxide from amorphous to crystalline phase increasing the photocatalytic activity, a sol-gel technique was used to coat magnetite particles with silica, in order to avoid the oxidation of magnetite at high temperatures and therefore the loss of its magnetic properties.
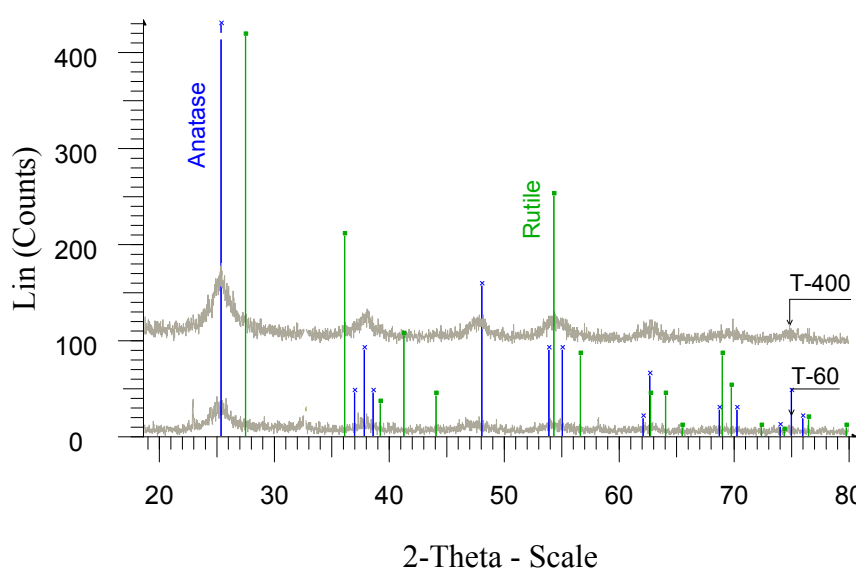
Figure 5.1: XRD patterns of T-60, T-400 and TiO_2 reference.

Figure 5.2 shows the XRD patterns for Fe_3O_4/TiO_2 (F/T) photocatalyst, along with the reference patterns for both magnetite and anatase. By means of the XRD analyses the presence of anatase and magnetite is confirmed. At 2θ equal to 25.3 a broad and strong peak which is characteristic for the anatase phase (00-021-1272 JCPDS card number) is clearly

seen. At 2θ equal to 35.4, 56.9 and 62.5 a narrow and well-defined peak can be attributed to crystal planes of the typical cubic magnetite Fe_3O_4 (00-019-0629 JCPDS card number).
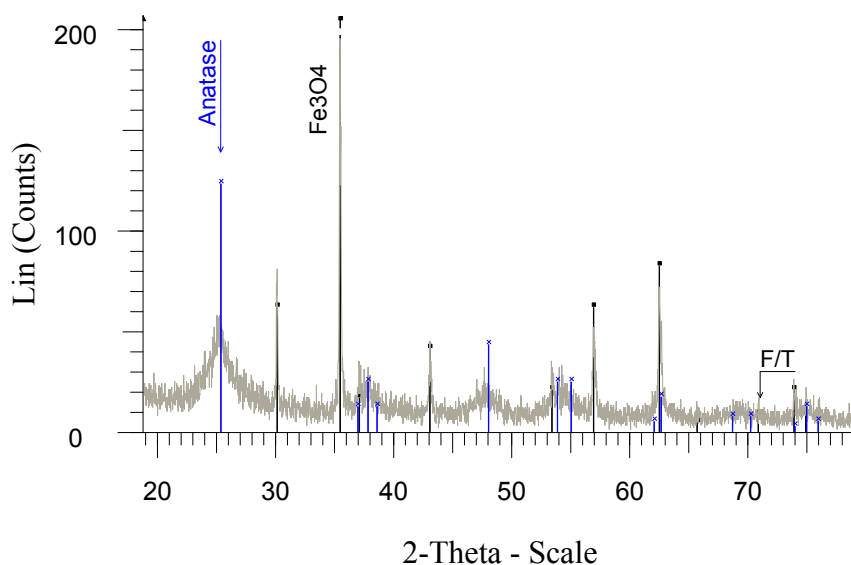
Figure 5.2: XRD analysis of F/T patterns in comparison with both magnetite and anatase reference patterns.
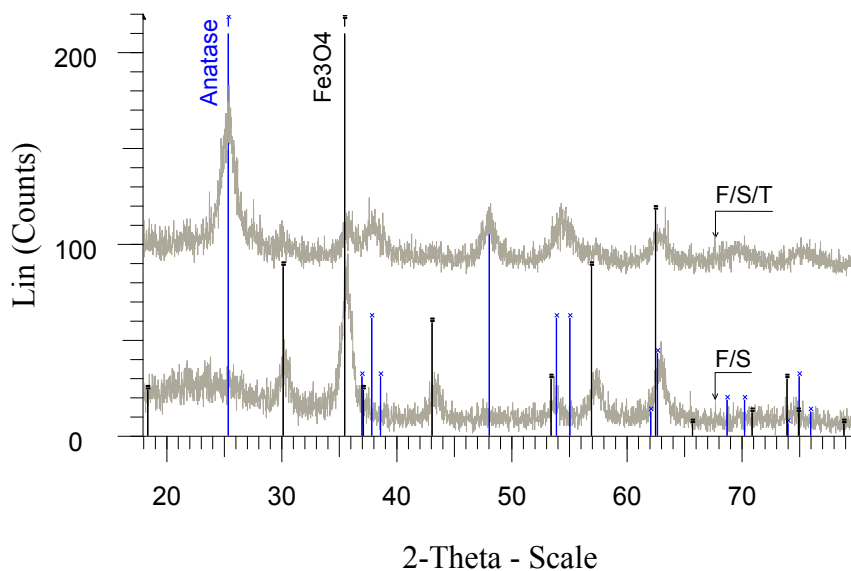
Figure 5.3: XRD analysis of F/S and F/S/T pattterns in comparison with both magnetite and anatase reference patterns.

Figure 5.3 shows the XRD patterns for both Fe_3O_4/SiO_2 (F/S) and $Fe_3O_4/SiO_2/TiO_2$ (F/S/T) samples, along with the reference patterns of anatase and magnetite. In this case the F/S

particles were used as a seed material on which the TiO_2 was deposited; by means of XRD analysis the presence of anatase phase in F/S/T material is confirmed. At 2θ equal to 25.3 a peak attributed to TiO_2 in the anatase phase structure (00-021-1272 JCPDS card number) can be clearly seen, while in the F/S material the TiO_2 peak is not present, indicating that the coating was successfully achieved. On the other hand for F/S material diffraction peaks observed at 2θ equal to 30.1, 35.4, 52.9 and 62.5 were well indexed to the cubic structured magnetite Fe_3O_4 (00-019-0629 JCPDS card number), thus, the presence of magnetite becomes evident. In the case of F/S/T is also possible to see the presence of magnetite although the peaks have a weak intensity, this could be attributed to due to the low weight percentage of magnetite in the sample.
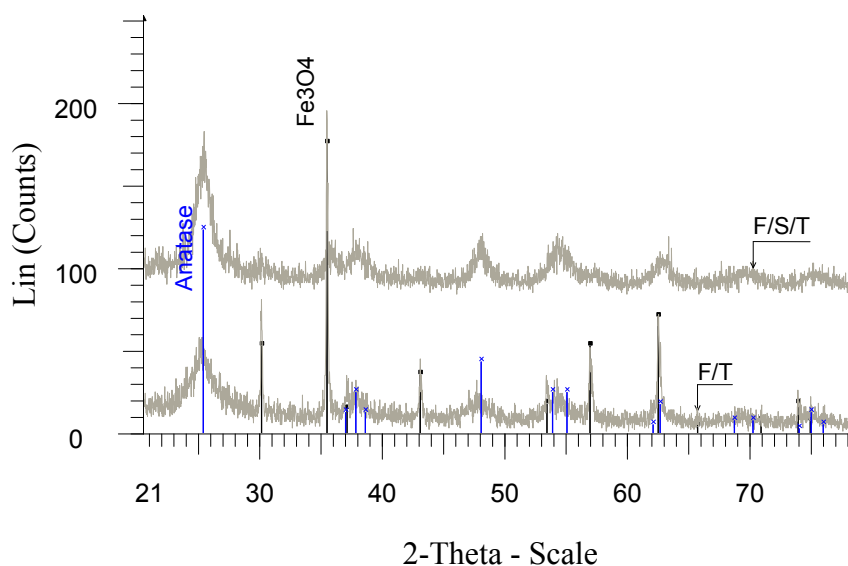
Figure 5.4: XRD analysis of both F/T and F/S/T patterns.

Figure 5.4 shows the XRD patterns for both Fe_3O_4/TiO_2 (F/T) and $Fe_3O_4/TiO_2/SiO_2$ (F/S/T). The diffraction peaks in Figure 5.4 appear at 2θ equal to 30.1, 35.4 and 62.5 corresponding to crystal planes of the cubic magnetite (00-019-0629 JCPDS card number) showing the presence of magnetite in both materials, it is seen that F/T has a well defined and narrow peaks at 2θ equal to 30.1, 35.4 and 62.5 and their intensities are stronger than the peaks of F/S/T. These differences can be attributed to the use of commercial magnetite which has a higher crystallinity as well as a major weight percentage in F/T of about 27% compared to 9.7% in F/S/T (see Table 5.2).

It should be appointed that the anatase peak which is present in both materials has a stronger intensity in F/S/T than F/T. This can be explained by the different temperatures at which the materials were dried, 60 and 400°C for F/T and F/S/T respectively, that is in accordance with the literature which states that a heat treatment process of a sample carried out at high temperatures promotes its crystallization (Zhang, Gao et al. 2000; Zhu, Zhang et al. 2000). Other possible explanation could be the different percentage of titania in the material, F/T and F/S/T have approximately a 72% and 84% respectively (see Table 5.2).

5.1.3   ESEM images

ESEM imaging techniques with EDAX analysis and multi-element mapping were combined to obtain information about the morphologies of the particles. The ESEM micrograph for the F/T particles is shown in Figure 5.5, the results confirm the presence of Ti and Fe, where it is possible to distinguish a cubic shape which can be attributed to Fe_3O_4. According to EDAX elemental maps of samples for Ti and Fe, the highest concentration of iron is found inside of the marked area while the highest concentration of titanium is found outside.
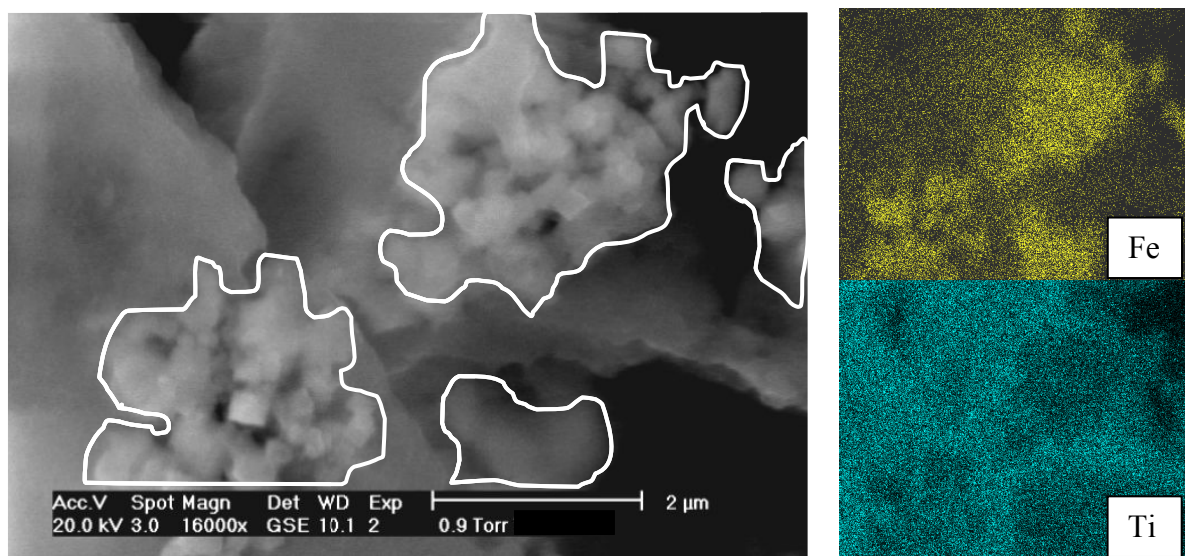
Figure 5.5: ESEM image of F/T and element maping of Ti and Fe.

Typical ESEM micrographs and EDAX analysis of the F/S/T material are shown in Figure 5.6. The EDAX spectrum for F/S/T shows different peaks which confirm the presence of titanium, iron and silicon in the material.
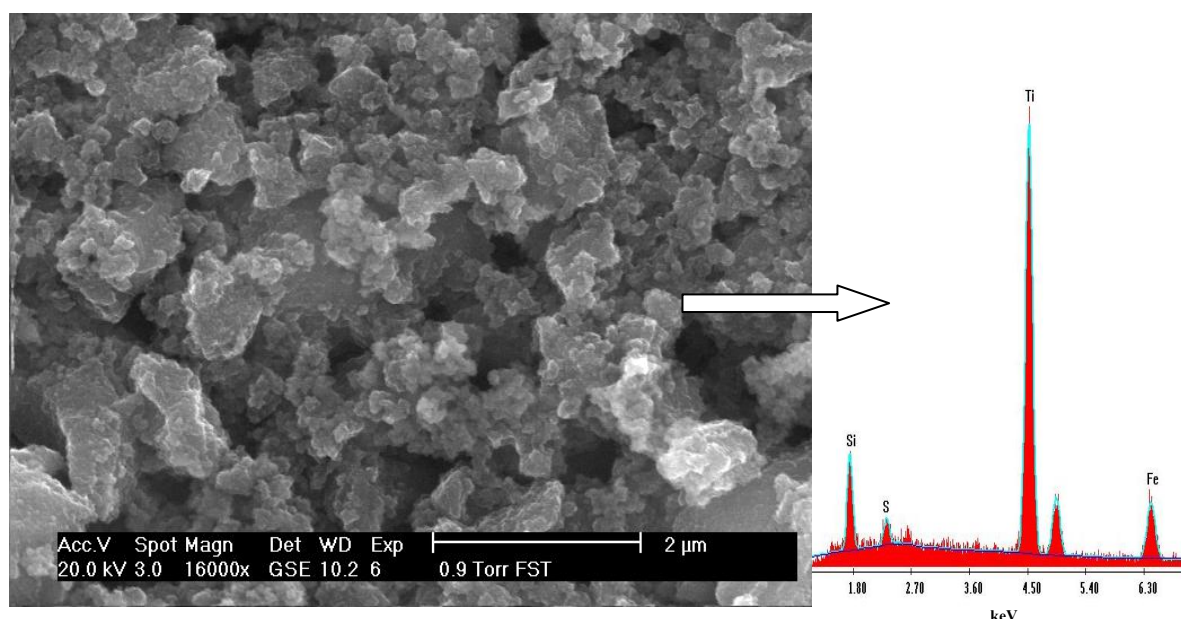
Figure 5.6: ESEM image of F/S/T and EDAX spectrum.

5.1.4 Distribution and size of the particles

Figure 5.7 shows the particle size analysis for F/S/T and F/T photocatalysts. F/S/T and F/T particles have a mean particle size of 1.84 μm and 6.6 μm respectively. According to the analysis software (Eyetech, Netherlands) 90% of the particles were under 4.3 and 14.9 μm for F/S/T and F/T respectively. The F/S/T and F/T photocatalysts have a particle size distribution between 0.6 to 6 μm and 0.6 to 20 μm respectively.

The difference of size and distribution of particles is mainly due to the magnetic materials used as seed particles, using commercial magnetite for F/T and synthesized silica coated magnetite for F/S/T.
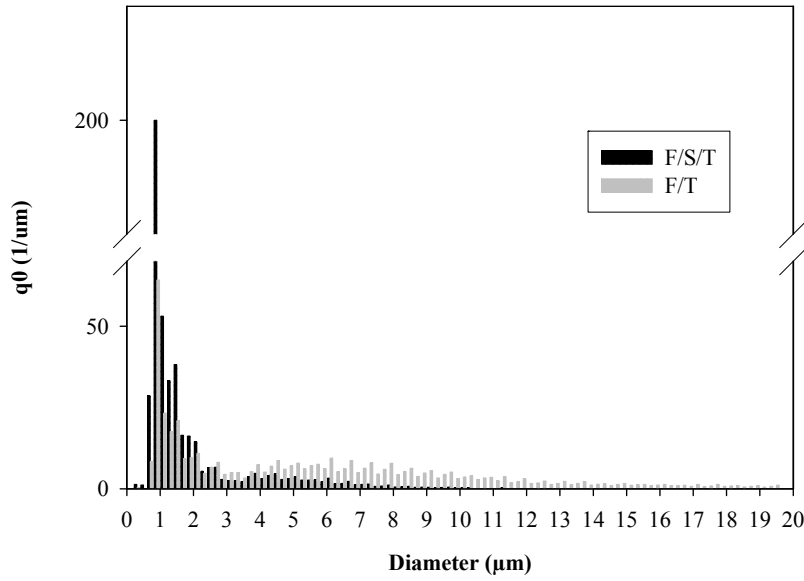
Figure 5.7: Distribution of particles size for F/S/T and F/T photocatalysts.

5.1.5   Zeta potential measurements

The zeta potential as function of the pH for both F/S/T and F/T is presented in Figure 5.8. The surface charge is due to adsorption of potential determining ions, for oxides these ions are H^+ and OH^- (David, Jaâfar et al. 2002). The point of zero charge $pH_{(PZC)}$ measured for F/T and F/S/T particles were found to be at pH 6.0 and 6.4 respectively, this is the pH at which the surface charge is equal to zero.

Since the surface of TiO_2 is mainly hydroxylated in contact with water. The surface groups can be protonated or deprotonated, depending on the pH value of the liquid phase. In the case of protonation a positive surface charge is generated, on the other hand, in the case of a deprotonation a negative surface charge is generated; the reactions are shown in Eq. 5.1 and Eq. 5.2.

$$Ti - OH_{(surf)} = Ti - O^- + H^+_{(aq.)} \qquad\qquad \text{Eq. 5.1}$$

$$Ti - OH_{(surf)} + H^+_{(aq.)} = Ti - OH_2^+ \qquad\qquad \text{Eq. 5.2}$$

It is known that the $pH_{(PZC)}$ varies according to the synthesis method of TiO_2. The $pH_{(PZC)}$ values for the synthesized particles prepared in this research are consistent with the values measured by other procedures. E.g., values in the range of pH 5 to 7 are reported for the study

of TiO_2 nanoparticles (Kosmulski 2002). According to the literature previously mentioned, the rutile phase shows a slightly lower $pH_{(PZC)}$ value than anatase phase.
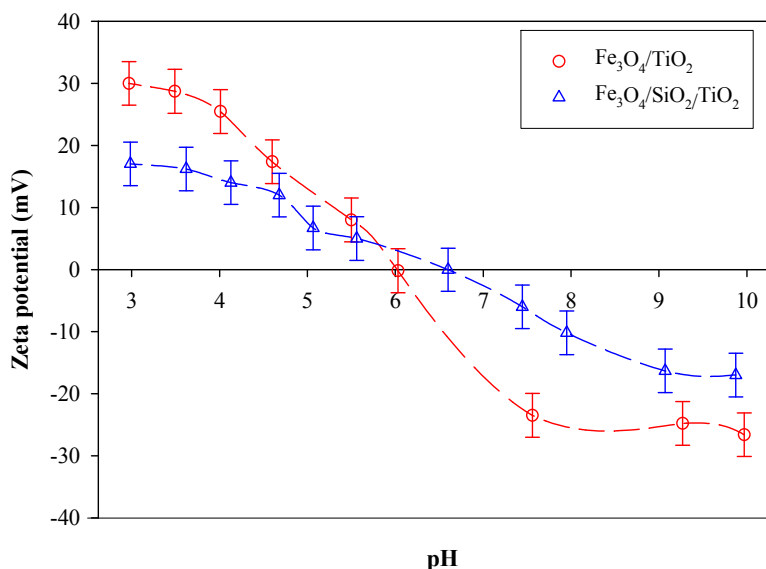
Figure 5.8: Zeta potential of F/T and F/T/S.

5.1.6 Specific surface area measurements

Table 5.2 shows a description regarding to the percentages of Fe_3O_4 and TiO_2 as well as the values of surface area obtained at different temperatures for the materials used in the photocatalytic investigation. According to Table 5.2, large surface areas for samples T-60 and T-400 were observed; 411 m^2 g^{-1} and 380 m^2 g^{-1} respectively. The amorphous characteristic of T-60 explains the highest value for BET against Fe_3O_4 which shows the lowest BET surface area (3-6 m^2 g^{-1}) value which can be attributed to its high crystallinity.

In general it was observed a decrease in the BET surface area values after coating TiO_2 onto magnetic particles. The decrease is clearly related to the ratio of magnetite and TiO_2 in the magnetic photocatalyst; thus, for F/T photocatalyst with a 27.7% of Fe_3O_4 the BET surface area value was 259 m^2 g^{-1} while for F/T-b with a 42.3% of Fe_3O_4 the BET surface area value was 204 m^2 g^{-1}.

The influence of temperature on the surface area values by means of a heat treatment of the materials was also observed. For both T-60 and T-400 particles as well as for F/S/T and F/S/T-b particles the BET values decreased as the temperature increased, as explained before this can be due to the crystal growth (Watson, Beydoun et al. 2002; Zhu, Yang et al. 2007).

The magnetic materials used as seed particles for the coating procedure (Fe_3O_4 and F/S) also have shown an influence on the final BET values for both F/T and F/S/T. For F/S the BET values were observed to be higher than those for Fe_3O_4, thus become obvious that this difference is noted in the final BET values being the surface area of F/S/T larger that F/T.

Table 5.2: Values of surface area (BET) of diferent particles used in photocatalytic oxidation.

Particle	Fe_3O_4 (%)	TiO_2 (%)	Dried T(°C)	BET surface area (m^2 g^{-1})
TiO_2 (T-60)	-	-	60	411
TiO_2 (T-400)	-	-	400	380
Fe_3O_4 (Bayoxide® E 8710)	98.0	-	-	3-6
Fe_3O_4/TiO_2 (F/T)	27.7	72.3	60	259
Fe_3O_4/TiO_2 (F/T-b)	42.3	57.7	60	204
Fe_3O_4/SiO_2 (F/S)	62.1	-	400	83
Fe_3O_4/SiO_2/TiO_2 (F/S/T-b)	9.7	84.0	60	361
Fe_3O_4/SiO_2/TiO_2 (F/S/T)	9.7	84.0	400	311

5.1.7 Magnetic characterization

The magnetic properties of the F/T and F/S/T particles are shown in Figure 5.9. In this figure, the magnetizations versus the applied magnetic field are graphically represented. As expected, it is seen that the magnetic saturation of F/T is higher than that of F/S/T.
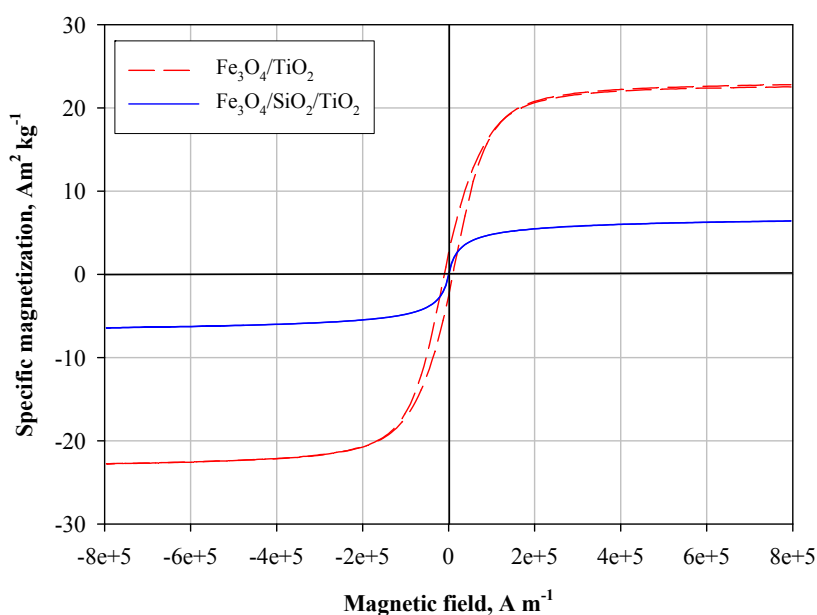
Figure 5.9: Magnetization curves of F/T and F/T/S.

The magnetic parameters such as saturation magnetization (M_s) and remanent magnetization (M_r) are given in Table 5.3. The differences of Ms between the particles are according with their Fe_3O_4 content in unit weight particle, thus F/T has a higher value than F/S/T. The low value of M_r for F/S/T particles indicates a superparamagnetic behaviour at room temperature. In the case of F/T particles the M_r value indicates a ferrimagnetic behaviour. The magnetic properties of the F/T and F/S/T particles allow the use of a magnet or a magnetic field for an easy solid/liquid separation. The low values of the M_r reduce considerably the aggregation of the particles after the separation by means of a magnet; therefore the photocatalysts can be easily dispersed in a solution for recycle.

Table 5.3: Magnetic parameters of the prepared samples.

Particle	M_s (Am^2 kg^{-1})	M_r (Am^2 kg^{-1})
Fe_3O_4/TiO_2 (F/T)	22.6	2.66
Fe_3O_4/SiO_2/TiO_2 (F/S/T)	6.4	0.08

5.1.8 Magnetic separation test

In order to have information about the solid/liquid magnetic separation of F/S/T and F/T photocatalysts, turbidity was measured. The results for measurements carried out for F/S/T photocatalyts are shown in Table 5.4.

Table 5.4: Turbidity of supernatants of F/S/T suspension at various settling times in deionized water, (1) no magnetic field, (2) under magnetic field of 0.4 T.

Time (min)	F/S/T [1] (NTU)	Residual percentage (%)	F/S/T [2] (NTU)	Residual percentage (%)
0	420	100	420	100
1	390	92.9	254	60.5
4	336	80	147	35
10	267	63.6	70	16.7
20	275	65.5	59	14
30	242	58	47	11.2
60	-	-	11.7	2.8

It has been observed that in presence of a magnetic field the settling of the suspension is much more effective than without its influence. Without a magnetic field the residual percentage is 58% at 30 min while this percentage is approximately reached (60.5%) at 1 min using a magnetic field.

Results obtained for F/T are shown in Table 5.5. As in the previous table for F/S/T photocatalyst, without a magnetic field the residual percentage at 30 min was 13.4% while by using a magnetic field this value is almost reached (15.9%) within the first minute. Residual percentages by using a magnetic field lie below 4.3% from 4 min and without a magnetic field this value is not reached even after 30 min.

Comparing the Table 5.4 and Table 5.5 it can be seen that the residual percentages without the application of a magnetic field obtained for F/T are lower than those for F/S/T; this is probably due to the different particle sizes between the materials (see Figure 5.7). Moreover, by using a magnetic field the trend is the same but the differences observed can be attributed

to the saturation magnetization, where F/T has a value of 22.6 Am^2 kg^{-1} and F/S/T a value of 6.4 Am^2 kg^{-1}.

Table 5.5: Turbidity of supernatants of F/T suspension at various settling times in deionized water, (1) no magnetic field, (2) under magnetic field of 0.4 T.

Time (min)	F/T [1] (NTU)	Residual percentage (%)	F/T [2] (NTU)	Residual percentage (%)
0	277	100	277	100
1	243	87.7	44	15.9
4	195	70.4	11.9	4.3
10	133	48	7.7	2.8
20	62	22.4	6.7	2.4
30	37.2	13.4	7	2.5

Turbidity measurements obtained for P25 TiO_2 are shown in Table 5.6. It can be observed that the application of a magnetic field has no influence on the settling of P25 TiO_2, this was expected because P25 TiO_2 is not magnetic. However, it is interesting that even at 30 min. the residual percentages are not below 92%, thus, the advantages of the magnetic separation exhibited of the both F/S/T and F/T photocatalysts is indirectly remarked.

Table 5.6: Turbidity of supernatants of P25 TiO_2 suspension at various settling times in deionized water, (1) no magnetic field, (2) under magnetic field of 0.4 T.

Time (min)	F/T [1] (NTU)	Residual percentage (%)	F/T [2] (NTU)	Residual percentage (%)
0	1950	100	1950	100
1	1946	99.8	1948	99.9
10	1900	97.4	1944	99.7
20	1846	94.7	1922	98.6
30	1808	92.7	1858	95.3

As can be seen in Table 5.4 and Table 5.5, the residual percentage values show a marked decline when the photocatalysts are separated from aqueous solution by using a magnet. Considering a large scale application, an almost complete separation of the photocatalysts could be achieved using a combined separation system consisting of magnetic flocculation device, a settling tank and a high gradient magetic separation (HGMS) device (see Figure 5.10). Although the photocatalysts could be separated by the HGMS system alone, this would require frequent washing of the magnetic filter and would result in a rather dilute recycling suspension of the particles. In order to reduce the loading rate of the HGMS device a settling tank could be installed. Previous to this step the particles would pass through a weak magnetic field induced by a magnet coil. According to the experimental data showed in Table 5.4 and Table 5.5, the sedimentation time for the majority of the particles would be around 30 min. At this time the residual percentages were of 11.2% and 2.5% for F/S/T and F/T respectively. Then the aqueous solution would be introduced into the HGMS unit where a final magnetic separation is performed. By means of this separation step the values of residual percentage will be well below 1%.

A.- Input of organic solution

B.- Outlet of clean solution

C.- Recovery of photocatalyst particles

D.- Particles resulting from cyclic filter washing

E.- Input of photocatalysts
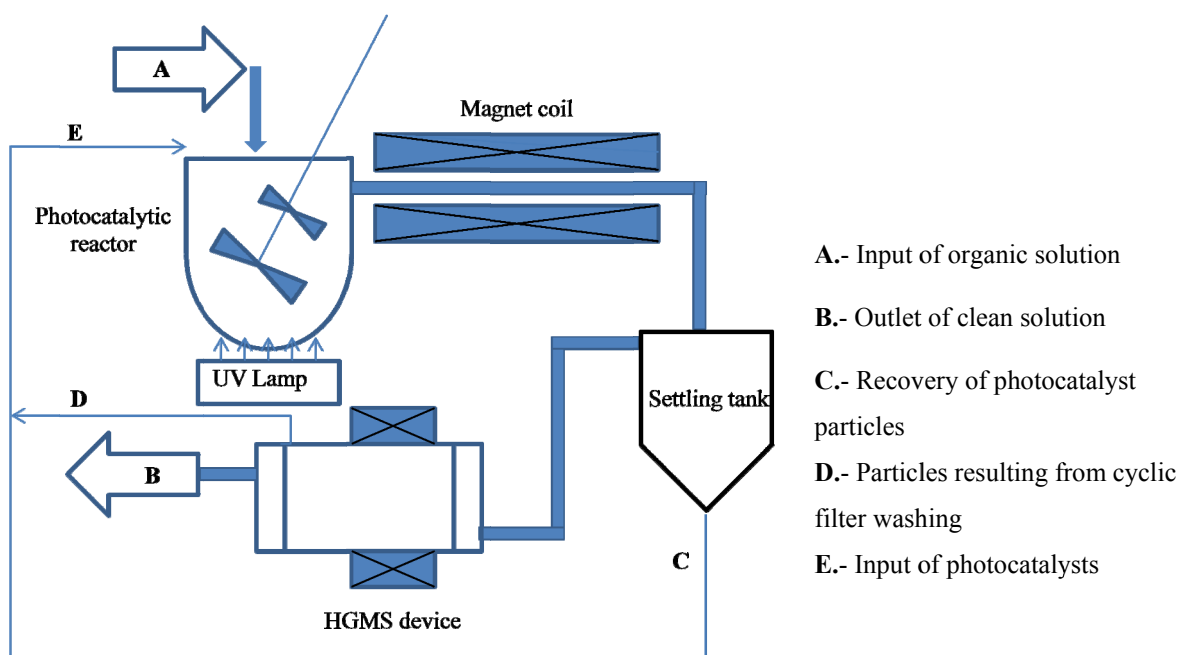
Figure 5.10: Illustration of a separation system by using a high gradient magnetic separation (HGMS).

5.2 Investigation of Adsorption

5.2.1 Adsorption of benzoic acid

The adsorption isotherms of benzoic acid onto F/T and F/S/T photocatalysts are shown in Figure 5.11. The Langmuir relationship has been applied for evaluation of the equilibrium data (see Table 3.2).

The representation of the reciprocals of q_e and C_e in the Langmuir isotherm is a straight line. From the intersection with the ordinate axis, it can be deduced the maximum adsorption capacity (q_{max}) and from the slope the coefficient K_L, which represents the equilibrium constant of the adsorption. This constant is related to the affinity of the adsorbent towards the adsorbate.
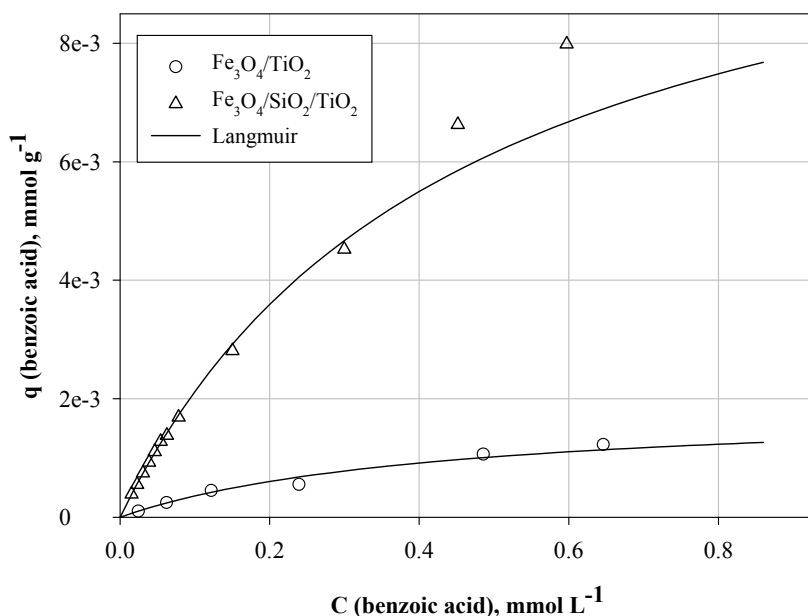
Figure 5.11: Adsorption isotherm of benzoic acid with F/T and F/S/T. T=25°C; pH=4.8; Catalyst=4 g L^{-1}.

Figure 5.12 shows a linear regression of q_e^{-1} versus C_e^{-1}. From the plot of q_e^{-1} as a function of C_e^{-1} the following data was obtained; q_{max}=0.0018 mmol g^{-1} and K_L=2.34 L mmol^{-1} using F/T; q_{max}=0.0117 mmol g^{-1} and K_L=2.207 L mmol^{-1} using F/S/T. Considering the maximum adsorption capacity per unit of surface area (q_{max}/A) and q_{max} values, the adsorption capacity of F/S/T was observed to be higher than that of F/T. The linear regression coefficients for the different particles are shown in the Table 5.7.

54

The experimental data can be adequately described by the Langmuir relationship with high correlation coefficients.
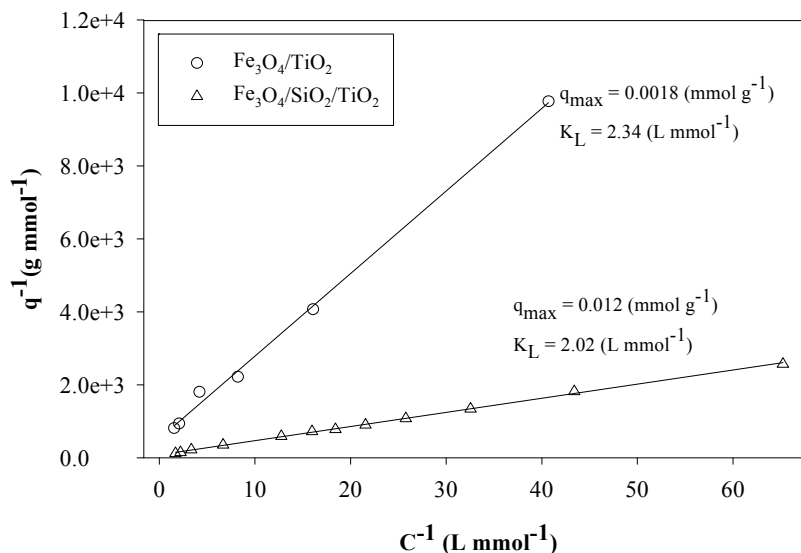
Figure 5.12: Linearization form of Langmuir isotherm of benzoic acid with (o) F/T and (Δ) F/S/T photocatalysts.

Table 5.7: Equilibrium parameters for sorption of benzoic acid.

Particle	q_{max} (mmol g^{-1})	q_{max} / A (mmol m^{-2})	K_L (L mmol^{-1})	R^2
Fe_3O_4/TiO_2 (F/T)	1.8×10^{-3}	6.94×10^{-6}	2.34	0.997
$Fe_3O_4/SiO_2/TiO_2$ (F/S/T)	1.2×10^{-2}	3.85×10^{-5}	2.02	0.999

Many others adsorbents have been used for the adsorption of benzoic acid. The results of those studies have shown adsorption capacities significantly higher than the values obtained using F/T and F/S/T particles. For example, the high area activated carbon cloth has a q_{max} of 2.97 mmol g^{-1}; the commercial activated carbon has a q_{max} of 1.48 mmol g^{-1} (Ayranci and Duman 2006); the granular activated carbon (Taipei Chemical Corp., Taiwan) has a q_{max} of 18.94 mmol g^{-1} (Chern and Chien 2001). From those investigations it can be deduced that the benefits of the synthesized particles are related to its photocatalytic activity and not to the adsorptive capacity.

5.2.2 Adsorption of methyl orange

Figure 5.13 shows isotherms for the adsorption of methyl orange onto F/T and F/S/T photocatalysts. The relationship between q_e and C_e is almost linear at low concentrations of methyl orange; concentrations lower than 0.026 mmol L^{-1} in the case of F/S/T, and for concentration lower than 0.0053 mmol L^{-1} using F/T.
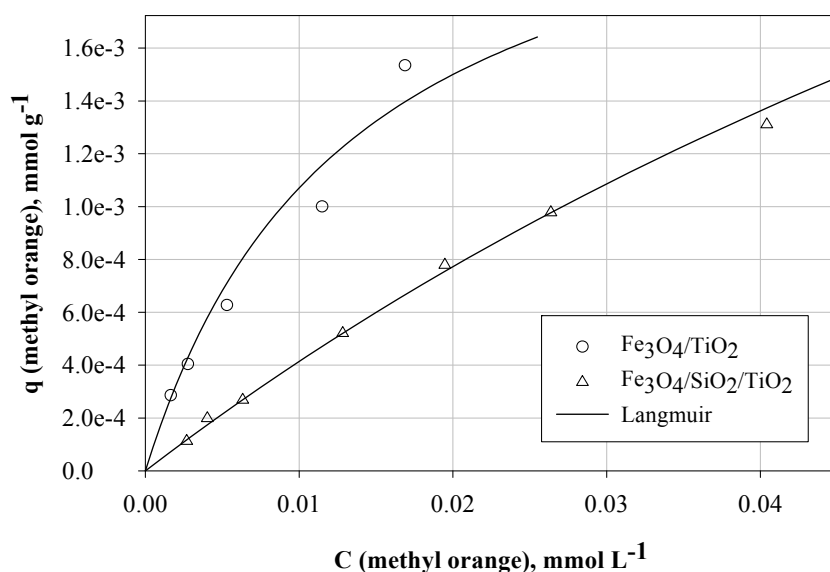
Figure 5.13: Adsorption isotherm of methyl orange with F/T and F/S/T. T=25°C; pH=3.7; Catalyst=4 g L^{-1}.

Values of q_{max} and C_e obtained by means of the application of a Langmuir relationship are summarized in Table 5.8. Comparing the results of both photocatalysts it can be observed that F/S/T has a q_{max} and q_{max}/A approximately 2.2 and 1.9 times higher than q_{max} and q_{max}/A obtained for F/T respectively, regarding to K_L values it was seen that K_L for F/T was approx. 9.5 times higher than the value obtained for F/S/T.

Table 5.8: Equilibrium parameters for sorption of methyl orange.

Particle	q_{max} (mmol g^{-1})	q_{max}/A (mmol m^{-2})	K_L (L $mmol^{-1}$)	R^2
Fe_3O_4/TiO_2 (F/T)	2.5×10^{-3}	9.65×10^{-6}	74	0.987
$Fe_3O_4/SiO_2/TiO_2$ (F/S/T)	5.7×10^{-3}	1.83×10^{-5}	7.7	0.999

5.2.3 Adsorption of SRB

Figure 5.14 shows the adsorption isotherms of SRB onto F/T and F/S/T photocatalysts. It can be observed for both photocatalysts the q_{max} values were similar being 6.5×10^{-4} mmol g^{-1} for F/S/T and 7.0×10^{-4} mmol g^{-1} for F/T, the same behaviour was found for the values of q_{max}/A. The K_L value obtained for the F/T material was 2.5 times higher compared to the F/S/T material (see Table 5.9).
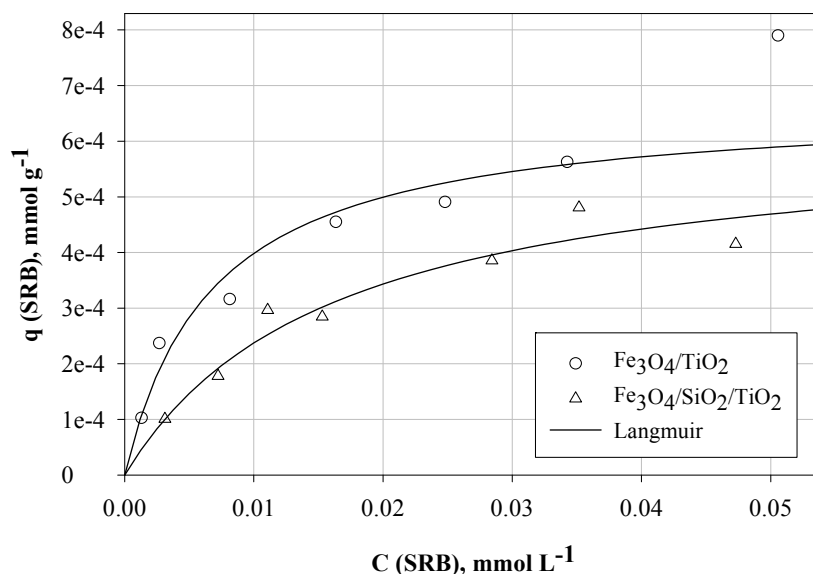
Figure 5.14: Adsorption isotherms of SRB onto both F/T and F/S/T photocatalysts. T=25°C; pH=3.5; Catalyst=4 g L^{-1}.

Figure 5.15 shows the influence of pH on the adsorption capacity of SRB onto F/S/T. The q_{max} values obtained at pH 3.5 and pH 5.4 are 6.5×10^{-4} and 8.0×10^{-4} respectively. The Langmuir constant, K_L, at pH 3.5 the value is approximately 2 times higher than the value obtained at pH 5.4 (see Table 5.9). At pH 2.5, the q values are higher in comparison to those obtained at pH 3.5 and 5.4. This is probably due to the greatest positive potential of the particle surface at this pH.
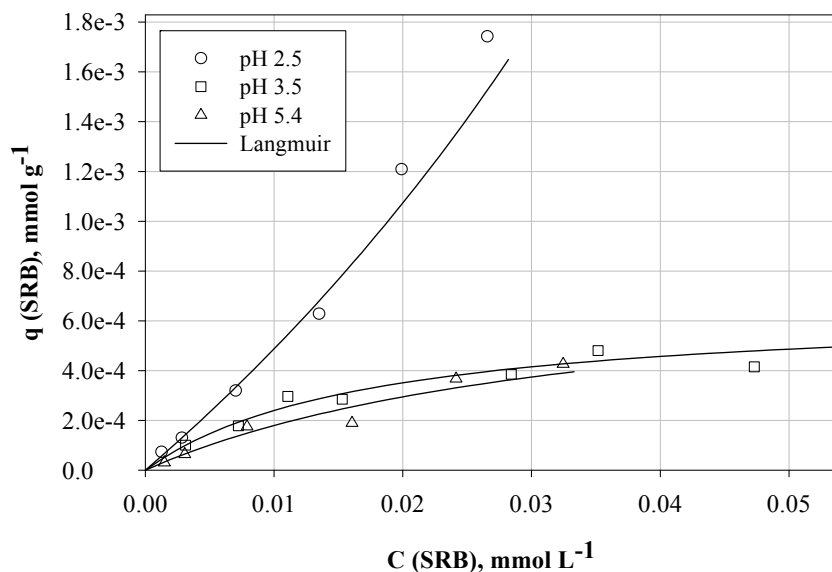
Figure 5.15: pH influence on the adsorption of SRB onto F/S/T photocatalyst. T=25°C; Catalyst=4 g L^{-1}.

Figure 5.16 shows the influence of pH on the adsorption capacity of SRB onto F/T. The results were similar to those obtained for the adsorption of SRB onto F/S/T (see Figure 5.15). The maximal adsorption capacity, q_{max}, at pH 3.5 and pH 5.4, was 7.0 x 10^{-4} and 5.4 x 10^{-4} respectively. The Langmuir constant, K_L, at pH 3.5 was 1.5 times higher compared to the value obtained at pH 5.4 (see Table 5.9). At pH 2.5, as in the case of the F/S/T material, the q values are higher than at pH 3.5 and 5.4.

As noted in the Table 5.9, it is shown that the values of q_{max} as well as q_{max}/A for both the F/T and F/S/T materials are very similar and cannot distinguish a clear difference between them. The Langmuir constant, K_L, follows a similar trend and the values obtained for F/T material were higher than the values obtained for F/S/T. For both materials at pH 3.5 the highest values of K_L were obtained and also in both cases the isotherms at pH 2.5 were slightly unfavorable.
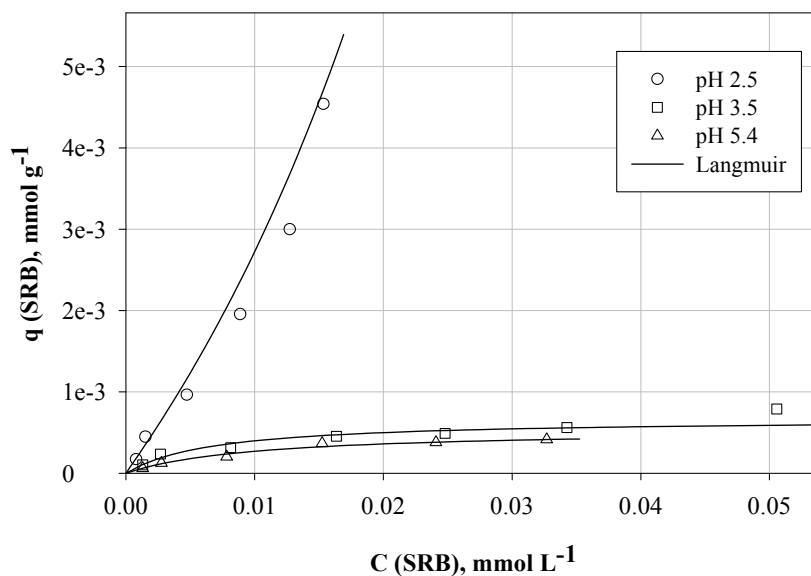
Figure 5.16: pH influence on the adsorption of SRB using F/T. T=25°C; Catalyst=4 g L^{-1}.

Table 5.9: Equilibrium parameters for sorption of SRB.

Particle	pH	q_{max} (mmol g^{-1})	q_{max} / A (mmol m^{-2})	K_L (L mmol^{-1})	R^2
Fe$_3$O$_4$/TiO$_2$ (F/T)	2.5	-	-	-	-
Fe$_3$O$_4$/TiO$_2$ (F/T)	3.5	7.0 x 10^{-4}	2.7 x 10^{-6}	147	0.967
Fe$_3$O$_4$/TiO$_2$ (F/T)	5.4	5.4 x 10^{-4}	2.1 x 10^{-6}	99	0.993
Fe$_3$O$_4$/SiO$_2$/TiO$_2$ (F/S/T)	2.5	-	-	-	-
Fe$_3$O$_4$/SiO$_2$/TiO$_2$ (F/S/T)	3.5	6.5 x 10^{-4}	2.1 x 10^{-6}	57	0.985
Fe$_3$O$_4$/SiO$_2$/TiO$_2$ (F/S/T)	5.4	8.0 x 10^{-4}	2.6 x 10^{-6}	28	0.974

The adsorption isotherms of the model compounds such as benzoic acid, methyl orange and sulforhodamine B (SRB) can be adjusted to the Langmuir isotherm.

The pH influence is based on the change of the polarity of the catalyst surface. Benzoic acid, methyl orange and SRB are preferably adsorbed at low pH values, because in the pH range studied (pH$_{BA}$=4.8, pH$_{MO}$=3.7 and pH$_{SRB}$=2.5-5.4) the organic compounds are negatively charged, and since the F/T and F/S/T particles at pH < 6.0 and pH < 6.4 respectively are positively charged.

5.3 Investigation of the Photooxidation

5.3.1 Oxidation of benzoic acid
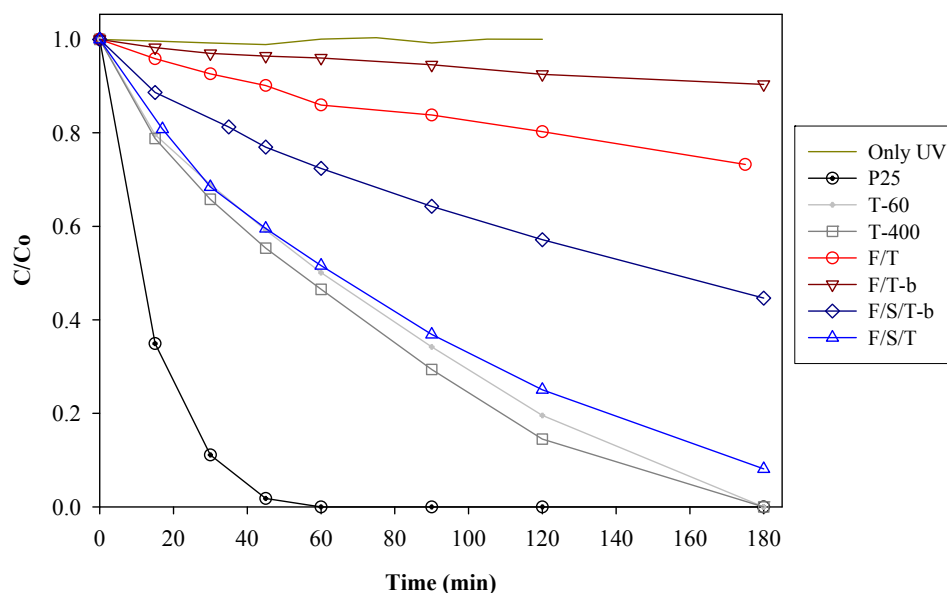
Figure 5.17: Oxidation of BA by using different materials. Catalyst=0.5 g L^{-1}; pH=4.8, C_{BA}=0.25 mmol L^{-1}; T=25°C; I_{UV}=20 mW cm^{-2}.

Figure 5.17 shows the oxidation of benzoic acid by using various photocatalysts under UV irradiation. To obtain relevant information about the photocatalytic degradation, it was necessary to carry out experiments from which direct photolysis was excluded. As seen in Figure 5.17 no disappearance of benzoic acid was observed in the absence of photocatalyst under UV irradiation. P25 TiO$_2$ used as a reference material showed the best photocatalytic performance to degrade benzoic acid; within the first 60 min of UV irradiation a complete degradation was reached. Excluding the P25 TiO$_2$, as expected the synthesized TiO$_2$, T-60 and T-400, have shown among the materials the best photocatalytic performance and between them T-400 shows the best result. This is consistent with the fact that the structure of T-400 has a greater amount of crystal phase than T-60, and this is directly related to the performance in the photooxidation. Among the materials with magnetic properties, F/S/T and F/S/T-b have shown the best results for the photooxidation of benzoic acid reaching values of 92% and 56% of degradation respectively. The difference in the degradation percentage is due to the degree of crystallinity of TiO$_2$ in the material, being much higher in F/S/T than in F/S/T-b. Finally F/T and F/T-b showed the lowest responses in the photooxidation experiment, reaching at 180

60

min of UV irradiation only a 27% and 10% of degradation respectively. Due to the different mass percentage and amorphous nature of TiO_2 present in both materials the results were expected to be as shown in Figure 5.17. However it should be pointed out that these materials have shown the best response for the solid/liquid magnetic separation due to the mass percentage of Fe_3O_4 present in both.

On the basis of the results shown in Figure 5.17, a linear dependence of $\ln(C_0/C)$ on irradiation time was obtained for all the materials used. In this case the simplified kinetic equation that describes the process is:

$$r = -\frac{dC}{dt} = k_{app}C$$
Eq. 5.3

k_{app}, apparent first-order reaction rate constant and C, the concentration of substrate in each moment when $t > 0$.

Integration of Eq. 5.3 will lead to a linear plot of $\ln(C_0/C)$ versus time with a slope of k_{app} the apparent rate constant (see Eq. 5.4).

$$\ln(C_0 / C) = k_{app}t$$
Eq. 5.4

where, C_0, initial organic concentration and, t, irradiation time.
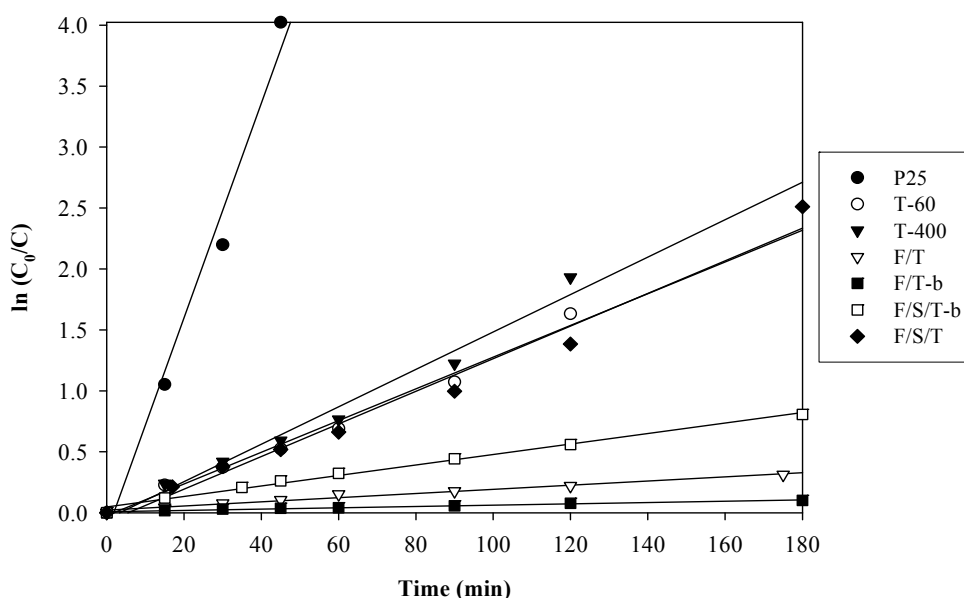
Figure 5.18: Apparent first-order linear transform $\ln(C_0/C)$ vs. time by using different materials. Catalyst=0.5 g L^{-1}; pH=4.8, C_{BA}=0.25 mmol L^{-1}; T=25°C; I_{UV}=20 mW cm^{-2}.

Table 5.10: Pseudo-first-order apparent constant values.

Particle	k_{app} (min^{-1})	R^2
P25	0.0881	0.981
T-60	0.0130	0.987
T-400	0.0154	0.981
F/T	0.0017	0.981
F/T-b	0.0005	0.978
F/S/T-b	0.0043	0.981
F/S/T	0.0127	0.981

The values of k_{aap} are in agreement with the behaviour of the materials showed in Figure 5.17. Among the materials P25 TiO$_2$ showed the highest k_{aap} value in contrast to F/T-b which showed the lowest value. The correlation coefficients (R^2) suggest that Eq. 5.4 can be used as a proper description for the different materials at the conditions used.

To investigate the photocatalytic degradation of benzoic acid the experiments were carried out in the photocatalytic system previously mentioned (see section 4.5). In these experiments, the photocatalysts F/S/T and F/T were used. The effect of the following parameters was observed; amount of catalyst, concentration of benzoic acid, pH and temperature. The light intensity (λ=315-400 nn) of 20 mW cm^{-2} was kept constant for all the measurements (see section 4.5.1).

5.3.1.1 Influence of the amount of catalyst

To determine the dependence of the oxidation with respect to the catalyst amount, experiments have been conducted with different amounts of F/S/T (0.003 to 1.0 g L^{-1}). Figure 5.19 shows a representation of the concentration of benzoic acid plotted as C/Co versus time.
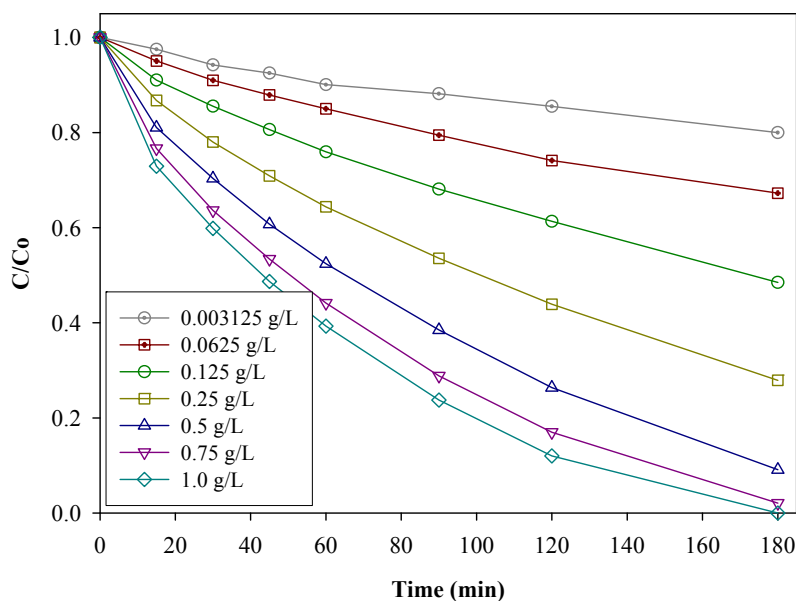
Figure 5.19: Influence of the amount of F/S/T photocatalyst. C_{BA}=0.25 mmol L^{-1}; pH=4.8; T=25°C; I_{UV}=20 mW cm^{-2}.

It is shown in Figure 5.19 that an increase in the amount of catalyst leads to an increase in the degradation rate of BA, reaching a 100% of degradation within 180 min using 1.0 g L^{-1} of catalyst. The increment of catalyst amount only until 0.5 g L^{-1} is significant, above this value there is not much improvement in the degradation rate of BA.

Figure 5.20 shows the influence of the amount of F/T photocatalyst used for the oxidation of BA. Similar to Figure 5.19, it is noted that at greater amounts of F/T the concentration of BA decreased. At 0.75 g L^{-1} a maximal degradation rate for BA on F/T was found. For F/T amounts above 0.75 g L^{-1} the degradation rate is reduced, this can be attributed to the shielding effect of the suspended F/T particles hindering the penetration of light.
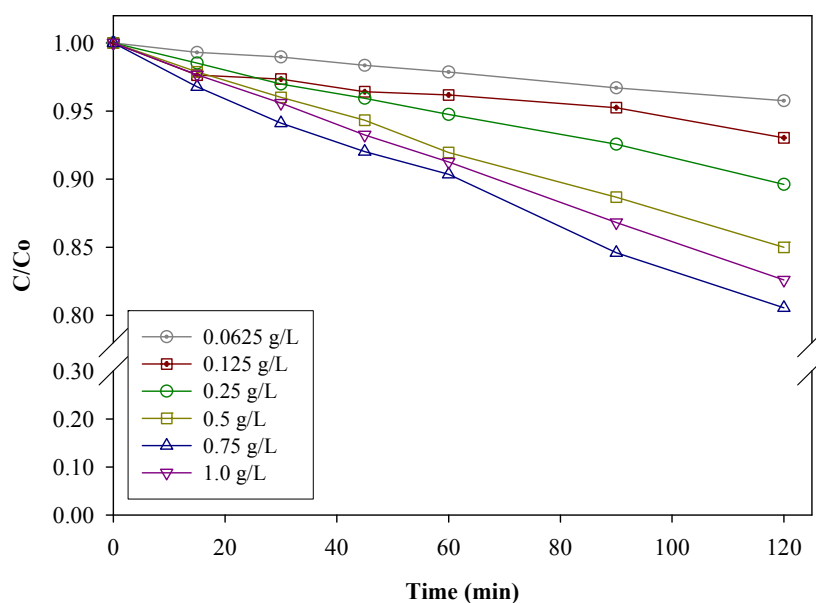
Figure 5.20: Influence of the amount of F/T photocatalyst. C_{BA}=0.25 mmol L^{-1}; pH=4.8; T=25°C; I_{UV}=20 mW cm^{-2}.

The degradation of benzoic acid on different amounts of catalyst was also subjected to kinetic analysis. The data for F/S/T and F/T were subjected to pseudo-first-order kinetics, which in its usual form is given by Eq. 5.4. The apparent rate constant and correlation values for various amounts of catalyst are given in Table 5.11.

Table 5.11: Pseudo-first-order apparent constant and correlation values.

F/S/T			F/T		
k_{app} (min^{-1})	Catalyst (g L^{-1})	R^2	k_{app} (min^{-1})	Catalyst (g L^{-1})	R^2
0.0012	0.03125	0.998	0.0004	0.0625	0.998
0.0024	0.0625	0.995	0.0005	0.125	0.903
0.004	0.125	0.992	0.0009	0.25	0.997
0.0067	0.25	0.996	0.0013	0.5	0.999
0.0107	0.5	0.997	0.0018	0.75	0.996
0.0143	0.75	0.996	0.0016	1.0	0.999
0.0169	1.0	0.991			

Figure 5.21 shows the k_{app} values (min^{-1}) as a function of catalyst mass. A comparison between the two photocatalysts was obtained from <u>Table 5.11</u>. The dependence of the amount of catalyst on the k_{app} values follows a similar relationship found as $(C_{cat})^n$.
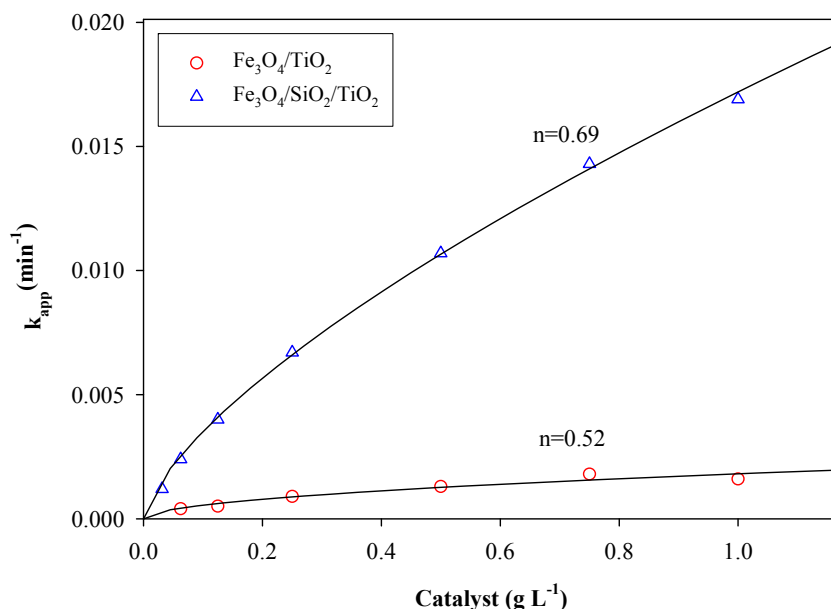
Figure 5.21: Comparison of the photooxidation of BA. Influence of the amount of catalyst. C_{BA}=0.25 mmol L^{-1}; pH=4.8; T=25°C; I_{UV}=20 mW cm^{-2}.

The k_{app} values increase proportionally to a function $(C_{cat})^n$ with the mass of catalyst. This indicates a true heterogeneous photocatalytic regime. For low amounts of catalyst, it can be observed that the k_{app} increases rapidly with the amount of catalyst, because most of the photocatalyst is irradiated by light. However, above a certain amount of catalyst, the rising became fairly smooth, because there is a shielding effect and not all the catalyst is used. In the case of an amount of the F/T = 0.5 g L^{-1} the value of k_{app} is about 1.3 x 10^{-3} min^{-1} and for an amount of F/S/T = 0.5 g L^{-1} the value is approximately 1.1 x 10^{-2} min^{-1}. The k_{app} value of F/T photocatalyst was about 8.5 times slower than for F/S/T.

5.3.1.2 Influence of the concentration of benzoic acid

The relative concentration of benzoic acid was studied as a function of the initial benzoic acid concentration in the range 0.04 to 0.63 mmol L^{-1}, for an amount of 0.5 g L^{-1} of F/S/T. The results are reported in Figure 5.22.
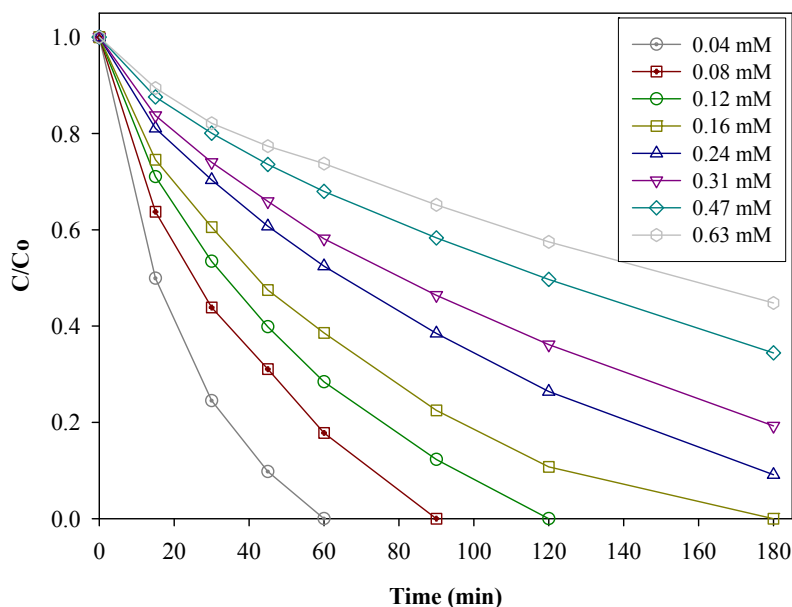
Figure 5.22: Influence of the BA concentration using F/S/T. Catalyst=0.5 g L^{-1}; pH=4.8; T=25°C; I_{UV}=20 mW cm^{-2}.

It is evident that the initial concentration of benzoic acid has a pronounced effect on the rate of the photooxidation; for the same irradiation time the remaining fraction of the initial concentration increases strongly for higher initial concentration.

Figure 5.23 shows the relative concentration of benzoic acid as a function of its initial concentration in the range 0.04 to 0.60 mmol L^{-1}, for an amount of 0.5 g L^{-1} of F/T. As in the Figure 5.22, the values of relative concentration decreased slowly at higher initial concentrations of benzoic acid, however, the values of relative concentration reached for a determined time are markedly higher than in the previous case, e.g., for a concentration of 0.04 mmol L^{-1} the value of relative concentration reached after 60 min of irradiation using F/T was 0.75 and using F/S/T was zero.
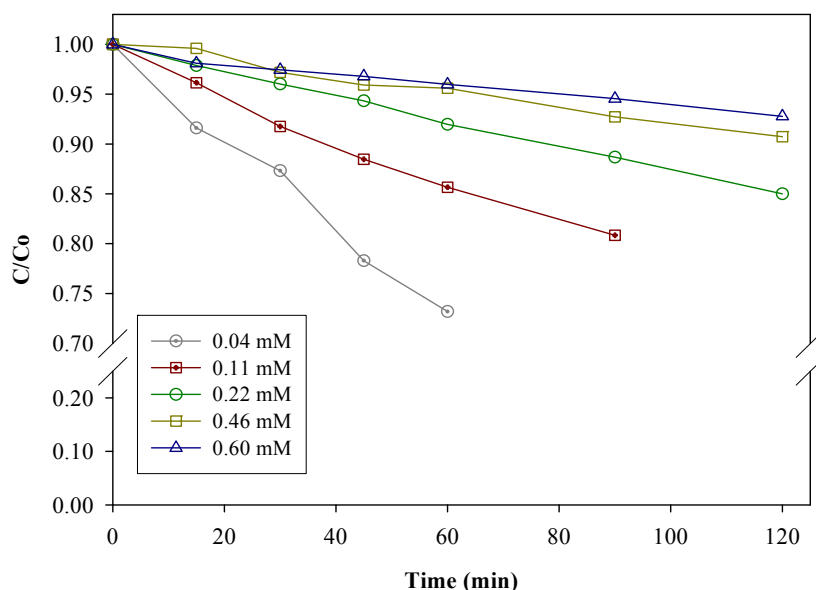
Figure 5.23: Influence of the BA concentration using F/T. Catalyst=0.5 g L^{-1}; pH=4.8; T=25°C; I$_{UV}$=20 mW cm^{-2}.

It should be noted that, unlike the relative concentration decreased, the efficiency of the process in terms of mass of benzoic acid degraded increased at higher initial concentrations. E.g., in the case of F/S/T (see Figure 5.22), the amount of benzoic acid degraded after 60 min of irradiation was observed to be 0.04 and 0.16 mmol L^{-1} at 0.04 and 0.63 mmol L^{-1} initial concentrations, respectively. In the case of F/T (see Figure 5.23), the amount of benzoic acid degraded after 60 min of irradiation was 0.010 and 0.024 mmol L^{-1} at 0.04 and 0.60 mmol L^{-1} initial concentrations, respectively.

The degradation kinetic was evaluated by noting the degradation rate of benzoic acid (r$_{BA}$) as determined from the variation of BA concentration within the first 30 min irradiation time.

Figure 5.24 shows the influence of the concentration of benzoic acid on the degradation rate on the both F/T and F/S/T materials based on the data of Figure 5.22 and Figure 5.23.

The kinetic results indicated that the r$_{BA}$ increased from 9.9 x 10^{-4} to 2.7 x 10^{-3} mmol L^{-1} min^{-1} when the concentration increased from 0.04 to 0.31 mmol L^{-1} for F/S/T; and from 1.6 x 10^{-4} to 4.3 x 10^{-4} mmol L^{-1} min^{-1} when the concentration increased from 0.04 to 0.46 mmol L^{-1} for F/T. A further increase in the BA concentration, led to a slight increases in the r$_{BA}$ for both photocatalysts; by using F/S/T to 3.7 x 10^{-3} at 0.63 mmol L^{-1} and by using F/T to 5.2 x 10^{-4} mmol L^{-1} min^{-1} at 0.6 mmol L^{-1}.
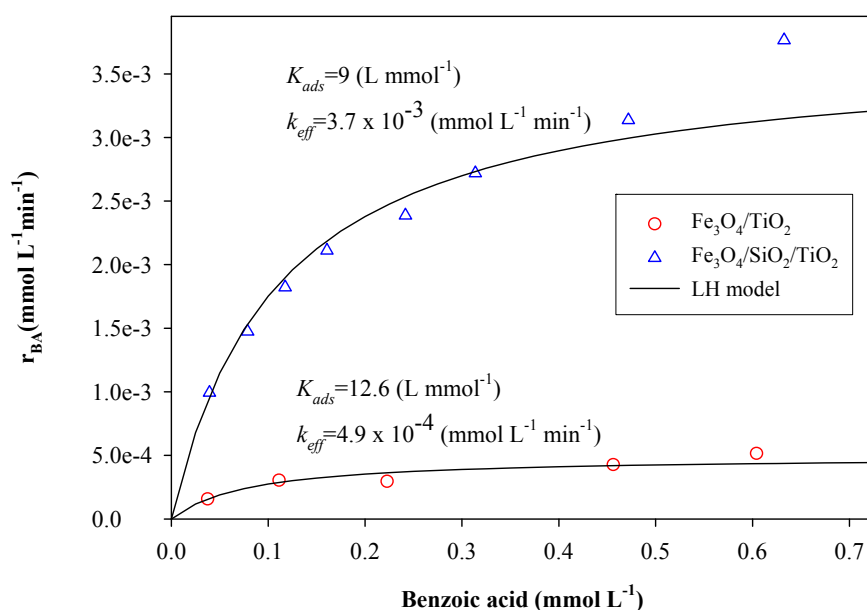
Figure 5.24: Comparison of the photooxidation of BA. Influence of BA concentration. Catalyst=0.5 g L^{-1}; pH=4.8; T=25°C; I$_{UV}$=20 mW cm^{-2}.

Figure 5.24 indicates that at low concentrations of benzoic acid the degradation rate increases as the concentration of benzoic acid is increased, where at higher concentrations a plateau was reached.

The Langmuir-Hinshelwood expressions has been successfully used for determining the relationship between the degradation rate and the concentration of the organic substrate for reactions which take place at the solid-liquid interface within the heterogeneous photocatalytic processes and is expressed by the Eq. 3.23.

The plot of the reciprocal rate r$_{BA}$ as a function of the reciprocal of the concentration C, shown in the Eq. 3.24, yields for constant particle dosage of F/T and F/S/T at 0.5 g L^{-1} a straight line (see Figure 5.25), confirming the Langmuir-Hinshelwood relationship for the rates of degradation. The k_{eff} and K_{ads} values were calculated according to Eq. 3.24 from the slope of each straight line and from the intercept with the r$_{BA}$$^{-1}$ axis were, in the case of F/S/T, k_{eff}=3.7 x 10^{-3} mmol L^{-1} min^{-1} and K_{ads}=9 L mmol^{-1} and, respected in the case of F/T, k_{eff}=4.9 x 10^{-4} mmol L^{-1} min^{-1} and K_{ads}=12.6 L mmol^{-1}.

Figure 5.25: Comparison of the photooxidation of BA. Influence of BA concentration. Catalyst=0.5 g L^{-1}; pH=4.8; T=25°C; I$_{UV}$=20 mW cm^{-2}.

Some researchers have reported that for many organic compounds the adsorption constants obtained from the equilibrium in dark are different from those obtained by means of the Langmuir-Hinshelwood model (Parra, Olivero et al. 2002).

The K_{ads} values obtained for the photocatalytic degradation of benzoic acid for both F/T and F/S/T by means of the Langmuir-Hinshelwood model have been 5.4 and 4.5 times greater than those obtained for K$_L$ measured in the dark, respectively (see Table 5.7). These results are consistent with those reported by other authors, where the adsorption constant K_{ads}, determined in the photocatalytic degradation experiments have always shown higher values than the adsorption values measured in the dark (Parra, Olivero et al. 2002).

The difference of the adsorption constants in the two cases may be related to changes in the adsorbing sites onto the catalyst surface under UV irradiation and competitive adsorption among reaction products. The possibilities of significant photoadsorption and/or occurring of reaction steps in the double layer may also contribute to such observations. Furthermore, studies have shown that the adsorption constant K_{ads} is a function of the light intensity and the electronic properties of the TiO$_2$ surface and can undergo dramatic changes upon irradiation, altering the adsorption sites (Xu and Langford 2000).

Summarizing the investigated dependencies it is known that the reaction rate depends on the factors that influence the photocatalytic process (initial concentration, catalyst mass,

temperature, UV intensity, pH ...). Taking into account the concentration of organic and the amount of catalyst the follow equation was deduced:

$$r = k^0 \times \frac{K_{ads} C_B}{1 + K_{ads} C_B} \times \left(\frac{C_{cat}}{g / L} \right)^n$$

Eq. 5.5

C_B = organic concentration in bulk solution (mmol L^{-1}).

C_{cat} = catalyst mass (g L^{-1}).

n = constant value obtained from the function $(C_{cat})^n$ for each catalyst.

K_{ads} = adsorption equilibrium constant (L mmol^{-1}).

k^0 could be interpreted as the degradation rate at given pH, temperature and catalyst dosage C_{cat}=1 g L^{-1}, when the surface of the catalyst is saturated with the organic compound.

Compared with Eq. 5.5 one finds:

$$k_{eff} = k^0 \times \left(\frac{C_{cat}}{g / L} \right)^n$$

Eq. 5.6

The experimental data reported in Figure 5.21 and Figure 5.24 were used in Eq. 5.6 to obtain the value of k^0. The results are summarized in Table 5.12. As noted, the k^0 value for F/S/T is approximately 8.5 times higher than for F/T.

Table 5.12: Parameter values for the reaction rate of benzoic acid.

Particle	n	k_{eff} (mmol L^{-1} min^{-1})	k^0 (mmol L^{-1} min^{-1})
Fe$_3$O$_4$/TiO$_2$ (F/T)	0.52	4.9 x 10^{-4}	7.02 x 10^{-4}
Fe$_3$O$_4$/SiO$_2$/TiO$_2$ (F/S/T)	0.69	3.7 x 10^{-3}	5.97 x 10^{-3}

5.3.1.3   Influence of pH

The results of the effect of the pH on the efficiency of the photocatalytic process of benzoic acid by F/S/T are shown in Figure 5.26.
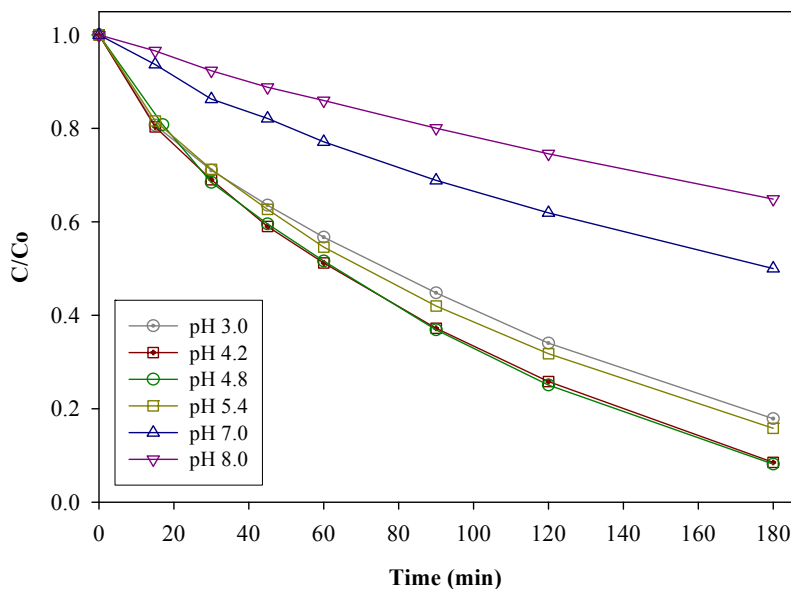
Figure 5.26: pH effect using F/S/T. Catalyst=0.5 g L^{-1}; C_{BA}=0.25 mmol L^{-1}; pH=4.8; T=25°C; I_{UV}=20 mW cm^{-2}.

The range of pH varied from acidic conditions (pH 3.0) to alkaline conditions (pH 8.0). A rapid degradation of benzoic acid at pH values of 4.2 and 4.8 was observed.

Figure 5.27 shows the effect of the pH on the relative concentration of BA using F/T. As in the previous case, the pH values varied from acidic conditions (pH 3.0) to alkaline conditions (pH 8.0), where the fastest degradation was reached at pH 4.8.
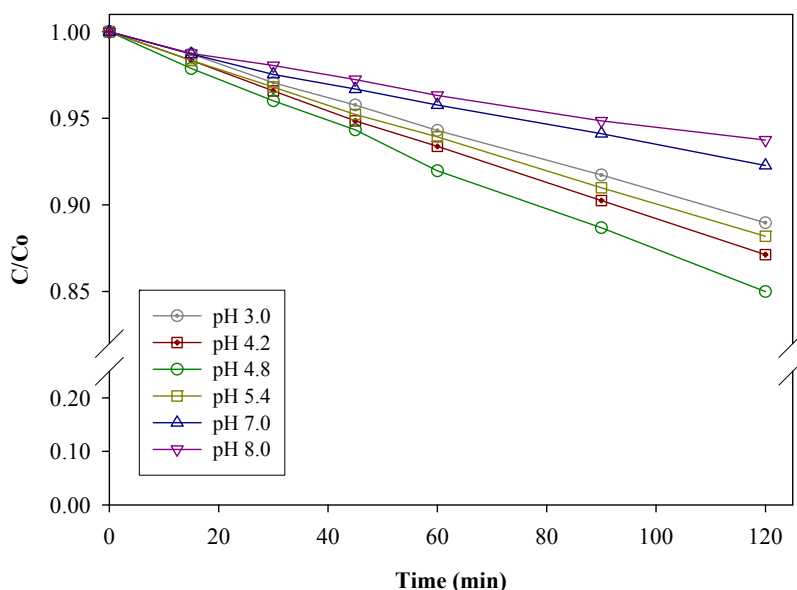
Figure 5.27: Effect of pH using Fe_3O_4/TiO_2. Catalyst=0.5 g L^{-1}; C_{BA}=0.25 mmol L^{-1}; pH=4.8; T=25°C; I_{UV}=20 mW cm^{-2}.

The influence of pH on the apparent first-order reaction rate constant is shown in the Figure 5.28. By means of the evaluation of the data obtained from Figure 5.26 and Figure 5.27 with the application of the pseudo-first-order kinetic model (see Eq. 5.4) the k_{app} values were deduced.

In both cases, either using F/T or F/S/T, the pH has a similar effect on the apparent first-order reaction rate constant values. For both materials k_{app} reaches maximum values at pH 4.8, where for F/S/T the absolute value is approximately 8.6 times higher than for F/T.

Titanium dioxide exhibits an amphoteric character when suspended in water, so that either a positive or a negative charge can be developed on its surface (Kosmulski 2002). The point of zero charge $pH_{(PZC)}$ for F/T and F/S/T were 6.0 and 6.4 respectively (see Figure 5.8). At pH values below the $pH_{(PZC)}$, the surface is positively charged and the surface is negatively charged at pH values above the $pH_{(PZC)}$. Benzoic acid is a weak acid with a pK_a of 4.2, once dissolved in water it exist partly in its anionic state and, at pH values above the pK_a the percentage of its anionic state is higher, therefore, an electrostatic attraction is expected to develop between the benzoic acid and the positively charged catalyst at pH values below 6 and 6.4 for F/T and F/S/T respectively.

The extent of substrate adsorption onto the catalyst would be then favored at 4.2 < pH < 6.0 for F/T and at 4.2 < pH < 6.4 for F/S/T which is consistent with the results obtained. On the other hand, at pH values above 6.0 and 6.4 for F/T and F/S/T respectively, the surface of catalyst is negatively charged, and the substrate is negatively charged too, therefore, the adsorption should be very low, due to electrostatic repulsion. Again this is consistent with the results obtained, since above these pH values the lowest initial degradation rates are obtained. At pH < 4.2 a reduction of the initial degradation rate was also observed, probably due to a major decrease of the available active centers on the catalyst surface, which in turn causes a reduction on the adsorbed photon.
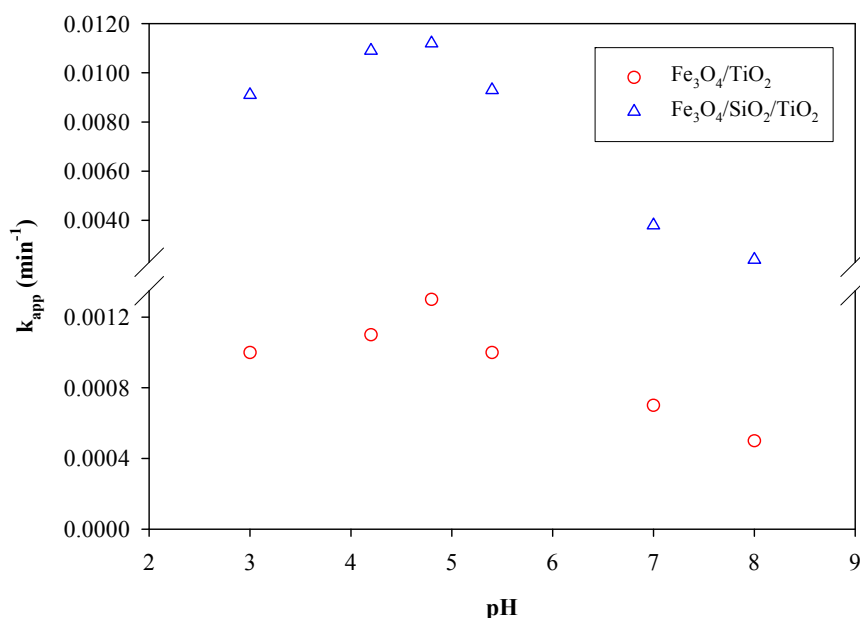
Figure 5.28: Influence of pH on the photooxidation of BA by using F/T and F/S/T materials. Catalyst=0.5 g L^{-1}; C_{BA}=0.25 mmol L^{-1}; pH=4.8; T=25°C; I_{UV}=20 mW cm^{-2}.

5.3.1.4 Influence of temperature

The temperature influence onto BA degradation with both photocatalysts F/S/T and F/T was studied.

Figure 5.29 shows the temperature effect onto BA degradation by F/S/T plotted in the form of relative benzoic acid concentration versus time.
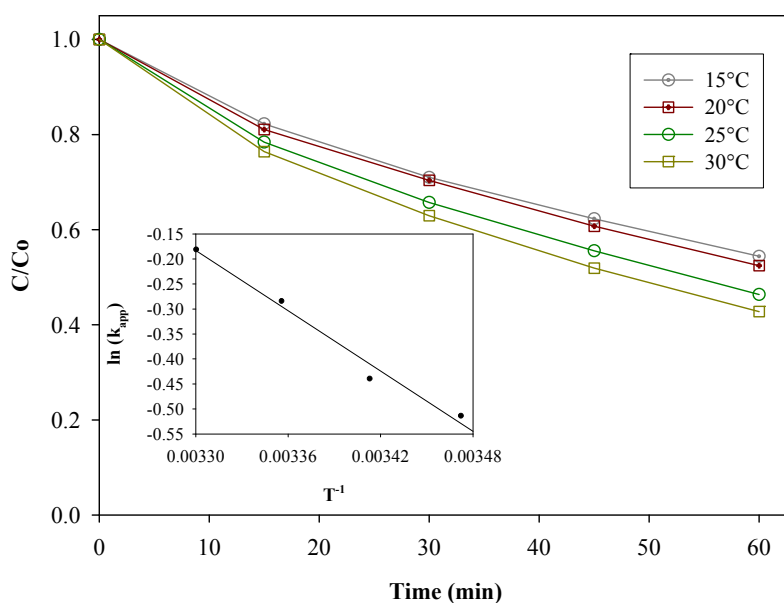
Figure 5.29: Effect of temperature in the degradation of BA by using F/S/T as photocatalyst. Catalyst=0.5 g L^{-1}; C_{BA}=0.25 mmol L^{-1}; pH=4.8; I_{UV}=20 mW cm^{-2}. In the insert: Plot of ln(k_{app}) vs 1/T.

The temperature was varied in the range of 15 to 30°C and although that the trend indicates that at higher temperature results in a greater decrease in the concentration of benzoic acid, the temperature has only a minor influence. E.g., between 25°C (standard temperature for the experiments) and 30°C for times up to 60 min was observed an increase in the degradation percentage of only a 4%. This can be attributed to the fact that in the formation of the hydroxyl radical, which occurs through activation of the catalyst with UV irradiation, thermal energy has a minor role (see section 3.4.1.5).

Figure 5.30 shows the temperature effect onto BA degradation by F/T plotted in the form of relative benzoic acid concentration versus time.
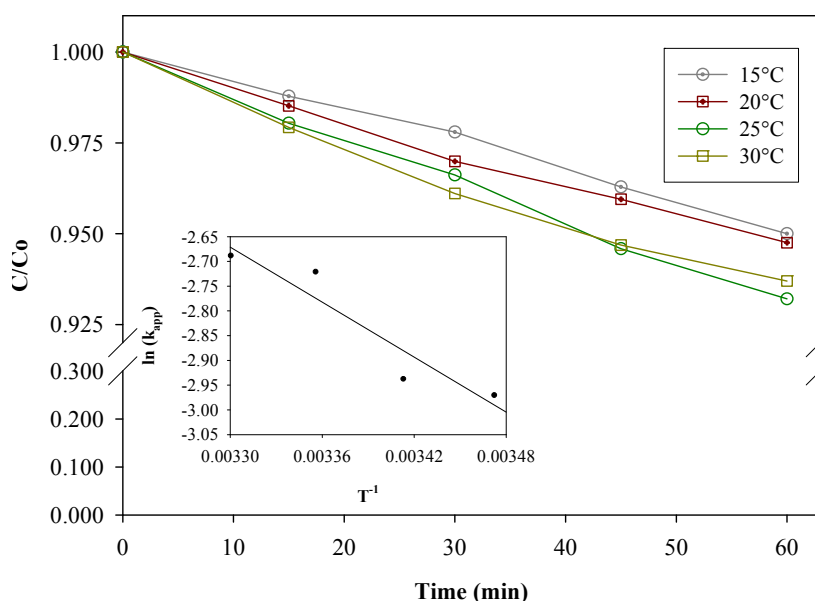
Figure 5.30: Effect of temperature in the degradation of BA by using F/T as photocatalyst. Catalyst=0.25 g L^{-1}; C_{BA}=0.24 mmol L^{-1}; pH=4.8; I_{UV}=20 mW cm^{-2}. In the insert: Plot of ln(k_{app}) vs 1/T.

As in the previous case there is small tendency to increase the degradation rate as the temperature increases but this effect plays a minor role.

The apparent activation energy (E_a) has been deduced by means of the Arrhenius equation (see Eq. 3.27) for both F/S/T and F/T photocatalyst.

The plot of ln(k_{app}) versus T^{-1}, which is shown in the insert of Figure 5.29 and Figure 5.30 for F/S/T and F/T photocatalysts, gives a straight line whose slope is equal to -E_a/R. From the data obtained, the E_a is 17 kJ mol^{-1} for F/S/T and 15 kJ mol^{-1} for F/T.

The overall process of photocatalysis is usually not very temperature sensitive. The low E_a values obtained for the two photocatalyst are comparable with the reported values by Chen (Chen and Ray 1998) that were in the range of 5-20 kJ mol^{-1}, therefore, the influence of temperature can be estimated as weak.

5.3.1.5 DOC mineralization

The degradation and mineralization of benzoic acid using different amounts of F/S/T particles is shown in Table 5.13. The experimental conditions were: C_{BA}=0.24 mmol L^{-1}; t=180; pH=4.8; I_{UV}=20 mW cm^{-2}. The percentages of degradation and mineralization were deduced according to the following equations:

% degradation = $100 \times (1 - C/C_0)$ Eq. 5.7

% mineralization = $100 \times (1 - DOC/DOC_0)$ Eq. 5.8

Table 5.13: Influence of the amount of catalyst on both degradation and mineralization of benzoic acid.

pH	$C_{F/S/T}$ (g L^{-1})	Degradation (%)	Mineralization (%)
4.8	0.25	72	41
4.8	0.5	91	64
4.8	1.0	100	90

It can be concluded that at higher amount of catalyst in the suspension, also the percentage of both degradation and mineralization is higher.

The degradation percentage of benzoic acid by using an amount of 0.25, 0.5 and 1.0 g L^{-1} of F/S/T particles was 72, 91 and 100%. However, only 41, 64 and 90% respectively was converted to CO_2; therefore, benzoic acid degradation is faster than its mineralization. This indicates that although a substantial portion of benzoic acid was mineralized, a fraction of the benzoic acid is converted to intermediates products as a consequence longer irradiation times are needed to achieve a complete mineralization.

The determination of DOC becomes an important analysis because it is very difficult to identify all the intermediary products that are involved in the mineralization process.

5.3.1.6 Reusability of photocatalyst

The reusability of the catalysts can be considered as a key point for the application of the photocatalysis technology in practical uses, being economically attractive. The reuse of both F/S/T and F/T was tested for the oxidation of benzoic acid; the results are shown in Figure 5.31 and Figure 5.32 respectively.
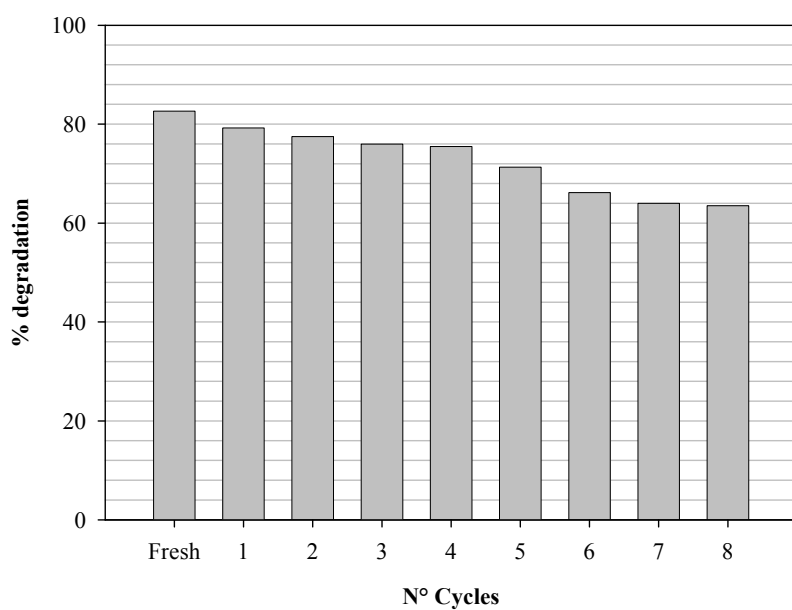
Figure 5.31: Degradation of BA with recycled F/S/T photocatalyst. Catalyst=0.5 g L^{-1}; C_{BA}=0.008 mmol L^{-1}; t=60 min; pH=4.8; T=25°C; I_{UV}=20 mW cm^{-2}.
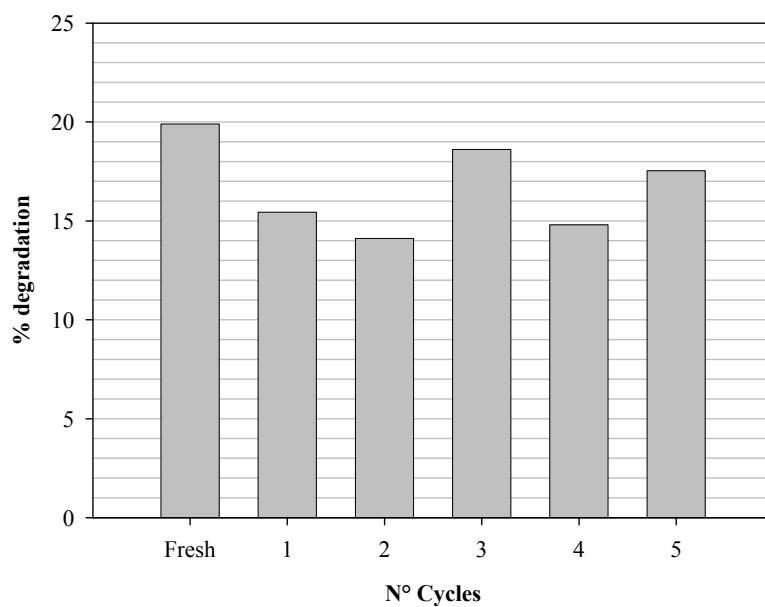
Figure 5.32: Degradation of BA with recycled F/T photocatalyst. Catalyst=0.5 g L^{-1}; C_{BA}=0.008 mmol L^{-1}; t=60 min; pH=4.8; T=25°C; I_{UV}=20 mW cm^{-2}.

F/S/T and F/T particles were repeatedly used for 8 and 5 cycles respectively. The photocatalytic activity of the photocatalyst weakened slowly when it was recycled. It can be

seen from Figure 5.31 that the degradation percentage of benzoic acid by using F/S/T was higher than 64% even after 8 cycles, which indicates that there is only a decrease of 23% in the degradation respect to the fresh one; this difference may be due to loss of catalyst in the recovery steps. By using F/T particles it was observed (see Figure 5.32) that after 5 cycles, the activity for degradation of benzoic acid still remained good, showing a decrease of only a 12% in the degradation at the fifth cycle. F/S/T presents a loss of 13% of the degradation respect to the fresh one at the fifth cycle, being comparable to loss of photoactivity degradation exhibited by F/T.

5.3.2 Oxidation of methyl orange

The absorption spectra of methyl orange at different pH are shown in Figure 8.2. Depending on the pH, methyl orange has two different maxima of absorption; at 467 nm for pH values above 4 and, at 505 nm for strong acid medium. In the range of 320 and 400 nm there is an absorbance between 7-15% (C_{MO}=0.014 mmol L^{-1}; pH=3.7).

5.3.2.1 Influence of the amount of catalyst

The influence of the amount of F/S/T photocatalyst on the relative concentration of methyl orange versus time was tested at pH 3.7 and is shown in Figure 5.33. The mass per volume of photocatalyst was in the range between 0.03125 and 1.0 g L^{-1}.
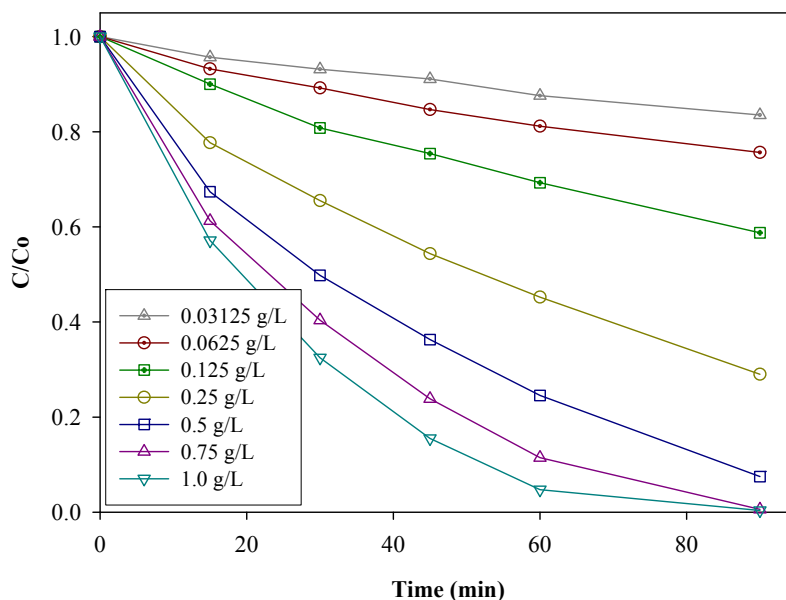
Figure 5.33: Influence of the amount of F/S/T photocatalyst. Influence of the amount of F/S/T photocatalyst. C_{MO}=0.014 mmol L^{-1}; pH=3.7; T=25°C; I_{UV}=20 mW cm^{-2}.

The results indicate that with an increase in the amount of catalyst an increase in the degradation also occurs, reaching a 100% of degradation at 90 min in both cases 0.75 and 1.0 g L^{-1}, while in the cases of 0.03125 and 0.0625 g L^{-1} less than 25% degradation was reached. This can be explained by the fact that a greater amount of catalyst results in a larger surface area available to adsorb the dye.

The relative concentration of methyl orange measured for different amounts of F/T photocatalyst is shown in Figure 5.34. The amounts of catalyst were in the range of 0.03125 and 1.0 g L^{-1}. As in the previous case, C/Co drops gradually as the amount of catalyst is increased from 0.03125 to 1.0 g L^{-1}. As can be seen for amounts of catalyst below 0.125 g L^{-1} less than 25% of degradation is reached and for amounts of 1.0 g L^{-1} an 88% of degradation is reached after 90 min of UV irradiation. It should be noted that the relative concentration decreases slowly within the first minutes and it decreases rapidly as the time of irradiation is increased. This behaviour could be explained by the UV light absorption of methyl orange; when methyl orange is degraded the available UV light for the activation of the photocatalyst increases.
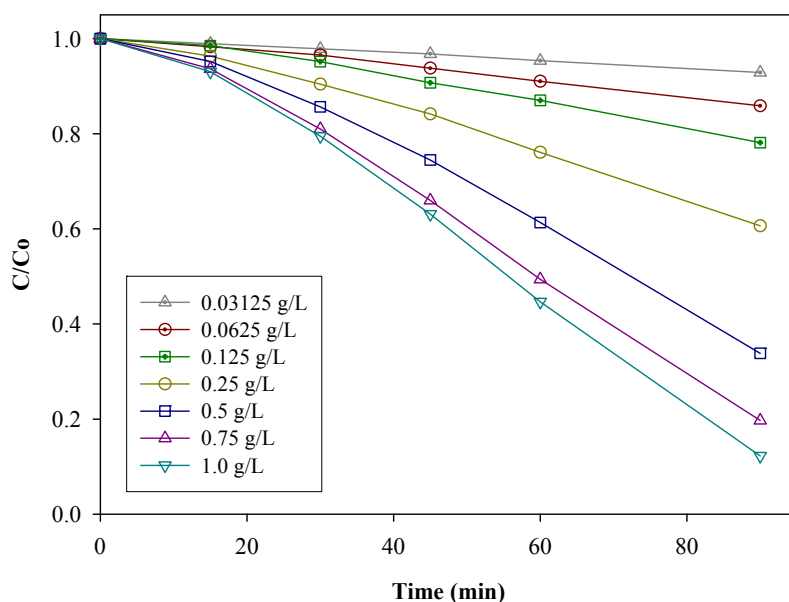
Figure 5.34: Influence of the amount of F/T photocatalyst. C_{MO}=0.014 mmol L^{-1}; pH=3.7; T=25°C; I_{UV}=20 mW cm^{-2}.

The relative decrease in the methyl orange concentration C/C_0 with irradiation time as shown in Figure 5.33 and Figure 5.34 was followed for various amount of catalyst. In the case of F/S/T as is shown in Figure 5.33, the experimental decay of C/C_0 appears to agree with pseudo-first-order kinetics (Eq. 5.3). Integration of Eq. 5.3 gives the Eq. 5.4, from the plot of $\ln(C_0/C)$ versus time the k_{app} is deduced. In the case of F/T as is seen in Figure 5.34, this behaviour seems to deviate from pseudo-first-order kinetics to zero-order. From the linear relationship between C/C_0 and time the k_{app} is deduced.

Figure 5.35 shows a comparison of the influence of the amount of catalyst for both F/T and F/S/T on the k_{app} values for the degradation of methyl orange. The comparison between the two photocatalysts was obtained from the Figure 5.33 and Figure 5.34. The dependence of the catalyst mass on the k_{app} values follows a power law-type empirical relationship found as $(C_{cat})^n$.
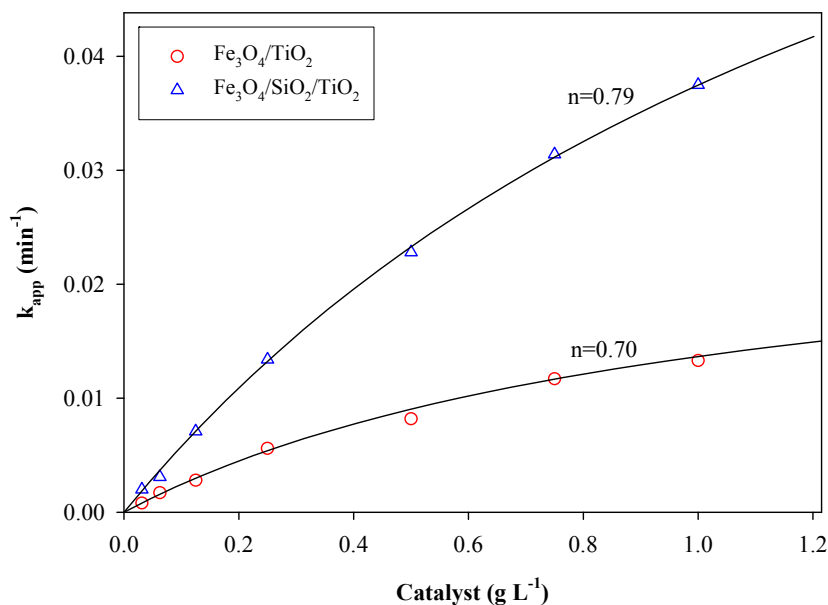
Figure 5.35: Comparison of the photooxidation of MO. Influence of amount of catalyst. C_{MO}=0.014 mmol L^{-1}; pH=3.7; T=25°C; I_{UV}=20 mW cm^{-2}.

As in the case of benzoic acid, the k_{app} values of methyl orange increases when the amounts of catalyst increase. In Figure 5.35 the differences of k_{app} between F/S/T and F/T can be seen where F/S/T has shown a value approximately 3.5 times faster than F/T using 0.5 g L^{-1} of catalyst. For both photocatalysts is observed that as the amount of catalyst increases the k_{app} values increases, these increases are faster at small amounts of catalyst than at high catalyst amounts. An increase in amount of catalyst also increases the darkness of the solution leading to a decrease in the penetration of the light flux in the reactor decreasing the photocatalytic reaction rate.

5.3.2.2 Influence of the concentration of methyl orange

The effect of varying the initial concentration of methyl orange on the initial degradation rate was also studied in the range of 0.003 to 0.0219 mmol L^{-1}, for an amount of 0.5 g L^{-1} of F/S/T at pH 3.7. The results are shown in Figure 5.36.

As expected, the effect of an increment in the initial concentration of MO is a decreasing of the degradation percentage, thus at the same time of irradiation, C/Co is smaller if the methyl orange concentration is small.
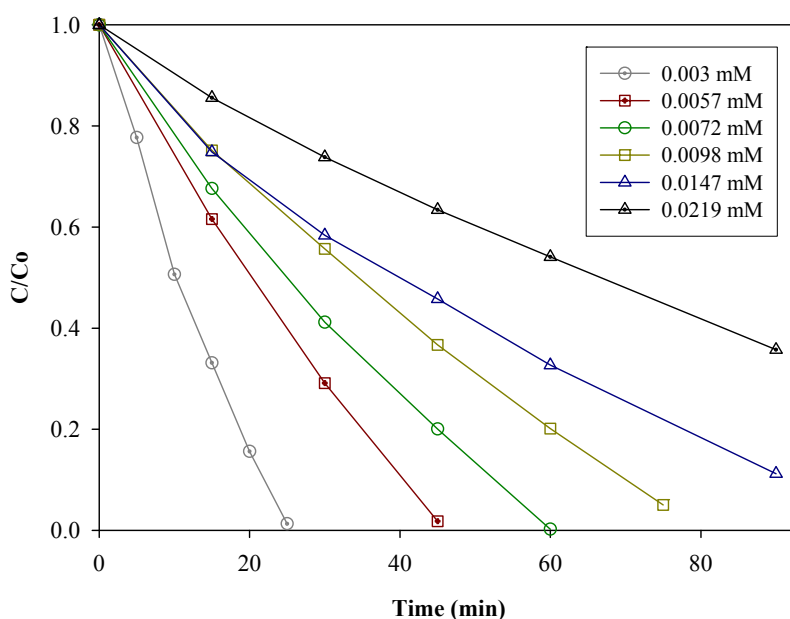
Figure 5.36: Influence of the MO concentration using F/S/T. Catalyst=0.5 g L^{-1}; pH=3.7; T=25°C; I_{UV}=20 mW cm^{-2}.

Figure 5.37 shows the relative concentration of methyl orange as a function of the initial methyl orange concentration in the range 0.0015 to 0.0177 mmol L^{-1}, for an amount of F/T (0.5 g L^{-1}) at pH 3.7.

As in Figure 5.36, the relative concentration decreased slowly at higher concentrations of methyl orange. However, the efficiency of the process in terms of mass of methyl orange degraded increased at higher initial concentrations. E.g. in the case of F/S/T (see Figure 5.36), the amount of methyl orange degraded after 45 min of irradiation was 0.003 and 0.0057 mmol L^{-1} at 0.003 and 0.0057 mmol L^{-1} initial concentrations, respectively. In the case of F/T (see

Figure 5.37), the amount of methyl orange degraded after 45 min of reactions was 0.0036 and 0.004 mmol L^{-1} at 0.0037 and 0.0063 mmol L^{-1} initial concentrations, respectively.
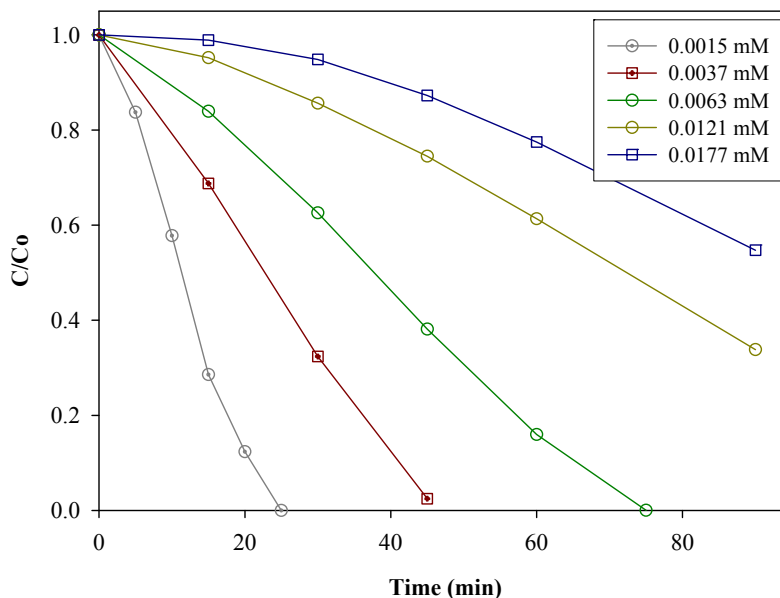
Figure 5.37: Influence of the MO concentration using F/T. Catalyst=0.5 g L^{-1}; pH=3.7; T=25°C; I$_{UV}$=20 mW cm^{-2}.

Kinetic of photocatalytic degradation of methyl orange was evaluated by noting the degradation rate of methyl orange (r$_{MO}$) as determined from the variation of MO concentration within the first 30 min irradiation time.

Figure 5.38 shows the degradation rate of methyl orange as a function of methyl orange concentration on of the F/S/T and F/T photocatalysts. This graph was based on the data from Figure 5.36 and Figure 5.37.
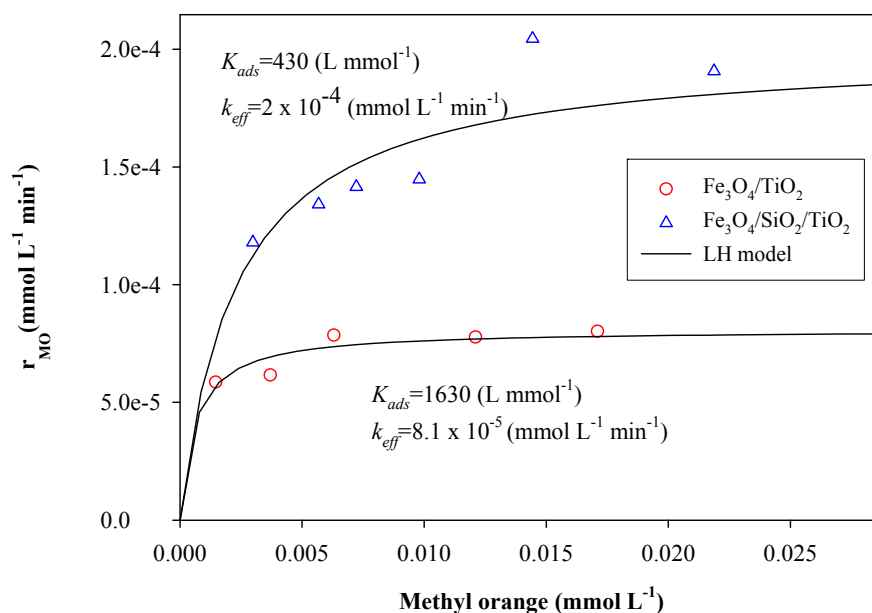
Figure 5.38: Comparison of the photooxidation of MO. Influence of MO concentration. Catalyst=0.5 g L^{-1}; pH=3.7; T=25°C; I$_{UV}$=20 mW cm^{-2}.

Figure 5.38 indicates that at small concentrations of methyl orange the degradation rate increases as the concentration of methyl orange is increased and at great concentration of methyl orange the degradation rate reaches a saturation limit. This means that the surface of the catalyst can only adsorb a certain amount of methyl orange. Hence, if there is an increase in the concentration, no further increase in the reaction rate can be achieved as no further methyl orange can be adsorbed onto the surface of the catalyst.

Experimental data of the degradation rate of methyl orange as function of the concentration were evaluated by means of the Langmuir-Hinshelwood relationship. The k_{eff} and K_{ads} values were deduced according to Eq. 3.24 which showed a linear variation, confirming the Langmuir-Hinshelwood relationship. The constants values obtained for F/S/T were k_{eff}=2 x 10^{-4} mmol L^{-1} min^{-1} and K_{ads}=430 L mmol^{-1} and, for F/T, k=8.1 x 10^{-5} mmol L^{-1} min^{-1} and K_{ads}=1630 L mmol^{-1}.

The data showed in Figure 5.35 and Figure 5.38 were used to obtain k^0 value from Eq. 5.6 for F/T and F/S/T. The results are summarized in Table 5.14. It can be seen that the k^0 value for F/S/T is higher approximately 2.7 times than for F/T, the same tend was observed in the case of benzoic acid. The initial degradation rate of methyl orange can be estimated by the application of Eq. 5.5.

Table 5.14: Parameter values for the reaction rate of methyl orange.

Particle	n	k_{eff} (mmol L^{-1} min^{-1})	k^o (mmol L^{-1} min^{-1})
Fe$_3$O$_4$/TiO$_2$ (F/T)	0.70	8.1 x 10^{-5}	1.3 x 10^{-4}
Fe$_3$O$_4$/SiO$_2$/TiO$_2$ (F/S/T)	0.79	2.0 x 10^{-4}	3.5 x 10^{-4}

5.3.2.3 Influence of pH

The influence of pH on the apparent first-order reaction rate constant for F/S/T and F/T photocatalysts is shown in Figure 5.39. The influence was investigated in the range of pH 2 to 8.7. By means of the application of the pseudo-first-order kinetic (see Eq. 5.4) the k_{app} values were deduced.

The curves presented in Figure 5.39 for both F/S/T and F/T photocatalysts, show a similar behaviour for the apparent first-order reaction rate constant for methyl orange at various pH values. A strong effect of pH on the apparent first-order reaction rate constant for the degradation of methyl orange was observed. In both cases at pH 3.7 the highest degradation rate was obtained; F/S/T was approximately 2.0 times faster than F/T. These results are in accordance with the values of Table 5.8 where the q_{max} of F/S/T was also greater than F/T.

The pH$_{(PZC)}$ for F/T and F/S/T were at pH 6.0 and 6.4 respectively (see Figure 5.8) therefore under acidic condition, a positively charged photocatalyst surface is available for the absorption of negatively charged methyl orange facilitating the degradation reaction, and high photocatalytic efficiency is obtained. On the other hand, at pH values above pH$_{(PZC)}$, the absorption of methyl orange onto the photocatalyst surface decreases by the effect of electrostatic repulsion forces between the negative catalyst surface and methyl orange anions resulting in the decrease of the degradation rate.
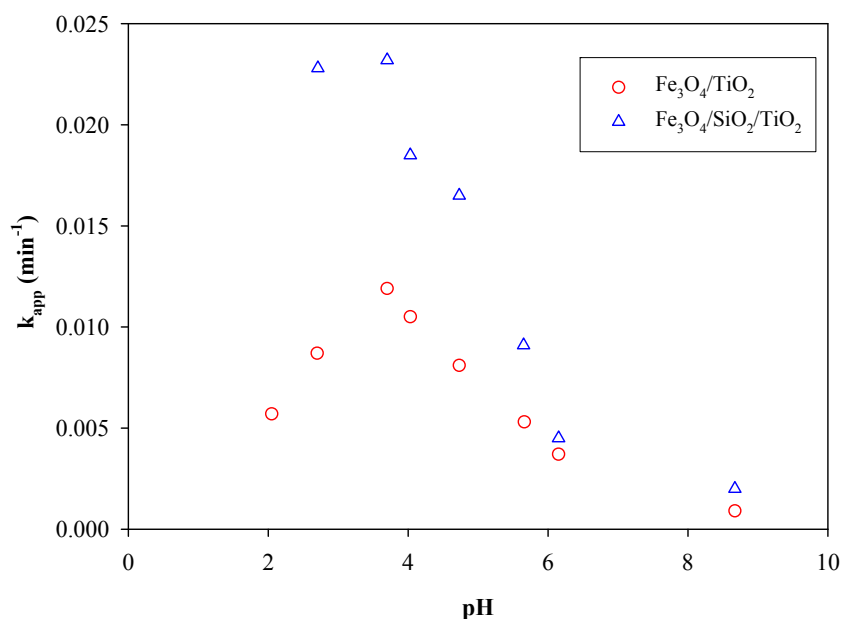
Figure 5.39: Influence of pH on photooxidation of MO. Catalyst=0.5 g L^{-1}; C$_{MO}$=0.014 mmol L^{-1}; T=25°C; I$_{UV}$=20 mW cm^{-2}.

5.3.2.4 Reusability of photocatalyst

The reusability of both F/S/T and F/T was performed in the photocatalytic oxidation of methyl orange. The results are shown in Figure 5.40 and Figure 5.41 respectively.

F/S/T and F/T photocatalysts were used repeatedly in 5 cycles. It was observed that the photocatalytic activity of F/S/T decreased slowly as the number of reuse cycles increased. It can be seen in Figure 5.40 that for methyl orange the degradation percentage by using F/S/T was higher than 70% even after 5 cycles, which indicates that the degradation was diminished only a 25% compared to the fresh one. This difference can be due to losses of catalyst in the recovery steps. By using F/T particles it was observed (see Figure 5.41) that after 5 cycles, the degradation activity for methyl orange was 50% smaller than the degradation of the fresh material. Unlike the results presented using benzoic acid, it can be seen a clear difference between the photocatalysts, where F/S/T shows a better reusability than F/T.
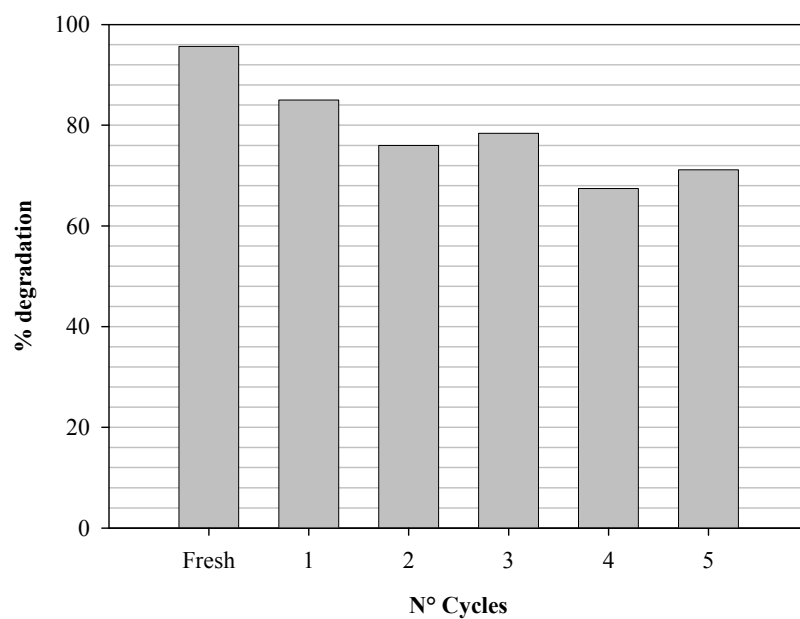
Figure 5.40: Degradation of MO with recycled F/S/T. Catalyst=0.5 g L^{-1}; C$_{MO}$=0.014 mmol L^{-1}; t=90 min; pH=3.7; T=25°C; I$_{UV}$=20 mW cm^{-2}.
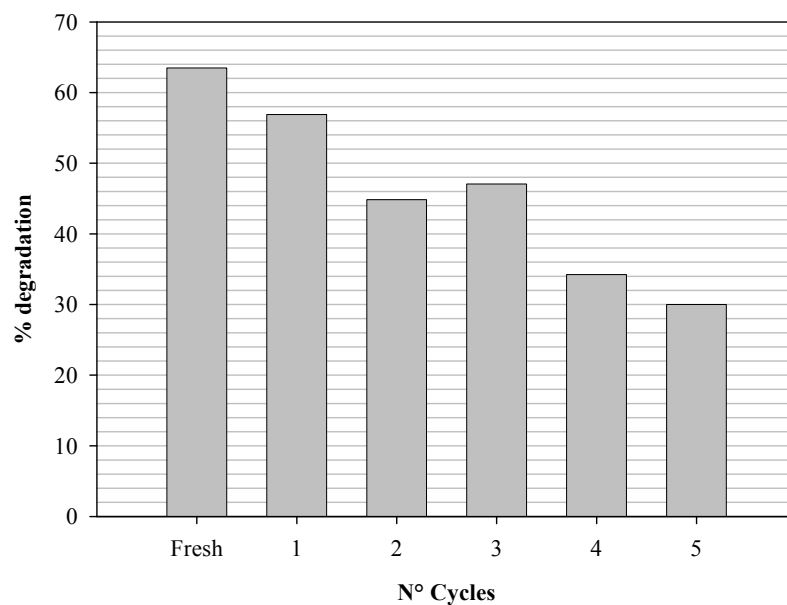
Figure 5.41: Degradation of MO with recycled F/T. Catalyst=0.5 g L^{-1}; C$_{MO}$=0.015 mmol L^{-1}; t=90 min; pH=3.7; T=25°C; I$_{UV}$=20 mW cm^{-2}.

5.3.3 Oxidation of SRB

The absorption spectra of SRB in aqueous solution at different pH are shown in Figure 8.3. SRB has shown a maximum absorption value at 565 nm for the complete pH range investigated. The absorbance measured in the range of 320-400 was less than 5% ($C_{SRB}=0.007$ mmol L^{-1}).

5.3.3.1 Influence of the amount of catalyst

The effect of the amount of F/S/T on the relative concentration of SRB is shown in Figure 5.42. The photodegradation of 0.007 mmol L^{-1} of SRB at pH 3.5 using F/S/T in the range amount of 0.00625 to 1.0 g L^{-1} was examinated.
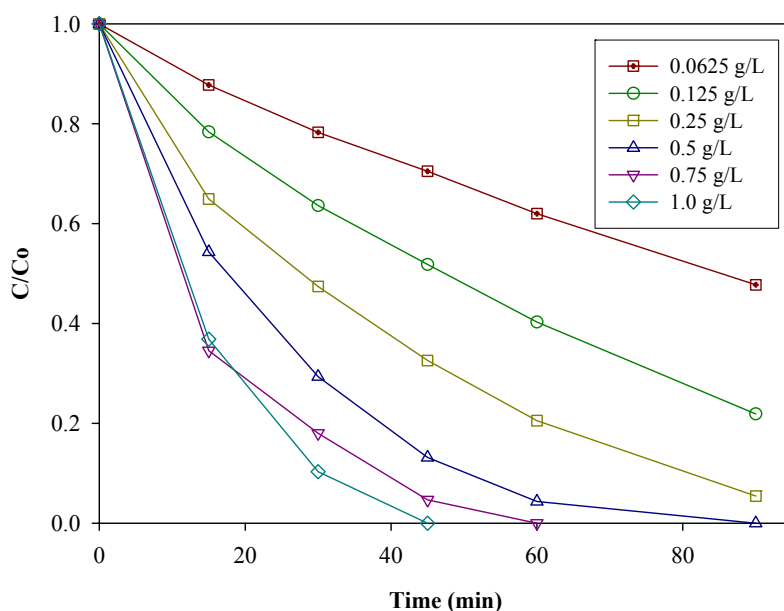
Figure 5.42: Influence of the amount of F/S/T. $C_{SRB}=0.007$ mmol L^{-1}; pH=3.5; T=25°C; $I_{UV}=20$ mW cm^{-2}.

Similar to benzoic acid and methyl orange experiments (influence of amount of catalyst), the increase on the amount of catalyst has an increase in the degradation which is again due to the increase in the surface area of the catalyst.

The results shown in Figure 5.42 indicate that with an increase in the amount of catalyst an increase in the degradation also occurs, reaching a 100% of degradation at 45, 60 and 90 min

using 1.0, 0.75 and 0.5 g L^{-1} of F/S/T respectively, while in the case of 0.00625 g L^{-1} the C/Co was 0.47 corresponding to 52% of degradation.

The effect of the amount of F/T photocatalyst on the relative concentration of SRB is shown in Figure 5.43. The amount of catalyst was in the range of 0.00625 - 1.0 g L^{-1}. In the same manner as for F/S/T catalyst, in Figure 5.43 can be seen that the C/Co decreases as the amount of catalyst is increased from 0.00625 to 1.0 g L^{-1}. E.g., after 90 min of irradiation the C/Co decreased from 0.72 to 0.58 and to 0.35 for 0.0625, 0.125 and 0.25 g L^{-1} of amount of catalyst respectively, the corresponding values expressed in SRB degradation were 28%, 42% and 65%. Further increase of the amount of catalyst to 0.5, 0.75 and 1.0 g L^{-1} shows C/Co values very close among them corresponding to 91%, 86% and 99% of degradation respectively.
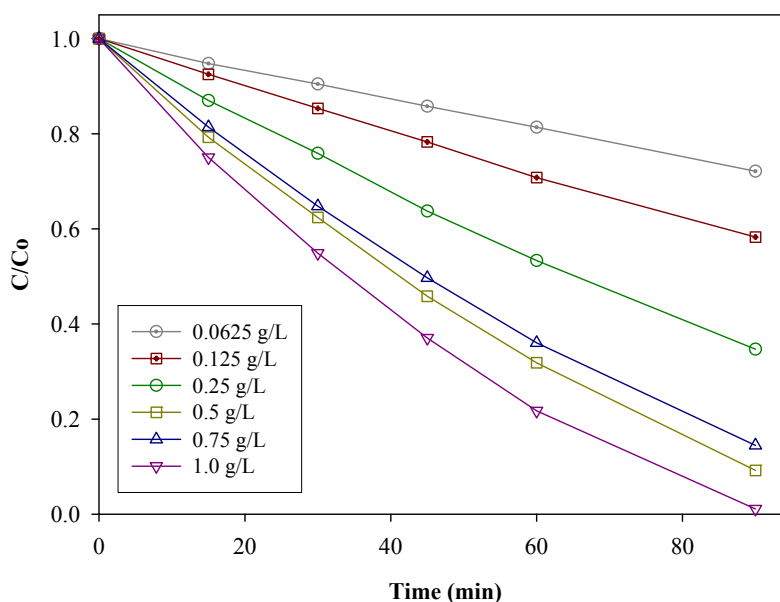
Figure 5.43: Influence of the amount of F/T. C_{SRB}=0.007 mmol L^{-1}; pH=3.5; T=25°C; I_{UV}=20 mW cm^{-2}.

The relative decrease in the SRB concentration C/C_0 with irradiation time as shown in Figure 5.42 and Figure 5.43 was followed for various amount of catalyst. The experimental decay of C/C_0 appears to agree with pseudo-first-order kinetics (Eq. 5.3). Integration of Eq. 5.3 gives the Eq. 5.4, from the plot of ln(C_0/C) versus time the k_{app} is deduced.

Figure 5.44 shows the k_{app} values obtained for SRB as a function of the amount of catalyst. The comparison between the two photocatalysts was obtained from Figure 5.42 and Figure

5.43. The dependence of the catalyst mass on the k_{app} values follows a power law-type empirical relationship found as $(C_{cat})^n$.
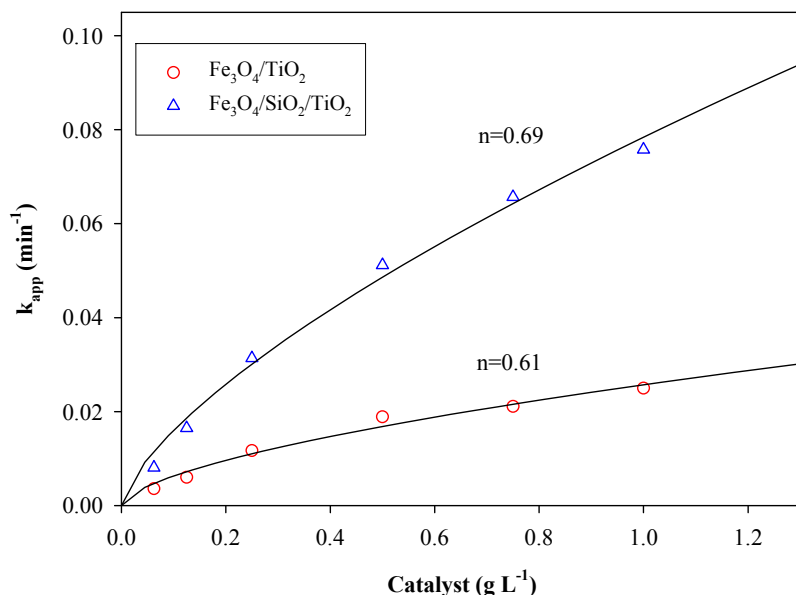
Figure 5.44: Comparison of the photooxidation of SRB. Influence of the amount of catalyst. C_{SRB}=0.007 mmol L^{-1}; pH=3.5; T=25°C; I_{UV}=20 mW cm^{-2}.

As in the cases of benzoic acid and methyl orange (see Figure 5.21 and Figure 5.35), the k_{app} values of SRB increased as the amount of catalyst also increased. Figure 5.44 shows the differences of k_{app} between F/S/T and F/T, where F/S/T was approximately 3 times faster than F/T using a dosage of 0.5 g L^{-1}. In both cases, the k_{app} values increase proportionally to a function $(C_{cat})^n$ with the amount of catalyst.

5.3.3.2   Influence of the concentration of sulforhodamine B

The effect of the initial concentration of SRB on the initial degradation rate is shown in Figure 5.45. The concentration of SRB used for this investigation was in the range of 0.0035 to 0.0172 mmol L^{-1}, using an amount of 0.5 g L^{-1} of F/S/T at pH 3.5.

It has been seen that the influence of the initial concentration of SRB was the same as for benzoic acid and methyl orange, a decrease in the SRB concentration results in an increase in the degradation rate, thus at the same irradiation time e.g. 60 min using a concentration of 0.0172 mmol L^{-1} a C/Co=0.22 is reached, corresponding to 78% of degradation and using a concentration of 0.0035 mmol L^{-1} a 100% of degradation is obtained.
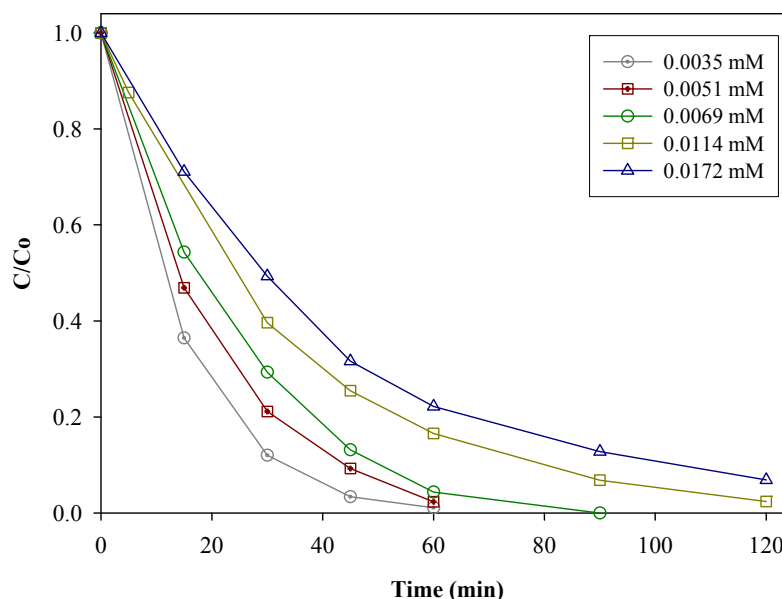
Figure 5.45: Influence of the SRB concentration using F/S/T. Catalyst=0.5 g L^{-1}; pH=3.5; T=25°C; I$_{UV}$=20 mW cm^{-2}.

Figure 5.46 shows the relative concentration of SRB as a function of the initial SRB concentration in the range 0.0031 to 0.0136 mmol L^{-1}, for an amount of 0.5 g L^{-1}of F/T at pH 3.5. It can be seen a similar behaviour compared with F/S/T photocatalyst, even using other organics such as benzoic acid and methyl orange. The relative concentration decreased more slowly at higher concentrations of SRB. E.g., at 90 min of irradiation the C/Co using a concentration of 0.0136 mmol L^{-1} is 0.433 and using a concentration of 0.0031 mmol L^{-1} was zero.

However, it should be noted that the efficiency of the process in terms of mass of SRB degraded increased at higher initial concentrations. E.g. in the case of F/S/T, the amount of SRB degraded after 90 min of irradiation was 0.0069 and 0.015 mmol L^{-1} at 0.0069 and 0.0172 mmol L^{-1} initial concentrations, respectively. In the case of F/T, the amount of SRB degraded after 90 min of irradiation was 0.0031 and 0.008 mmol L^{-1} at 0.0031 and 0.0136 mmol L^{-1} initial concentrations, respectively.
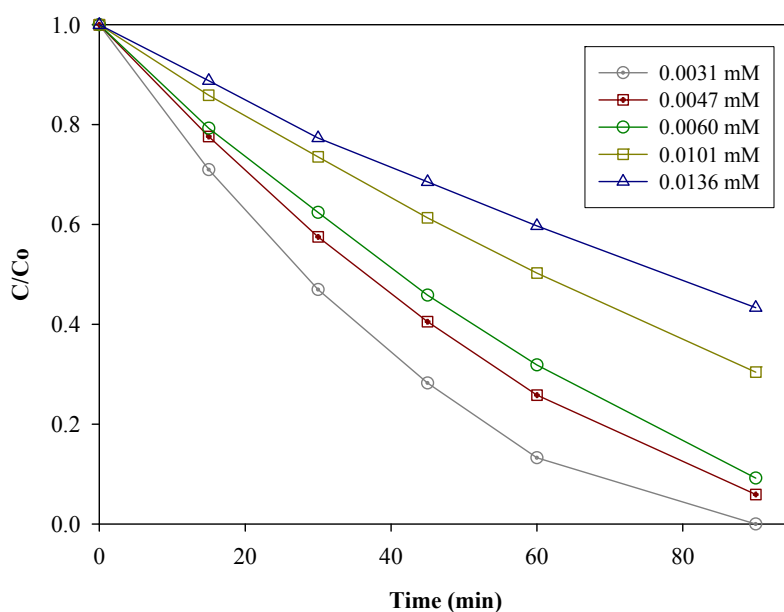
Figure 5.46: Influence of the SRB concentration using F/T. Catalyst=0.5 g L^{-1}; pH=3.5; T=25°C; I_{UV}=20 mW cm^{-2}.

The degradation kinetic was evaluated by noting the degradation rate of SRB (r_{SRB}) as determined from the variation of SRB concentration within the first 30 min irradiation time.

Figure 5.47 shows the degradation rate as a function of the SRB initial concentration for F/S/T and F/T photocatalysts. The graph was based on the data of Figure 5.45 and Figure 5.46.
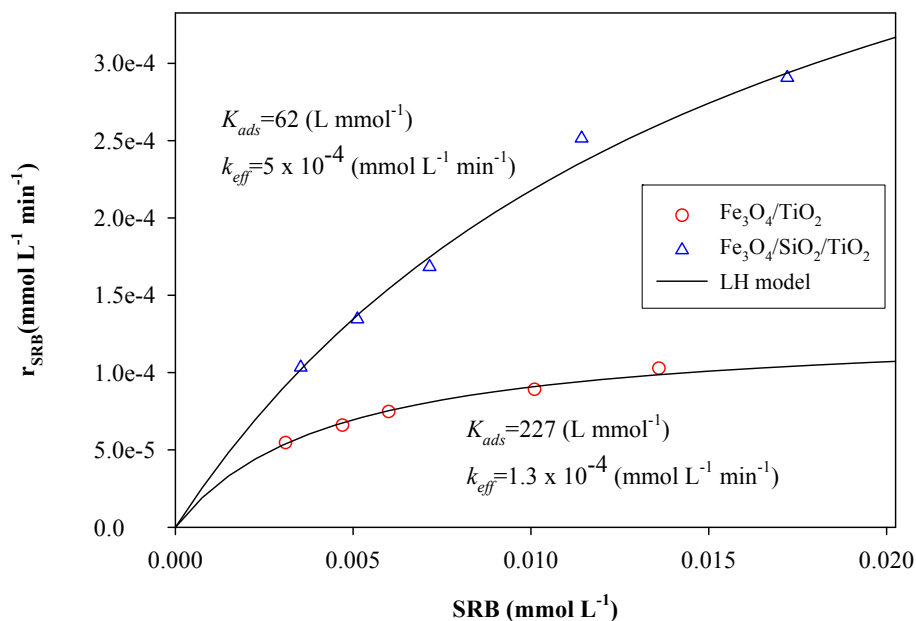
Figure 5.47: Comparison of the photooxidation of SRB. Influence of SRB concentration. Catalyst=0.5 g L^{-1}; pH=3.5; T=25°C; I$_{UV}$=20 mW cm^{-2}.

Figure 5.47 shows that at small SRB concentrations the degradation rate increases as the SRB concentration also increases and at greater concentration a plateau is reached.

At small concentrations of SRB, the photocatalytic degradation is limited by the amount of substrate available at the catalyst surface. Increasing the concentration of SRB in the bulk solution enhanced the opportunity of SRB to be adsorbed onto the surface of the catalyst, which improved the photocatalytic degradation. However, at greater concentration of SRB, the increase in the concentration did not result in a proportionate increase in the adsorption of SRB onto catalyst surface. Additionally, due to the fact that SRB could absorb UV light, an increase in its concentration may lead to an inhibition in light absorption for the photocatalytic degradation.

The data of the degradation rate of SRB versus concentration were evaluated by applying the Langmuir-Hinshelwood relationship. The k_{eff} and K_{ads} values were deduced according to Eq. 3.24 which presented a linear expression, thus, the Langmuir-Hinshelwood relationship was confirmed. The constants values were for F/S/T, k_{eff}=5 x 10^{-4} mmol L^{-1} min^{-1} and K_{ads}=62 L mmol^{-1} and, for F/T, k_{eff}=1.3 x 10^{-4} mmol L^{-1} min^{-1} and K_{ads}=227 L mmol^{-1}.

The K_{ads} values obtained by means of the Langmuir-Hinshelwood model, for both F/T and F/S/T photocatalysts were very similar to those obtained from the sorption equilibrium of SRB, being only 1.5 and 1.09 times greater respectively (see Table 5.9). In the previous cases for benzoic acid and methyl orange, the K_{ads} values obtained from the photocatalytic degradation experiments have shown greater values compared to the adsorption equilibrium.

k^0 value were deduced with the application of Eq. 5.6 by using the data presented in Figure 5.44 and Figure 5.47. The results are summarized in Table 5.15. It can be seen that the k^0 value for F/S/T is higher approximately 4 times than for F/T, the same tend was also observed in the case of benzoic acid as well as methyl orange. Values of degradation rate of SRB can be calculated by using Eq. 5.5.

Table 5.15: Parameter values for the reaction rate of SRB.

Particle	n	k_{eff} (mmol L^{-1} min^{-1})	k^0 (mmol L^{-1} min^{-1})
Fe$_3$O$_4$/TiO$_2$ (F/T)	0.61	5.0 x 10^{-4}	1.98 x 10^{-4}
Fe$_3$O$_4$/SiO$_2$/TiO$_2$ (F/S/T)	0.69	1.3 x 10^{-4}	8.07 x 10^{-4}

5.3.3.3 Influence of pH

Apparent first-order reaction rate constant of SRB depending on the pH of the aqueous suspensions of F/S/T and F/T are illustrated in Figure 5.48. The pH investigated was in the range of 2.5 – 8.7. By means of the application of the pseudo-first-order kinetic (see Eq. 5.4) the k_{app} values were deduced.

For both F/S/T and F/T photocatalysts the pH has a marked influence; at pH 3.5 the maximum values for the apparent first-order reaction rate constant were obtained where F/S/T was approximately 2.6 times faster than F/T.

In Table 5.9 it can be seen that the adsorption of SRB at pH 3.5 onto both F/S/T and F/T photocatalysts was very similar, therefore, the differences of k_{app} in the photodegradation of SRB showed in Figure 5.48 cannot be attributed to this factor, thus, it can be deduced that the major difference between these two photocatalysts lies in both the quantity and the crystallinity of TiO$_2$ present by F/S/T compared to F/T.

As previously seen, the surface of F/S/T and F/T are positively charged when immersed in acid media, this is at pH values below 6.4 and 6.0 respectively, whereas they are negatively

94

charged under alkaline conditions, pH values above 6.4 and 6.0 respectively. The SRB molecule has two sulfonic acid groups which ensure its existence in the form of a charged anion in aqueous solutions within the pH 2-12 (Mchedlov-Petrossyan, Shapovalov et al. 1995). As a result, the anionic SRB can be chemisorbed significantly by electrostatic forces on the surface of the catalysts in acid media, which benefit the photocatalytic degradation of the SRB.

On the other hand, under alkaline conditions, the absorption of SRB onto the surface of the photocatalyst decreases by the electrostatic repulsion between the negative catalyst surface and SRB anions resulting in the decrease of degradation rate.
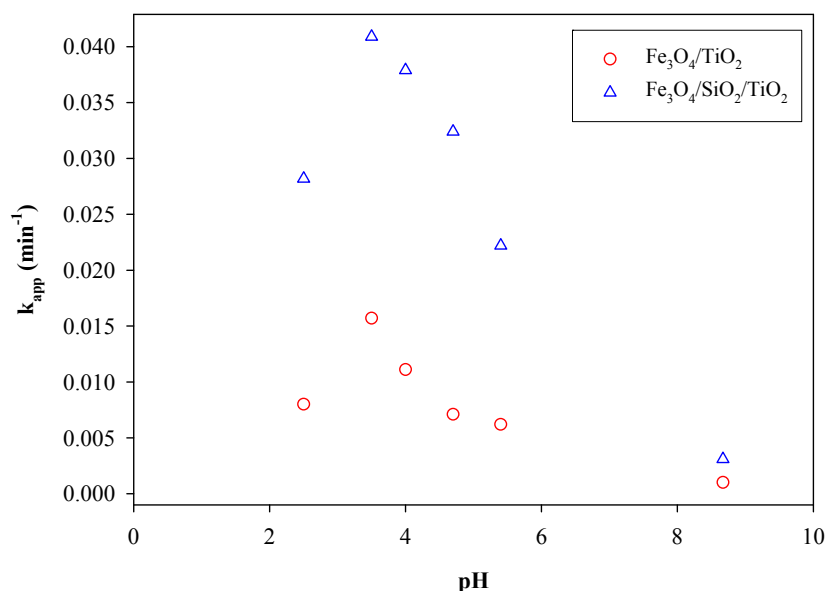
Figure 5.48: Comparison of the photooxidation of SRB. Influence of pH. C_{SRB}=0.007 mmol L^{-1}; Catalyst=0.5 g L^{-1}; T=25°C; I_{UV}=20 mW cm^{-2}.

5.3.3.4 Influence of HCO$_3^-$

The effect of the HCO$_3^-$ ions on the relative concentration of SRB by using F/T as photocatalyst was tested and is shown in the Figure 5.49. It was expected to have a negative effect of HCO$_3^-$ on the degradation of SRB, due to their ability to act as hydroxyl radical scavengers by the following reaction (Bekbölet and Balcioglu 1996):

$$HCO_3^- + OH^\bullet \rightarrow CO_3^{\bullet-} + H_2O \hspace{3cm} \text{Eq. 5.9}$$

These ions may also block the photocatalytic sites on the TiO_2 surface thus deactivating the catalyst toward the SRB molecules.

Nevertheless, Figure 5.49 shows that no noticeable effect of HCO_3^- on the SRB degradation is seen, probably due to the small concentration range of HCO_3^- investigated. In the literature similar case has been presented where it is suggested that at HCO_3^- concentrations smaller than 0.05 mol L^{-1} there is no influence on the degradation (Lair, Ferronato et al. 2008).
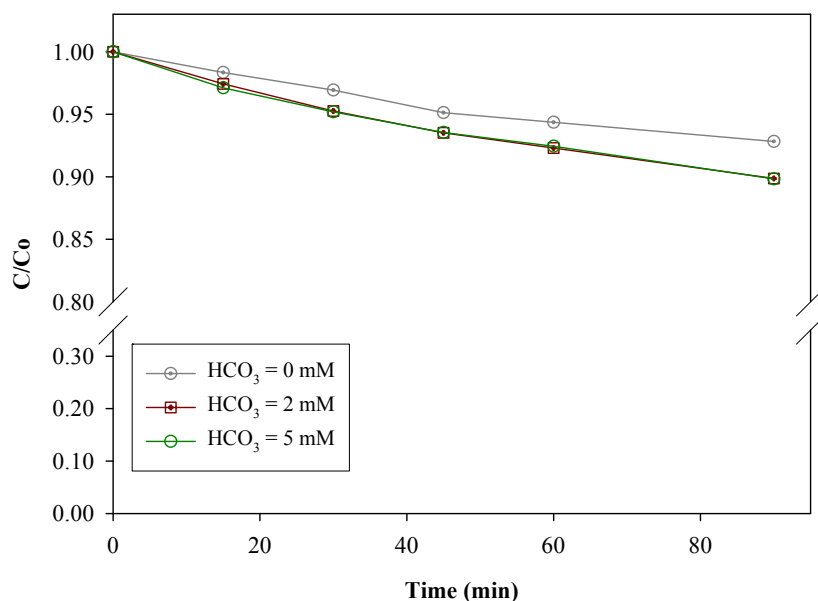
Figure 5.49: HCO_3^- effect using F/T. C_{SRB}=0.007 mmol L^{-1}; Catalyst=0.5 g L^{-1}; pH=8.67; T=25°C; I_{UV}=20 mW cm^{-2}.

5.3.3.5 Influence of H_2O_2

Figure 5.50 shows the influence of the concentration of H_2O_2 on the relative concentration of SRB by using F/T as photocatalyst. The concentration of H_2O_2 was used in the range 0 to 5 mmol L^{-1}, using an amount of 0.5 g L^{-1} of F/T at pH 8.67.

The presence of H_2O_2 resulted in a small increase in the degradation rate, thus, as the H_2O_2 concentration increases the degradation rate is increased. At a concentration of 5 mmol L^{-1} H_2O_2, the degradation of SRB has been increased by 10% compared to the values obtained in its absence. This effect can be explained by means of radical reaction mechanisms, where the

amount of H_2O_2 added could accelerate the reaction by producing hydroxyl radicals according to Eq. 3.12 and Eq. 3.13.
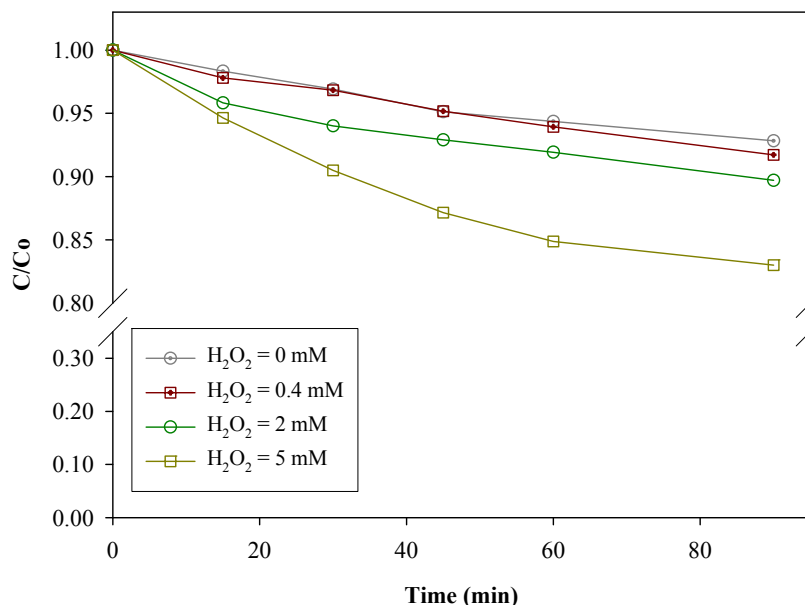
Figure 5.50: H_2O_2 effect using F/T. C_{SRB}=0.007 mmol L^{-1}; Catalyst=0.5 g L^{-1}; pH=8.67; T=25°C; I_{UV}=20 mW cm^{-2}.

5.3.3.6 Reusability of photocatalyst

The reusability of both F/S/T and F/T was carried out for the oxidation of SRB. The results are shown in the Figure 5.51 and Figure 5.52 respectively.

F/S/T and F/T photocatalysts were used repeatedly for 5 cycles. As in the previous cases the fresh material has shown for both F/S/T and F/T high degradation percentages reaching values of 95% and 68% respectively, while a slight decrease in photoactivity was noticed with the reuse cycles. Figure 5.51 shows that the degradation percentage of SRB using F/S/T was higher than 75% even after 5 cycles, therefore, there is only a decrease by 20% compared to the fresh material. F/T photocatalyst has shown that after 5 cycles, the activity for the degradation of SRB decreases in a 30% respect to the fresh material (see Figure 5.52). The differences between the values of the fresh material and that using in five cycles can be due to losses of catalyst in the recovery step. From the figures it is deduced that F/S/T shows a better performance in the reusability than F/T.
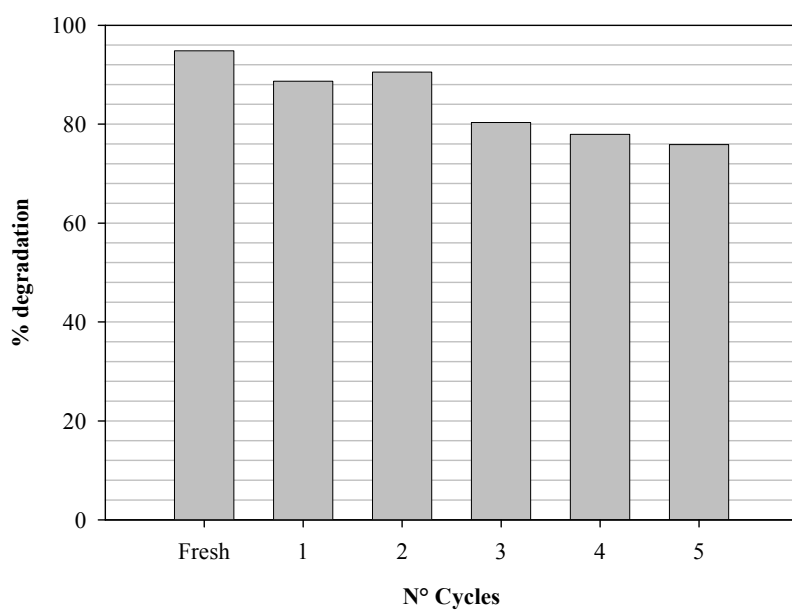
Figure 5.51: Degradation of SRB with recycled F/S/T. Catalyst=0.5 g L^{-1}; C_{SRB}=0.007 mmol L^{-1}; t=60 min; pH=3.5; T=25°C; I_{UV}=20 mW cm^{-2}.
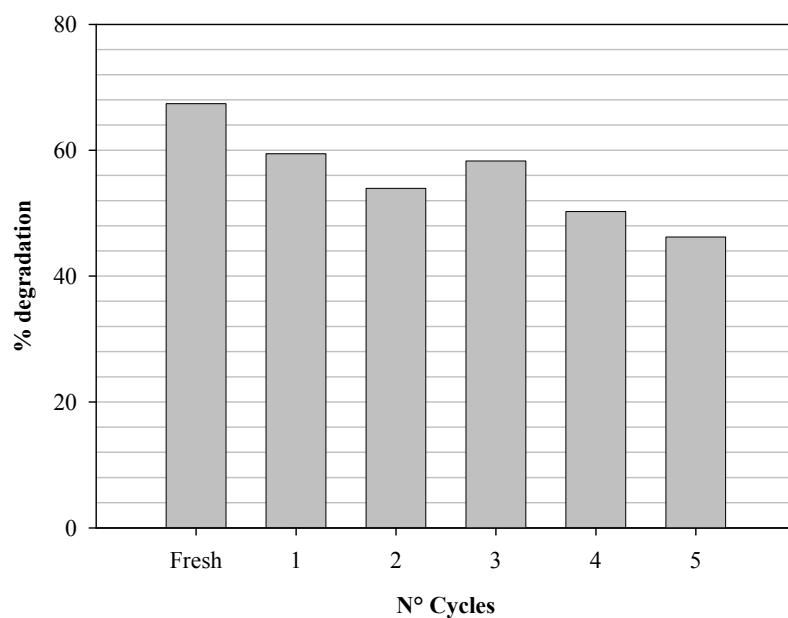
Figure 5.52: Degradation of SRB with recycled F/T. Catalyst=0.5 g L^{-1}; C_{SRB}=0.007 mmol L^{-1}; t=60 min; pH=3.5; T=25°C; I_{UV}=20 mW cm^{-2}.

5.3.4 Kinetic model of organic photooxidation

A kinetic model was proposed which involves the parameters of catalyst mass and initial concentration of organic compound (see Eq. 5.5). The constants of this model, k^0 and n for the three studied organic compounds and for the two photocatalysts were calculated, this values are shown in Table 5.12, Table 5.14 and Table 5.15. The deduced values of the K_{ads} for each organic compound and photocatalyst are shown in Figure 5.24, Figure 5.38 and Figure 5.47. This kinetic model allows the estimation of the degradation rate for a certain compound.

E.g. at an organic concentration of 0.025 mmol L^{-1}, catalyst mass of 0.5 g L^{-1} and at the pH value at which each organic compound showed the fastest k_{app} value (min^{-1}), the following degradation rates are obtained (Table 5.16).

Table 5.16: Values of degradation rate for the three organic compounds for F/T and F/S/T photocatalyst.

Particle	C_0 (mmol L^{-1})	Catalyst (g L^{-1})	r (mmol L^{-1} min^{-1}) BA	MO	SRB
F/T	0.025	0.5	1.20 x 10^{-4}	7.81 x 10^{-5}	1.11 x 10^{-4}
F/S/T	0.025	0.5	6.80 x 10^{-4}	1.85 x 10^{-4}	3.04 x 10^{-4}

T=25°C; I_{UV}=20 mW cm^{-2}.

Table 5.16 shows that for F/S/T, BA has the highest value of degradation rate being 3.7 and 2.2 times higher than MO and SRB respectively. In the case of F/T the degradation rate values are very similar; although that the same behaviour is observed where BA is 1.5 and 1.08 times higher than MO and SRB respectively.

A comparison between the photocatalysts shows that the values of degradation rate obtained by using F/S/T are higher compared to F/T. The values were approximately 5.7, 2.4 and 2.7 times faster for BA, MO and SRB than for F/T respectively. This is coincident with the trends observed according to the k_{app} values.

6 CONCLUSION

The overall aim of this PhD thesis was to develop a magnetic and photoactive photocatalyst of enhanced separation properties for application in photocatalytic slurry systems. In the present investigation several important conclusions are generated regarding to its preparation, as well as factors affecting the photocatalytic process.

Preparation of the magnetic photocatalyst

Titanium dioxide has been synthesized by sol-gel technique. The crystal phases of titania were characterized in terms of XRD, which clearly indicates the presence of anatase and rutile. The heat treatment of 1 h at 400°C was found to be beneficial with respect to the conversion of amorphous titania into a crystalline phase.

Titanium dioxide was successfully deposited onto seed magnetic particles (Fe_3O_4 or Fe_3O_4/SiO_2) by using a coating technique. This was demonstrated by the physicochemical characterization of the samples. Analysis such as XRD and ESEM showed the presence of magnetite and anatase together in the same sample, indicating that the coating process occurred.

The two photocatalysts showed magnetic characteristics, using the same magnetic field at given time, it can be seen that the magnetic separation of F/T is faster compared to F/S/T, which is absolutely consistent with the results obtained from the magnetization curves. The influence of applying a magnetic field on the settling for both F/S/T and F/T accelerated significantly the solid/liquid separation process. Moreover, it was verified that P25 TiO_2 is not affected by a magnetic field and the settling rates are very slow, enhancing the importance of the magnetic coating. It was proposed a high gradient separation system (HGMS) for the solid/liquid separation, where the catalyst removal will be over 99%. According to the residual percentage values shown in the magnetic separation test, it was estimated a time of 30 min in the sedimentation tank, for a removal of 89% and 97.5% of F/S/T and F/T respectively, thus the loading of the HGMS device is reduced.

The silica coating was effective for the protection of magnetite against the oxidation during the heat treatment for 1 h in air atmosphere, showing a magnetization saturation of 6.4 Am^2 kg^{-1}.

It can be concluded that a main objective of this research work that involved the synthesis of a photocatalyst with magnetic characteristics which can be easily recovered from a slurry system by mean of an external magnetic field, was achieved.

Adsorption investigation

Adsorption of benzoic acid, methyl orange and sulforhodamine onto F/S/T and F/T was investigated.

Adsorption isotherms data for the systems studied were well modelled by means of Langmuir isotherm relationship, with values of R^2 higher than 0.97, for all the systems.

In general, the model compounds were better adsorbed onto F/S/T than F/T, an exception was only observed in the case of SRB where the adsorption was almost the same for both photocatalysts.

The adsorption isotherms for each model compound were carried out at the pH where the value for k_{app} (min^{-1}) in the photocatalytic system was the maximum observed. Under these conditions, it can be concluded that in the case of F/T the values of q_{max} follow the order BA ~ MO > SRB, because the q_{max} values between BA and MO are very similar. For F/S/T, the values of q_{max} follow clearly the order BA > MO > SRB.

The adsorption isotherms for SRB using both photocatalysts, showed similar behaviour and even a similar q_{max} values.

Important paramenters influencing the photocatalytic process

The photocatalytic activity of F/S/T and F/T was studied using a benzoic acid, methyl orange and sulforhodamine B as a model compounds in a batch system. The treatment of these organic compounds by photocatalysis causes its oxidation, which was followed by determining the variation of organic concentrations.

Under the same conditions, the photocatalysts were tested on the degradation of benzoic acid. Hence, the photocatalysts F/S/T and F/T were selected for the following photooxidation experiments, between them F/S/T has shown a better performance than F/T. It is concluded that without a photocatalyst no degradation of benzoic acid is possible, an important point to test the effectiveness of the photocatalytic process, because the degradation cannot be attributed to photolysis. The best photocatalytic performance to degrade benzoic acid was P25 TiO_2, which was used as a reference material. The decrease of relative concentration versus

irradiation time was adjusted with pseudo-first-order kinetics. The relationship was well fitted by a straight line; this is confirmed by the high values of the correlation coefficients.

The influence of the amount of catalyst was studied for both F/S/T and F/T photocatalysts in the range of 0.0031-1.0 g L^{-1}, for the three model compounds. By means of the application of the pseudo-first-order reaction the kinetic evaluation was adjusted. The results indicated that the apparent first-order reaction rate constant increased with an increase in the amount of catalyst until according to a function $(C_{cat})^n$. It was interesting to determine the minimum amount of catalyst required to degrade the maximum amount of the model compound at a particular experimental conditions. Although the k_{app} value is increased if the amount of catalyst is greater than 0.5 g L^{-1}, significant increment is observed until this amount of catalyst. After that the k_{app} value increases only gradually. Thus, the amount of catalyst selected for the degradation of all the organic compounds was 0.5 g L^{-1}.

A series of BA, MO and SRB solutions with different concentrations were used to determine the influence of the initial concentration on the photocatalytic degradation for both F/S/T and F/T photocatalysts. It is evident that the photodegradation rate depends on the initial concentration of the organic compounds. Due to that the lifetime of hydroxyl radicals is very short (only a few nanoseconds), they can only react at or near the location where they are formed. A high concentration of organics logically enhances the probability of collision between organic matter and the oxidizing species, leading to an increase in the degradation rate. The three model compounds have been evaluated quite well by applying the Langmuir-Hinshelwood relationship.

A comparison among the different model compounds can be made taking into account the pH value at which each organic compound showed the fastest k_{app} value (min^{-1}). Under these conditions, the k_{app} values follow the order BA > MO > SRB being BA the fastest, this occur using both F/S/T as F/T photocatalysts. This behaviour is consistent with the values obtained from adsorption isotherms, confirming that the initial degradation rate is dependent on the adsorption.

The efficiency of the photocatalytic processes strongly depends on the pH of the reaction solution. The effect of pH on the oxidation can be explained by its effect on the adsorption. The high adsorption of the organics on the photocatalyst material leads to a fast decrease of the organic concentration in the photocatalytic process. The k_{app} values of BA, MO and SRB were found to be the faster at pH 4.8, pH 3.7 and pH 3.5, for both F/S/T and F/T photocatalyts

in the pH range from 3 to 8, respectively. The different values of pH can be attributed to the electrostatic interactions between charged photocatalysts and organic compounds.

The temperature showed a slight influence on the degradation of benzoic acid for both F/S/T and F/T photocatalysts. In the range of 25-30°C only an increase of 4% in the degradation percentage for F/S/T was observed, on the other hand, by using F/T the influence of temperature at these conditions was negligible, which can be attributed to the small activation energy of the photocatalytic reaction.

The influence of H_2O_2 and HCO_3^- was investigated by using F/T photocatalyst for the degradation of SRB. The addition of H_2O_2 caused only a moderate increase of the degradation of SRB, improving a 10% the degradation percentage with 5 mmol L^{-1} compared to its absence, whereas the addition of HCO_3^- showed only a negligible effect on the SRB degradation, probably due to the small concentrations used.

The degradation and mineralization of benzoic acid by using F/S/T photocatalyst was investigated. It can be concluded that mineralization is a slower process in comparison to the degradation. E.g., using 0.5 g L^{-1} of catalyst, the benzoic acid degradation percentage was 91% and only a partial mineralization of 64% after 180 min of irradiation was reached. This is indicative of the presence of intermediate reaction products, leading to the conclusion that longer illumination times are needed for the complete conversion to inorganic end products.

The reusability of F/S/T and F/T photocatalysts was evaluated for the three model compounds. This was probably one of the most significant experiments, as it is in direct relation to the practical application of the catalyst. The easy separation and reusability of the catalyst is an important cost factor. A very effective solid/liquid separation of the catalysts from solutions by the application of a magnetic field was effective and a good reproducibility of the photocatalytic activity of the recycled catalysts was observed. It should be noted that the performance exhibited by F/S/T was better than F/T; thus, the photocatalytic degradation of BA, MO and SRB by F/S/T was diminished in a 13, 25 and 20% compared to the fresh material after 5 cycles, respectively, while by using F/T the reduction was 12, 50 and 30% after 5 cycles, for the same organic compounds. The small decreases of degradation observed could be accounted by losses of catalysts mass during the recycle steps. The differences in the performance of the catalyst can be attributed to the different pH values of the organic solutions. Thus, F/S/T also exhibited the best reproducibility, probably due to the greater stability provided by the silica coating.

Finally, by means of the combination of the empirical models obtained from the parameters that involve the amount of catalyst and the initial organic concentrations, a general kinetic model for the estimation of the degradation rate for the organic compounds studied is established.

Recommendations

The results of this PhD thesis exhibit a great potential. The present study shows that organic pollutants can be effectively degraded by a photocatalytic oxidation process using titanium dioxide with magnetic properties, thus, the separation problem was successfully solved.

Further studies are recommended based on the current preparation method as well as on the exploration of alternative preparation methods in order to optimize the catalyst.

This investigation was carried out in a batch operation system for each experimental run. In order for the present findings to be implemented in industrial applications, a scale-up system based on the design of the proposed solid/liquid separation needs to be investigated to test how effective the photocatalyst can work in an industrial unit.

The efficient practical use of a light source should be investigated. Instrumental setup may be improved for an efficient utilization of solar light as irradiation source to save operational cost.

7 LIST OF REFERENCES

Agustina, T. E., H. M. Ang, et al. (2005). "A review of synergistic effect of photocatalysis and ozonation on wastewater treatment." Journal of Photochemistry and Photobiology C: Photochemistry Reviews **6**(4): 264-273.

Al-Sayyed, G., J.-C. D'Oliveira, et al. (1991). "Semiconductor-sensitized photodegradation of 4-chlorophenol in water." Journal of Photochemistry and Photobiology A: Chemistry **58**(1): 99-114.

Alfano, O. M., D. Bahnemann, et al. (2000). "Photocatalysis in water environments using artificial and solar light." Catalysis Today **58**(2-3): 199-230.

Angelidis, T. N., M. Koutlemani, et al. (1998). "Kinetic study of the photocatalytic recovery of Pt from aqueous solution by TiO_2, in a closed-loop reactor." Applied Catalysis B: Environmental **16**(4): 347-357.

Araña, J., E. Tello Rendón, et al. (2001). "High concentrated phenol and 1,2-propylene glycol water solutions treatment by photocatalysis: Catalyst recovery and re-use." Applied Catalysis B: Environmental **30**(1-2): 1-10.

Arslan, I. and I. A. Balcioglu (1999). "Degradation of commercial reactive dyestuffs by heterogenous and homogenous advanced oxidation processes: a comparative study." Dyes and Pigments **43**(2): 95-108.

Assabane, A., Y. Ait Ichou, et al. (2000). "Photocatalytic degradation of polycarboxylic benzoic acids in UV-irradiated aqueous suspensions of titania.: Identification of intermediates and reaction pathway of the photomineralization of trimellitic acid (1,2,4-benzene tricarboxylic acid)." Applied Catalysis B: Environmental **24**(2): 71-87.

Augugliaro, V., E. Davì, et al. (1990). "Influence of hydrogen peroxide on the kinetics of phenol photodegradation in aqueous titanium dioxide dispersion." Applied Catalysis **65**: 101-116.

Ayranci, E. and O. Duman (2006). "Adsorption of aromatic organic acids onto high area activated carbon cloth in relation to wastewater purification." Journal of Hazardous Materials **136**(3): 542-552.

Bacsa, R. R. and J. Kiwi (1998). "Effect of rutile phase on the photocatalytic properties of nanocrystalline titania during the degradation of p-coumaric acid." Applied Catalysis B: Environmental **16**(1): 19-29.

Baruth, E. E., E. American Society of Civil, et al. (2005). Water treatment plant design. New York, McGraw-Hill.

Bauer, C., P. Jacques, et al. (2001). "Photooxidation of an azo dye induced by visible light incident on the surface of TiO_2." Journal of Photochemistry and Photobiology A: Chemistry **140**(1): 87-92.

Bekbölet, M. and I. Balcioglu (1996). "Photocatalytic degradation kinetics of humic acid in aqueous TiO_2 dispersions: The influence of hydrogen peroxide and bicarbonate ion." Water Science and Technology **34**(9): 73-80.

Beydoun, D., R. Amal, et al. (2000). "Novel Photocatalyst: Titania-Coated Magnetite. Activity and Photodissolution." The Journal of Physical Chemistry B **104**(18): 4387-4396.

Blake, D. M. (1995). Bibliography of work on the heterogeneous photocatalytic removal of hazardous compounds from water and air: Update Number 1 to June, 1995. Other Information: PBD: Nov 1995**:** Medium: ED; Size: 103 p.

Blake, D. M., P.-C. Maness, et al. (1999). "Application of the Photocatalytic Chemistry of Titanium Dioxide to Disinfection and the Killing of Cancer Cells." Separation & Purification Reviews **28**(1): 1-50.

Boonstra, A. H. and C. A. H. A. Mutsaers (1975). "Relation between the photoadsorption of oxygen and the number of hydroxyl groups on a titanium dioxide surface." The Journal of Physical Chemistry **79**(16): 1694-1698.

Campostrini, R., G. Carturan, et al. (1994). "Sol-gel derived anatase TiO_2: morphology and photoactivity." Materials Chemistry and Physics **38**(3): 277-283.

Castillo, S., M. Morán-Pineda, et al. (1998). "Catalytic reduction of nitric oxide on Pt and Rh catalysts supported on alumina and titania synthesized by the sol-gel method." Applied Catalysis B: Environmental **15**(3-4): 203-209.

Chang, C.-F., C.-Y. Chang, et al. (2008). "Preparation and adsorptive application of novel superparamagnetic zirconia material." Colloids and Surfaces A: Physicochemical and Engineering Aspects **327**(1-3): 64-70.

Chang, C.-F., P.-H. Lin, et al. (2006). "Aluminum-type superparamagnetic adsorbents: Synthesis and application on fluoride removal." Colloids and Surfaces A: Physicochemical and Engineering Aspects **280**(1-3): 194-202.

Chen, D. and A. K. Ray (1998). "Photodegradation kinetics of 4-nitrophenol in TiO_2 suspension." Water Research **32**(11): 3223-3234.

Chen, D. and A. K. Ray (1999). "Photocatalytic kinetics of phenol and its derivatives over UV irradiated TiO2." Applied Catalysis B: Environmental **23**(2-3): 143-157.

Chen, F. and J. Zhao (1999). "Preparation and photocatalytic properties of a novel kind of loaded photocatalyst of $TiO_2/SiO_2/\gamma-Fe_2O_3$." Catalysis Letters **58**(4): 246-247.

Chern, J.-M. and Y.-W. Chien (2001). "Adsorption Isotherms of Benzoic Acid onto Activated Carbon and Breakthrough Curves in Fixed-Bed Columns." Industrial & Engineering Chemistry Research **40**(17): 3775-3780.

Ciston, S., R. M. Lueptow, et al. (2008). "Bacterial attachment on reactive ceramic ultrafiltration membranes." Journal of Membrane Science **320**(1-2): 101-107.

Crittenden, J. C., J. Liu, et al. (1997). "Photocatalytic oxidation of chlorinated hydrocarbons in water." Water Research **31**(3): 429-438.

Cunningham, J. and G. Al-Sayyed (1990). "Factors influencing efficiencies of TiO_2-sensitised photodegradation. Part 1.—Substituted benzoic acids: discrepancies with dark-adsorption parameters." Journal of the Chemical Society, Faraday Transactions **86**: 3935 - 3941.

David, H., F. Jaâfar, et al. (2002). "Dispersion and Grinding of Oxide Powders into an Aqueous Slurry." Journal of the American Ceramic Society **85**(2): 321-328.

de Lasa, H., B. Serrano, et al. (2005). Photocatalytic Reaction Engineering, Springer, USA.

Diebold, U. (2003). "The surface science of titanium dioxide." Surface Science Reports **48**(5-8): 53-229.

Ding, H., H. Sun, et al. (2005). "Preparation and characterization of mesoporous SBA-15 supported dye-sensitized TiO_2 photocatalyst." Journal of Photochemistry and Photobiology A: Chemistry **169**(1): 101-107.

Draper, R. B. and M. A. Fox (1990). "Titanium dioxide photosensitized reactions studied by diffuse reflectance flash photolysis in aqueous suspensions of TiO_2 powder." Langmuir **6**(8): 1396-1402.

Duonghong, D., E. Borgarello, et al. (1981). "Dynamics of light-induced water cleavage in colloidal systems." Journal of the American Chemical Society **103**(16): 4685-4690.

Epling, G. A. and C. Lin (2002). "Photoassisted bleaching of dyes utilizing TiO_2 and visible light." Chemosphere **46**(4): 561-570.

Fabbri, D., A. B. Prevot, et al. (2006). "Effect of surfactant microstructures on photocatalytic degradation of phenol and chlorophenols." Applied Catalysis B: Environmental **62**(1-2): 21-27.

Fox, M. A. and M. T. Dulay (1993). "Heterogeneous photocatalysis." Chemical Reviews **93**(1): 341-357.

Freundlich, H. (1906). "Über die Adsorption in Lösungen (Concerning adsorption in solutions)." Zeitschrift Fur Physikalische Chemie–Stochiometrie Und Verwandtschaftslehre **57**(385-470).

Fujishima, A. and K. Honda (1972). "Electrochemical photolysis of water at a semiconductor electrode." Nature **238**: 37-38.

Fujishima, A. and X. Zhang (2006). "Titanium dioxide photocatalysis: present situation and future approaches." Comptes Rendus Chimie **9**(5-6): 750-760.

Ganesh, R., G. D. Boardman, et al. (1994). "Fate of azo dyes in sludges." Water Research **28**(6): 1367-1376.

Gao, Y., B. Chen, et al. (2003). "Preparation and characterization of a magnetically separated photocatalyst and its catalytic properties." Materials Chemistry and Physics **80**(1): 348-355.

Garg, A. K. and L. C. de Jonghe (1990). "Microencapsulation of silicon nitride particles with yttria and yttria-alumina precursors." Journal of Materials Research **5**(1): 136-142.

Gaya, U. I. and A. H. Abdullah (2008). "Heterogeneous photocatalytic degradation of organic contaminants over titanium dioxide: A review of fundamentals, progress and problems." Journal of Photochemistry and Photobiology C: Photochemistry Reviews **9**(1): 1-12.

Gherardi, P. and E. Matijevic (1986). "Interactions of precipitated hematite with preformed colloidal titania dispersions." Journal of Colloid and Interface Science **109**(1): 57-68.

Glaze, W. H., J.-W. Kang, et al. (1987). "The Chemistry of Water Treatment Processes Involving Ozone, Hydrogen Peroxide and Ultraviolet Radiation." Ozone: Science & Engineering: The Journal of the International Ozone Association **9**(4): 335 - 352.

Gopal, M., W. Moberly Chan, et al. (1997). "Room temperature synthesis of crystalline metal oxides." Journal of Materials Science **32**(22): 6001-6008.

Guillard, C., H. Lachheb, et al. (2003). "Influence of chemical structure of dyes, of pH and of inorganic salts on their photocatalytic degradation by TiO_2 comparison of the efficiency of powder and supported TiO_2." Journal of Photochemistry and Photobiology A: Chemistry **158**(1): 27-36.

Hasnat, M. A., I. A. Siddiquey, et al. (2005). "Comparative photocatalytic studies of degradation of a cationic and an anionic dye." Dyes and Pigments **66**(3): 185-188.

Herrmann, J.-M. (1999). "Heterogeneous photocatalysis: fundamentals and applications to the removal of various types of aqueous pollutants." Catalysis Today **53**(1): 115-129.

Hidaka, H., J. Zhao, et al. (1992). "Photodegradation of surfactants. 8. Comparison of photocatalytic processes between anionic DBS and cationic BDDAC on the titania surface." The Journal of Physical Chemistry **96**(5): 2226-2230.

Hoffmann, M. R., S. T. Martin, et al. (1995). "Environmental Applications of Semiconductor Photocatalysis." Chemical Reviews **95**(1): 69-96.

Hong Kyu Park, D. K. K. C. H. K. (1997). "Effect of Solvent on Titania Particle Formation and Morphology in Thermal Hydrolysis of $TiCl_4$." Journal of the American Ceramic Society **80**(3): 743-749.

Hu, C., Y. Tang, et al. (2003). "Photocatalytic degradation of cationic blue X-GRL adsorbed on TiO_2/SiO_2 photocatalyst." Applied Catalysis B: Environmental **40**(2): 131-140.

Inel, Y. and D. Ertek (1993). "Photocatalytic deposition of bismuth(III) ions onto TiO_2 powder." Journal of the Chemical Society, Faraday Transactions **89**: 129-133.

Jackson, M. J. and W. Ahmed (2007). Surface engineered surgical tools and medical devices. New York, Springer

Jornitz, M. W. and T. H. Meltzer (2007). Filtration and Purification in the Biopharmaceutical Industry, Taylor & Francis, Inc.

Kajitvichyanukul, P., J. Ananpattarachai, et al. (2005). "Sol–gel preparation and properties study of TiO_2 thin film for photocatalytic reduction of chromium(VI) in photocatalysis process." Science and Technology of Advanced Materials **6**(3-4): 352-358.

Kaneko, M. and I. Okura (2002). Photocatalysis: Science and Technology, Springer.

Karakitsou, K. E. and X. E. Verykios (1993). "Effects of Altervalent Cation Doping of TiO_2 on its Performance as a Photocatalyst for Water Cleavage." Journal of physical chemistry **97**(6): 1184-1189.

Katoh, R., A. Furube, et al. (2004). "Kinetics and mechanism of electron injection and charge recombination in dye-sensitized nanocrystalline semiconductors." Coordination Chemistry Reviews **248**(13-14): 1195-1213.

Kosmulski, M. (2002). "The significance of the difference in the point of zero charge between rutile and anatase." Advances in Colloid and Interface Science **99**(3): 255-264.

Kuo, W. S. and P. H. Ho (2001). "Solar photocatalytic decolorization of methylene blue in water." Chemosphere **45**(1): 77-83.

Kwon, S., M. Fan, et al. (2008). "Photocatalytic Applications of Micro- and Nano-TiO$_2$ in Environmental Engineering." Critical Reviews in Environmental Science and Technology **38**(3): 197 - 226.

Lair, A., C. Ferronato, et al. (2008). "Naphthalene degradation in water by heterogeneous photocatalysis: An investigation of the influence of inorganic anions " Journal of Photochemistry and Photobiology A: Chemistry **193**(2-3): 193-203.

Langmuir, I. (1918). "THE ADSORPTION OF GASES ON PLANE SURFACES OF GLASS, MICA AND PLATINUM." Journal of the American Chemical Society **40**(9): 1361-1403.

Legrini, O., E. Oliveros, et al. (1993). "Photochemical processes for water treatment." Chemical Reviews **93**(2): 671-698.

Linsebigler, A. L., G. Lu, et al. (1995). "Photocatalysis on TiO$_2$ Surfaces: Principles, Mechanisms, and Selected Results." Chemical Reviews **95**(3): 735-758.

Litter, M. I. (1999). "Heterogeneous photocatalysis: Transition metal ions in photocatalytic systems." Applied Catalysis B: Environmental **23**(2-3): 89-114.

Liu, G., T. Wu, et al. (1999). "Photoassisted degradation of dye pollutants. 8. Irreversible Degradation of Alizarin Red under Visible Light Radiation in Air-Equilibrated Aqueous TiO$_2$ Dispersions." Environmental Science & Technology **33** (12): 2081-2087.

Maki, T. and Y. Susuki (1985). Benzoic acid and derivatives. Ullmann's encyclopedia of industrial chemistry. New York, Wiley-VCH. **A3:** 555-569.

Matthews, R. W. (1993). Photocatalysis in water purification: possibilities, problems and prospects. . Photocatalytic purification and treatment of water and air, Amsterdam, Elsevier Science Publishers.

Matthews, R. W. and S. R. McEvoy (1992). "Photocatalytic degradation of phenol in the presence of near-UV illuminated titanium dioxide." Journal of Photochemistry and Photobiology A: Chemistry **64**(2): 231-246.

Mchedlov-Petrossyan, N. O., S. A. Shapovalov, et al. (1995). "A New Application of Rhodamine 200 B (Sulfo Rhodamine B)." Dyes and Pigments **28**(1): 7-18.

Mengyne, Z., C. Shifn, et al. (1995). "Photocatalytical degradation of organophosphorus pesticides using thin films of TiO$_2$." Journal of Chemical Technology and Biotechnology. **64**: 339-334.

Mills, A., R. H. Davies, et al. (1993). "Water purification by semiconductor photocatalysis." Chem. Soc. Rev **22**: 417-425.

Mills, A. and S. Le Hunte (1997). "An overview of semiconductor photocatalysis." Journal of Photochemistry and Photobiology A: Chemistry **108**(1): 1-35.

Mills, A. and S. Morris (1993). "Photomineralization of 4-chlorophenol sensitized by titanium dioxide: a study of the initial kinetics of carbon dioxide photogeneration." Journal of Photochemistry and Photobiology A: Chemistry **71**(1): 75-83.

Mills, G. and M. R. Hoffmann (1993). "Photocatalytic degradation of pentachlorophenol on titanium dioxide particles: identification of intermediates and mechanism of reaction." Environmental Science & Technology **27**(8): 1681-1689.

Mohammad Hossein Habibi, M. K. M. M. (2004). "Photocatalytic Mineralisation of Aniline Derivatives in Aquatic Systems Using Semiconductor Oxides." Annali di Chimica **94**(5-6): 421-428.

Morrison, P. W., R. Raghavan, et al. (1997). "In Situ Fourier Transform Infrared Characterization of the Effect of Electrical Fields on the Flame Synthesis of TiO_2 Particles." Chemistry of Materials **9**(12): 2702-2708.

Munter, R. (2001). "Advanced Oxidation Processes- Current status and prospects." Proc. Estonian Acad.Sci.Chem **50**(2): 59-80.

Murakami, Y., T. Matsumoto, et al. (1999). "Salt Catalysts Containing Basic Anions and Acidic Cations for the Sol&Gel Process of Titanium Alkoxide: Controlling the Kinetics and Dimensionality of the Resultant Titanium Oxide." The Journal of Physical Chemistry B **103**(11): 1836-1840.

Ocaña, M., E. Matijevic, et al. (1991). "Preparation and properties of uniform-coated colloidal particles. 6. Titania on zinc oxide." Langmuir **7**(12): 2911-2916.

Okamoto, K., Y. Yamamoto, et al. (1985). "Heterogeneous photocatalytic descomposition of phenol over TiO2 powder." Bull. Chem. Soc. Jpn **58**: 2015.

Ollis, D. F. (1987). Process economics for water purification: a comparative assessment. Photocatalysis and environment, trends and applications M. Schiavello. Dordrecht, Kluwer Academic Publishers: 663-677.

Ollis, D. F., E. Pelizzetti, et al. (1991). "Photocatalyzed destruction of water contaminants." Environmental Science & Technology **25**(9): 1522-1529.

Ollis, D. F. and N. Serpone (1989). Heterogeneous Photocatalysis in the Environment: Application to Water Purification. Photocatalysis: Fundamentals and Applications. N. Serpone and E. Pelizzetti, John Wiley and sons**:** 650.

Pagga, U. and K. Taeger (1994). "Development of a method for adsorption of dyestuffs on activated sludge." Water Research **28**(5): 1051-1057.

Parent, Y., D. Blake, et al. (1996). "Solar photocatalytic processes for the purification of water: State of development and barriers to commercialization." Solar Energy **56**(5): 429-437.

Parra, S., J. Olivero, et al. (2002). "Relationships between physicochemical properties and photoreactivity of four biorecalcitrant phenylurea herbicides in aqueous TiO_2 suspension." Applied Catalysis B: Environmental **36**(1): 75-85.

Patil, S. S. and V. M. Shinde (1988). "Biodegradation studies of aniline and nitrobenzene in aniline plant wastewater by gas chromatography." Environmental Science & Technology **22**(10): 1160-1165.

Pozzo, R. L., M. A. Baltanás, et al. (1999). "Towards a precise assessment of the performance of supported photocatalysts for water detoxification processes." Catalysis Today **54**(1): 143-157.

Preety S. Mukherjee, A. K. R. (1999). "Major Challenges in the Design of a Large-Scale Photocatalytic Reactor for Water Treatment." Chemical Engineering & Technology **22**(3): 253-260.

Primet, M., P. Pichat, et al. (1971). "Infrared study of the surface of titanium dioxides. I. Hydroxyl groups." The Journal of Physical Chemistry **75**(9): 1216-1220.

Rajeshwar, K. and J. Ibanez (1997). Environmental Electrochemistry: Fundamentals and Applications in Pollution Abatement. San Diego., Academic Press.

Rao, C. N. R., S. R. Yoganarasimhan, et al. (1961). "Studies on the brookite-rutile transformation." Trans. Faraday Soc. **57**: 504-510.

Ray, A. K. (1999). "Design, modelling and experimentation of a new large-scale photocatalytic reactor for water treatment." Chemical Engineering Science **54**(15-16): 3113-3125.

Ray, A. K. and A. A. C. M. Beenackers (1996). A Photocatalytic Reactor Suitable for Water Purification as Well as a Process for the Purification of Waste Water by Means of Such a Photocatalytic Reactor. European patent **96200942.9-2104**.

Reemtsma, T. and M. Jekel (2006). Organic pollutants in the water cycle. Weinheim, Wiley-VCH.

Rideh, L., A. Wehrer, et al. (1997). "Photocatalytic Degradation of 2-Chlorophenol in TiO_2 Aqueous Suspension: Modeling of Reaction Rate." Industrial & Engineering Chemistry Research **36**(11): 4712-4718.

Saadoun, L., J. A. Ayllón, et al. (1999). "1,2-Diolates of titanium as suitable precursors for the preparation of photoactive high surface titania." Applied Catalysis B: Environmental **21**(4): 269-277.

Sclafani, A., L. Palmisano, et al. (1990). "Influence of the preparation methods of titanium dioxide on the photocatalytic degradation of phenol in aqueous dispersion." The Journal of Physical Chemistry **94**(2): 829-832.

Scott, J. P. and D. F. Ollis (1995). "Integration of chemical and biological oxidation processes for water treatment: Review and recommendations." Environmental Progress **14**(2): 88-103.

Serpone, N. (1995). "Brief introductory remarks on heterogeous photocatalysis." Solar Energy Materials and Solar Cells **38**(1-4): 369-379.

Serpone, N., D. Lawless, et al. (1995). "Subnanosecond Relaxation Dynamics in TiO_2 Colloidal Sols (Particle Sizes Rp = 1.0-13.4 nm). Relevance to Heterogeneous Photocatalysis." The Journal of Physical Chemistry **99**(45): 16655-16661.

Snoeyink, V. and R. S. Summers (1999). Adsorption of Organic Compounds. Water Quality and Treatment - A Handbook of Community Water Supplies. R. D. Letterman and A. American Water Works. New York., McGraw-Hill**:** 1248.

Sökmen, M. and A. Özkan (2002). "Decolourising textile wastewater with modified titania: the effects of inorganic anions on the photocatalysis." Journal of Photochemistry and Photobiology A: Chemistry **147**(1): 77-81.

Stashans, A., S. Lunell, et al. (1996). "Theoretical study of perfect and defective TiO_2 crystals." Journal of Physics and Chemistry of Solids **57**(9): 1293-1301.

Tang, W. Z. and A. Huren (1995). "UV/TiO_2 photocatalytic oxidation of commercial dyes in aqueous solutions." Chemosphere **31**(9): 4157-4170.

Tayade, R. J., P. K. Surolia, et al. (2007). "Photocatalytic degradation of dyes and organic contaminants in water using nanocrystalline anatase and rutile TiO_2." Science and Technology of Advanced Materials **8**(6): 455-462.

Turchi, C. S. and D. F. Ollis (1990). "Photocatalytic degradation of organic water contaminants: Mechanisms involving hydroxyl radical attack." Journal of Catalysis **122**(1): 178-192.

van Dyk, A. C. and A. M. Heyns (1998). "Dispersion Stability and Photo-activity of Rutile (TiO_2) Powders." Journal of Colloid and Interface Science **206**(2): 381-391.

Vidal, A., B. Sanchez, et al. (1994). Proc. of the First International Conference on Advanced oxidation technologies for water and air remediation, London.

Vinodgopal, K., D. E. Wynkoop, et al. (1996). "Environmental Photochemistry on Semiconductor Surfaces: Photosensitized Degradation of a Textile Azo Dye, Acid Orange 7, on TiO_2 Particles Using Visible Light." Environmental Science & Technology **30**(5): 1660-1666.

Warad, H. C., S. C. Ghosh, et al. (2005). "Luminescent nanoparticles of Mn doped ZnS passivated with sodium hexametaphosphate." Science and Technology of Advanced Materials **6**(3-4): 296-301.

Watson, S., D. Beydoun, et al. (2002). "Synthesis of a novel magnetic photocatalyst by direct deposition of nanosized TiO2 crystals onto a magnetic core." Journal of Photochemistry and Photobiology A: Chemistry **148**(1-3): 303-313.

Xu, N., Z. Shi, et al. (1999). "Effects of Particle Size of TiO_2 on Photocatalytic Degradation of Methylene Blue in Aqueous Suspensions." Industrial & Engineering Chemistry Research **38**(2): 373-379.

Xu, Y. and C. H. Langford (2000). "Variation of Langmuir adsorption constant determined for TiO2-photocatalyzed degradation of acetophenone under different light intensity." Journal of Photochemistry and Photobiology A: Chemistry **133**(1-2): 67-71.

Ying, J. Y. and T. Sun (1997). "Research Needs Assessment on Nanostructured Catalysts." Journal of Electroceramics **1**(3): 219-238.

Zaban, A., S. T. Aruna, et al. (2000). "The Effect of the Preparation Condition of TiO_2 Colloids on Their Surface Structures." The Journal of Physical Chemistry B **104**(17): 4130-4133.

Zhang, Q., L. Gao, et al. (2000). "Effect of hydrolysis conditions on morphology and crystallization of nanosized TiO_2 powder." Journal of the European Ceramic Society **20**(12): 2153-2158.

Zhang, Q. H., L. Gao, et al. (1999). "Preparation and characterization of nanosized TiO_2 powders from aqueous $TiCl_4$ solution." Nanostructured Materials **11**(8): 1293-1300.

Zhang, X., H. Yang, et al. (2007). "Preparation and characterization of $Pt-TiO_2-SiO_2$ mesoporous materials and visible-light photocatalytic performance." Materials Letters **61**(11-12): 2231-2234.

Zhang, Y., J. C. Crittenden, et al. (1994). "Fixed-bed photocatalysts for solar decontamination of water." Environmental Science & Technology **28**(3): 435-442.

Zhao, J., K. Wu, et al. (1998). "Photoassisted degradation of dye pollutants III: Evidence for the need for substrate adsorption on TIO2 particles." Environmental Science & Technology **32**: 2394-2400.

Zhu, J., J. Yang, et al. (2007). "Nanocrystalline anatase TiO$_2$ photocatalysts prepared via a facile low temperature nonhydrolytic sol-gel reaction of TiCl$_4$ and benzyl alcohol." Applied Catalysis B: Environmental **76**(1-2): 82-91.

Zhu, Y., L. Zhang, et al. (2000). "The synthesis of nanosized TiO$_2$ powder using a sol-gel method with TiCl$_4$ as a precursor." Journal of Materials Science **35**(16): 4049-4054.

8   APPENDIX

8.1   List of Symbols

E_a	Activation energy
γ	Activity coefficient of the substrate
K_{ads}	Apparent adsorption equilibrium constant (L mmol^{-1})
k_{eff}	Apparent effective reaction rate constant (mmol L^{-1} min^{-1})
k_{app}	Apparent reaction rate constant (min^{-1})
e^-_{cb}	Conduction band electron
e^-	Electron
E_{bg}	Energy gap or band gap
a	Equilibrium activity of the substrate in aqueous solution
C_e	Equilibrium concentration of sorptive (mmol L^{-1})
K_F	Freundlich constant
R	Gas constant (J mol^{-1} K^{-1})
h^+	Hole
C_0	Initial concentration of sorptive (mmol L^{-1})
r_0	Initial degradation rate (mmol L^{-1} min^{-1})
q_o	Initial loading (mmol g^{-1})
K_L	Langmuir constant (L mmol^{-1})
q_e	Loading at equilibrium (mmol g^{-1})
q_{max}	Maximum loading (mmol g^{-1})
E_{ph}	Photon energy
>TiOH	Primary hydrated surface functionality of TiO$_2$
A	Surface area (m^2 g^{-1})
θ	Surface coverage
>Ti^{III}OH	Surface-trapped conduction band electron
>Ti^{IV}OH$^{\bullet}$	Surface-trapped valence band hole
T	Temperature (°K or °C)
I_{UV}	UV light intensity (mW cm^{-2})
h_{vb}^+	Valence band hole
V_L	Volume of liquid phase (L)

8.2 Absorption Spectra of Model Compounds

The absorption spectra for the three organic compounds were determined by a spectrophotometer Spectroflex 6600 (WTW, Germany).
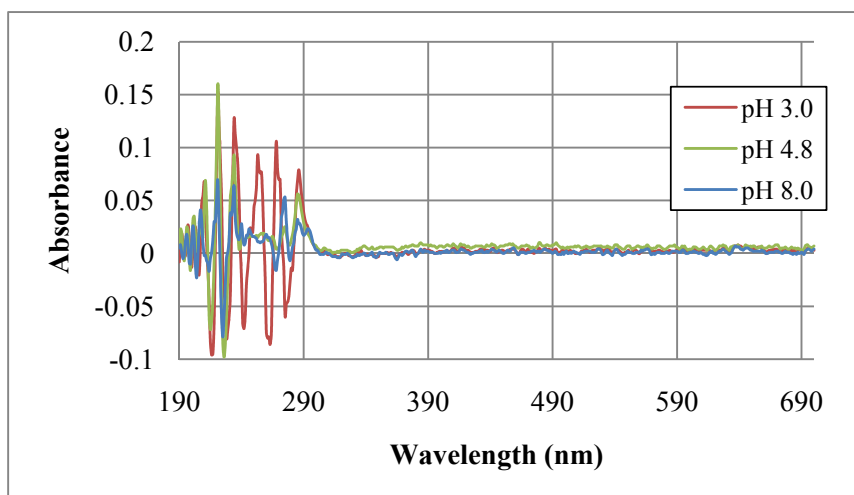
8.2.1 Benzoic acid (BA)

Figure 8.1: Absorption spectra of benzoic acid at different pH values; benzoic acid concentration 0.24 mmol L^{-1}.
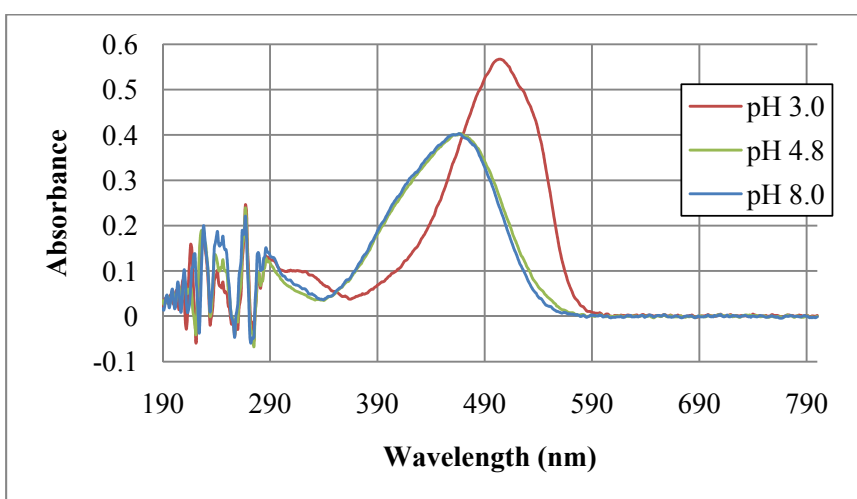
8.2.2 Methyl orange (MO)

Figure 8.2: Absorption spectra of methyl orange at different pH values; methyl orange concentration 0.014 mmol L^{-1}.
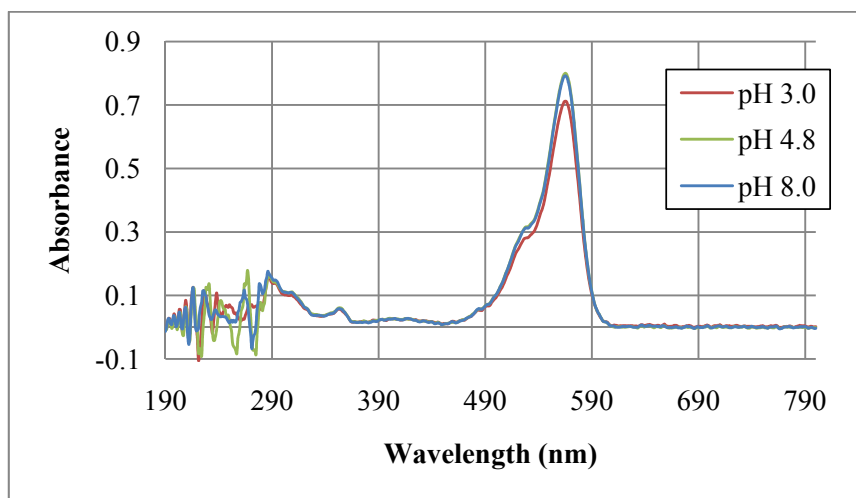
8.2.3 Sulfurhodamine B (SRB)

Figure 8.3: Absorption spectra of sulfurhodamine at different pH values; sulfurhodamine concentration 0.071 mmol L^{-1}.

Curriculum Vitae

Name	Marcelo José González Salazar
Date of Birth	November 24th, 1975.
Place of Birth	Santiago – Chile.
Nationality	Chilean.
E-Mail	mgonzalezs@msn.com

Academic Records

2006 - 2010	PhD Student, Technical University of Berlin, Germany. **PhD Thesis:** Development and application of titanium dioxide coated magnetic particles for photocatalytic oxidation of aqueous phase organic pollutants.
2002	Faculty of natural sciences, mathematics and environment. Metropolitan University of Technology. Santiago, Chile. **Degree:** Chemi Engineer.
2000 - 2001	Faculty of Chemical and Pharmaceutical Sciences, University of Chile, Santiago, Chile. **Thesis:** Study of the feasibility of the use of chitosan grafted as an agent of metallic ion Cu(II) removal from watery solutions by selective adsorption.
1995 - 2000	Faculty of natural sciences, mathematics and environment. Metropolitan University of Technology. Santiago, Chile. Chemical Engineering**.**
1994	Academic Aptitude Test. National Examination for applying to the Chilean universities.
1990 - 1993	Secondary Education. Instituto Nacional "José Miguel Carrera", Santiago, Chile.

Professional Experience

2006 – 2010	Karlsruhe Institute of Technology (formerly Forschungszentrum Karlsruhe), Germany. Researcher at Institute of Functional Interfaces.
2002 - 2005	Equilab Equipments Ltda., Chile. Sales Representative. Preparation of technical seminaries and assistance to clients on laboratory issues.
2001 - 2002	Laboratory of Homeopathy Lautaro Ltda., Chile. Planning and supervision of pharmaceutical procedures.
2000 - 2001	Faculty of Chemical and Pharmaceutical Sciences, University of Chile. Thesis.
1999	Faculty of Engineering, Pontifical Catholic University of Chile. Wastewater and Industrial water laboratory. Professional Practice.

Courses

2006	Techniques for the sustainable administration of hydraulic resources and Modeling of groundwaters. **Complutense University of Madrid. Spain.**
2000	Metallurgical - Mining Chemistry, Faculty of Chemical and Pharmaceutical Sciences, **University of Chile, Santiago, Chile.**
2000	Pollution and Wastewater Treatment, Faculty of Chemical and Pharmaceutical Sciences, **University of Chile, Santiago, Chile.**

Conferences and Publications

2008	Wasser 2008 - Jahrestagung der Wasserchemischen Gesellschaft Trier. Poster: Gonzalez M, Jekel M., Höll W.H. "Development and Application of Titanium Dioxide coated Magnetic particles for Photocatalytic Oxidation of Organic Pollutants in Aqueous Phase".
2008	Gonzalez, M., Hoell, W.H., Jekel, M. (2008). "Development and application of TiO_2/Fe_3O_4 catalyst for photodegradation of benzoic acid" Vom Wasser **106** (4): 22-26.
2007	Wasser 2007 - Jahrestagung der Wasserchemischen Gesellschaft Passau.

Languages

Spanish	Native Language.
English	Intermediate – Advanced.
German	Intermediate.